

Overall evaluation of drive-off procedures in a mild hybrid powertrain

An evaluation approach considering subjective and ecological evaluation aspects

Am Fachbereich Maschinenbau

an der Technischen Universität Darmstadt

zur

Erlangung des Grades eines Doktor-Ingenieurs (Dr.-Ing.)

genehmigte

DISSERTATION

vorgelegt von

PING HE, M.SC.

Berichterstatter:

Prof. Dr.-Ing. Stephan Rinderknecht

Mitberichterstatter:

Prof. Dr.-Ing. Michael Fister

Tag der Einreichung:


05.12.2023

Tag der mündlichen Prüfung:

13.02.2024

Darmstadt 2024

D17



He, Ping: Overall evaluation of drive-off procedures in a mild hybrid powertrain

Darmstadt, Technische Universität Darmstadt

Veröffentlichungsjahr der Dissertation auf TUpriints: 2024

Tag der mündlichen Prüfung: 13.02.2024

Veröffentlicht unter CC BY-SA 4.0 International

<https://creativecommons.org/licenses/>



Acknowledgements

I would like to give my sincere gratitude to my first supervisor, Professor Dr.-Ing. Stephan Rinderknecht, for his continuous support throughout the research project and this doctoral work. His guidance, insightful advice, and encouragement have been invaluable, shaping not only my research but also my career aspirations.

I also want to express my appreciation to my second supervisor, Professor Dr.-Ing. Michael Fister, who provided me with my first student job during my master study and offered me a glimpse into the world of research. I am grateful for his time spent supervising this work.

Special thanks are due to Magna PT and its staff members for their support in completing the research project. I want to acknowledge Andreas Pawlenka and Marius Schmiedt for their willingness to engage in the project, their collaborative spirit, and the inspiration they brought. Without their contributions, the success of the research results would not have been possible.

I am deeply thankful to friends and colleagues for their support, proofreading, and valuable advice. A very special thanks to Dr.-Ing. Edward Kraft and Dr.-Ing. Björn Bartholmai for their assistance.

Last but not least, heartfelt thanks to my parents, my parents-in-law, and my wife. Your understanding of the challenges I faced during this time has been a pillar of strength. Thank you for always being there, offering support, and allowing me the time to focus on this work. To my daughter Ella, your presence has been a constant source of joy, making it easier to confront all challenges. I love you all!



Abstract

This work deals with the combined investigation of subjective and ecological evaluation of the drive-off dynamics of passenger vehicles. The main focus is on the drive-off procedure in a mild hybrid powertrain. A connection between the subjective driving impression and ecological factors such as fuel consumption and the thermal load in the clutch is established.

In order to investigate the subjective evaluation of the drive-off dynamics, three test subject studies are conducted with the focus on influence factors maximum acceleration, mean jerk, response time, and engine speed changes. In each study, evaluation criteria related to driving dynamics and ride comfort are used. Statistical tests are carried out to identify the evaluation difference thresholds for these influence factors. The evaluation criteria, sportiness, jerkiness, and comfort, which are used in the ecological evaluation to assess the drive-offs, are objectivated by using a logistic regression model based on the maximum acceleration and mean jerk.

The hybrid modeling approach introduced for the ecological evaluation, which combines forward and backward modeling, ensures a precise simulation of the drive-off behavior. This approach also fulfills the requirement to maintain the neutrality of the battery's state of charge in the mild hybrid powertrain and to follow the reference driving cycle with high accuracy. The results show that the fuel consumption benefits of using the electric motor are most significant during drive-offs at low accelerator pedal positions, but this advantage decreases with increasing accelerator pedal positions due to compensatory fuel consumption for battery recharging.

Furthermore, the work underlines the ecological advantages of support by the electric motor in terms of reducing the thermal load in the clutch. It proves to be effective in reducing thermal load during drive-off and sequential gear upshifting when the electric motor operates as a drive. These advantages go beyond the immediate thermal load reduction and contribute to the goals of sustainable and efficient vehicle design.

For the calibration process, it is beneficial to understand the effects of changes in drive-off dynamics on user experience and ecological aspects. The results of this work provide valuable insights for the calibration process to facilitate fine-tuning of the drive-off characteristics taking into account both subjective driving impression and ecological factors.

Kurzfassung

Diese Arbeit beschäftigt sich mit der kombinierten Untersuchung der subjektiven und ökologischen Bewertung der Anfahrtdynamik von Personenkraftwagen. Der primäre Fokus liegt auf dem Anfahrvorgang in einem Mild-Hybrid-Antriebsstrang. Es wird ein Zusammenhang zwischen dem subjektiven Fahreindruck und ökologischen Faktoren wie Kraftstoffverbrauch und thermischer Belastung der Kupplung hergestellt.

Um die subjektive Bewertung der Anfahrtdynamik zu untersuchen, werden drei Probandenstudien durchgeführt, die sich auf die Einflussfaktoren maximale Beschleunigung, mittlerer Ruck, Reaktionszeit und Motordrehzahländerungen konzentrieren. In jeder Studie werden Bewertungskriterien im Zusammenhang mit Fahrtdynamik und Fahrkomfort verwendet. Statistische Tests werden durchgeführt, um die Differenzschwellen der Bewertung für diese Einflussfaktoren zu ermitteln. Die Bewertungskriterien Sportlichkeit, Ruckartigkeit und Komfort, die in der ökologischen Bewertung zur Beurteilung der Anfahrvorgängen herangezogen werden, werden mit Hilfe eines logistischen Regressionsmodells basierend auf der maximalen Beschleunigung und des mittleren Rucks objektiviert.

Der für die ökologische Bewertung eingeführte hybride Modellierungsansatz, der Vorwärts- und Rückwärtsmodellierung kombiniert, gewährleistet eine präzise Simulation des Anfahrverhaltens. Dieser Ansatz erfüllt auch die Anforderung, die Neutralität des Ladezustands der Batterie im Mild-Hybrid-Antriebsstrang einzuhalten und dem Referenzfahrzyklus mit hoher Genauigkeit zu folgen. Die Ergebnisse zeigen, dass die Kraftstoffverbrauchsvorteile beim Anfahren bei niedrigen Fahrpedalstellungen signifikant sind, dieser Vorteil jedoch mit zunehmender Fahrpedalstellung aufgrund des kompensatorischen Kraftstoffverbrauchs für das Aufladen der Batterie abnimmt.

Darüber hinaus unterstreicht die Arbeit die ökologischen Vorteile der Unterstützung durch den Elektromotor im Hinblick auf die Verringerung der thermischen Belastung in der Kupplung. Sie erweist sich als wirksam bei der Reduzierung der thermischen Belastung während des Anfahrens und des sequenziellen Hochschaltens, wenn der Elektromotor als Antrieb arbeitet. Diese Vorteile gehen über die unmittelbare Verringerung der thermischen Belastung hinaus und tragen zu den Zielen eines nachhaltigen und effizienten Fahrzeugdesigns bei.

Für den Kalibrierungsprozess ist es von Vorteil, die Auswirkungen von Veränderungen in der Anfahrtdynamik auf die Nutzererlebnis und ökologische Aspekte zu verstehen. Die Ergebnisse dieser Arbeit bieten wertvolle Einblicke für den Kalibrierungsprozess, um die Feinabstimmung der Anfahrcharakteristiken unter Berücksichtigung sowohl des subjektiven Fahreindrucks als auch der ökologischen Faktoren zu erleichtern.

Contents

Abstract.....	I
Kurzfassung	II
Contents.....	III
List of Figures	VI
List of Tables.....	IX
Nomenclature	X
Acronyms/Abbreviations.....	X
Latin Symbols.....	XI
Greek Symbols.....	XIV
Subscripts.....	XV
1 Introduction.....	1
1.1 Motivation	1
1.2 Research objectives	4
1.3 Structure of the content	7
2 Fundamentals and state of the art	9
2.1 Definition and evaluation of the drive-off procedure	9
2.2 The mild hybrid powertrain	13
2.3 The wet friction dual-clutches	16
2.3.1 Understanding wet friction dual-clutches.....	16
2.3.2 Degradation mechanisms	19
2.3.3 Lifetime prediction	21
2.4 Subjective evaluation of the driving dynamics	22
2.4.1 Perception of motion	22
2.4.2 State of the art of the subjective evaluation and perception threshold for linear motion and acceleration	24
2.4.3 Objectivation of the subjective evaluation.....	26
2.4.4 Longitudinal dynamic driving simulator	28
2.5 Ecological evaluation of the driving dynamics	31
2.5.1 State of the art of the ecological evaluation	32
2.5.2 Ecological evaluation objectives	33
2.6 Research gap and usability.....	34
3 Investigation of the subjective evaluation	36

3.1	Test subject study 1 – Investigation of the maximum acceleration and mean jerk ..	36
3.1.1	Design of the study.....	37
3.1.2	Results of the test subject studies	39
3.1.3	Objectivation of the subjective evaluation.....	44
3.2	Test subject study 2 – Investigation of the response time	47
3.2.1	Design of the test subject studies	48
3.2.2	Results of the test subject studies	50
3.3	Test subject study 3 – Investigation of the engine speed changes	54
3.3.1	Design of the test subject studies	54
3.3.2	Results of the test subject studies	56
3.4	Conclusion for the results of the test subject studies and the limitations	59
4	Powertrain model for ecological evaluation	62
4.1	Foundational modeling principle.....	62
4.2	Powertrain component modeling	66
4.2.1	Propulsion Units.....	66
4.2.2	DCT Modeling.....	70
4.2.3	Wheel modeling	74
4.2.4	Vehicle dynamics modeling	77
4.3	Extended clutch modeling.....	79
4.3.1	Thermal model for the clutch	79
4.3.2	Degradation model for the clutch	80
4.4	Control module.....	86
4.4.1	Drive-off controller.....	86
4.4.2	Backward modeling for torque request estimation	87
4.4.3	Control strategy for EMS	89
4.5	Analysis of the simulation results	93
4.5.1	Driving cycle	93
4.5.2	Evaluation criteria.....	94
4.5.3	Correctness of the vehicle simulation model	94
4.5.4	Performance of the control strategy.....	98
5	Results of the drive-off procedure evaluation.....	101
5.1	Subjective and ecological evaluation of the drive-off procedure.....	101
5.1.1	Analysis of the drive-off procedures.....	101
5.1.2	Subjective and ecological evaluation	107
5.2	Ecological evaluation of the thermal clutch load regarding the driving cycle.....	120
5.2.1	Proportion of the drive-off thermal load in the lifetime of the clutch.....	120
5.2.2	Outlook for the potential during shifting	120



6 Conclusion and perspectives 125

6.1 Conclusion 125

6.2 Perspectives 127

Reference 139



List of Figures

Figure 1.1: Illustration of the subjective and ecological evaluation of the drive-off procedures in a mild hybrid powertrain 5

Figure 2.1: Engine speed (green) and clutch output plate speed (orange) during a drive-off procedure, (a): Drive-off with a consistently increasing engine speed, (b): Drive-off with a flare in engine speed 10

Figure 2.2: Exemplary illustration of an acceleration profile of a drive-off..... 12

Figure 2.3: P2.5 hybrid configuration with an integrated EM connected mechanically to the second input shaft of the transmission via an intermediate gear, C1 and C2 represent the Clutches 1 and 2 15

Figure 2.4: Wet friction dual-clutch of VW (BorgWarner) [25]. 1 Inner plate carrier of the outer clutch; 2 Outer plate carrier of the outer clutch; 3 Inner plate carrier of the inner clutch; 4 Outer plate carrier of inner clutch; 5 Piston; 6 Compression spring; 7 Input hub; 8 Drum; 9 Sealing ring; 10 Driving plate 17

Figure 2.5: An exemplary illustration of a complete duty cycle of a wet friction clutch 18

Figure 2.6: interaction among the clutch degradation mechanisms [52] 19

Figure 2.7: Longitudinal dynamic driving simulator in side view (left) and front view (right) [22] 29

Figure 2.8: HMI in the driving simulator [22] (left) and the visual environment displayed in the VR Headset (right)..... 31

Figure 3.1: Drive-off profiles for the test subject study 1 37

Figure 3.2: Descriptive statistics for drive-off evaluation according to sportiness in study 1 40

Figure 3.3: Descriptive statistics for drive-off evaluation according to jerkiness in study 1 41

Figure 3.4: Descriptive statistics for drive-off evaluation according to comfort in study 1 41

Figure 3.5: Regression models for evaluating drive-off dynamics 45

Figure 3.6: Division of the evaluation of the drive-off dynamics 46

Figure 3.7: Descriptive statistics for drive-off evaluation according to agility in study 2..... 51

Figure 3.8: Descriptive statistics for drive-off evaluation according to sportiness in study 2..... 51

Figure 3.9: Descriptive statistics for drive-off evaluation according to comfort in study 2 52

Figure 3.10: Descriptive statistics for engine speed evaluation according to sportiness in study 3 56

Figure 3.11: Descriptive statistics for engine speed evaluation according to comfort in study 3 . 57

Figure 3.12: Descriptive statistics for engine speed evaluation according to acceptability in study 3 57

Figure 4.1: Overview of the P2.5 HEV model and control module, information flow for the drive-off procedure, and subsequent driving 63

Figure 4.2: LUTs from the Simulink® library for the simulation of the engine torque and fuel mass flow	67
Figure 4.3: The brake-specific fuel consumption	67
Figure 4.4: Efficiency map of EM including an inverter	69
Figure 4.5: Open circuit voltage (left) and internal resistance of the battery model (right).....	70
Figure 4.6: Switch condition for the clutch operating states	70
Figure 4.7: Torque transfer within the DCT	72
Figure 4.8: Overview of the wheel model [112].....	74
Figure 4.9: Schematic illustration of the wheel dynamics.....	75
Figure 4.10: Forces acting on a vehicle	77
Figure 4.11: A part of a test cycle in the endurance experiment (left) and the shifting process at the start of the test cycle	82
Figure 4.12: The changing of the reinforced CoF-slope over the test cycles represented by difference in the mean value of the reinforced CoF at high and low sliding speed.....	83
Figure 4.13: Peak amplitude of the sliding speed plotted over the test cycles	84
Figure 4.14: Characteristic diagram for the friction behavior of the clutch with consideration of the degradation process	85
Figure 4.15: Acceleration estimation based on vehicle speed deviation	87
Figure 4.16: Schematic representation of the „Time of Arrive“ concept	87
Figure 4.17: Gear shifting map, color bar shows the corresponding areas for each gear	89
Figure 4.18: Velocity profile of the WLTC Class 3b [126].....	94
Figure 4.19: Comparison between desired velocity and simulated velocity from HEV and conventional vehicle.	95
Figure 4.20: ICE operation points in the efficiency distribution diagram according to torque and speed in conventional operation mode	96
Figure 4.21: ICE operation points in the efficiency distribution diagram according to torque and speed in hybrid operation mode.....	97
Figure 4.22: ICE operation point distribution in conventional and hybrid operation modes.....	97
Figure 4.23: EM operation points in hybrid operation mode with the distribution diagram for torque and speed	98
Figure 4.24: SOC comparison between ECMS and A-ECMS.....	99
Figure 4.25: ICE and EM torque distribution under hybrid operation mode with ECMS and A-ECMS as control strategy for the EMS	100
Figure 5.1: LUTs for determining the desired engine torque and speed of the drive-off controller	102
Figure 5.2: Electric drive-off procedures for the APPs of 10 % and 20 %, supported without (left) and with (right) EM.....	103

Figure 5.3: Hybrid drive-off procedures for the APPs from 30 % to 50 %, supported without (left) and with (right) EM.....	104
Figure 5.4: Reduction of heat and surface temperature during drive-offs according to the APPs by using the EM	110
Figure 5.5: Cooling performance at different flow rates for drive-offs with and without the EM support at an APP of 50 %	111
Figure 5.6: Driving cycle for testing the fuel consumption improvement during drive-offs with EM support and recharging the battery with consideration of the energy recuperation	112
Figure 5.7: Distribution of the battery recharge by recuperation and ICE load point upshifting for drive-off with an APP of 10 %	113
Figure 5.8: Energy inputs (a) and Energy outputs and losses (b) during drive-offs with and without the support of the EM	116
Figure 5.9: Gear shifting at 3 rd gear without (a) and with (b) the EM support	122
Figure 5.10: Gear shifting at 4 th gear without (a) and with (b) the EM support during load point upshifting of the ICE	123

List of Tables

Table 2.1: Perception threshold for acceleration and jerk.....	26
Table 2.2: Actuator and platform specifications [78]	30
Table 3.1: Variation of the drive-off profiles for study 1	38
Table 3.2: Evaluation criteria for the experienced drive-off.....	39
Table 3.3: MANOVA Multivariate Tests (Wilks-Lambda).....	42
Table 3.4: ANOVA for investigating the significance of maximum acceleration and mean jerk...	42
Table 3.5: Pairwise comparisons for identifying the EDTs of maximum acceleration	43
Table 3.6: Pairwise comparisons for identifying the EDTs of mean jerk.....	44
Table 3.7: Drive-off profiles for the validation of the regression models	46
Table 3.8: Results for validation of the regression models.....	47
Table 3.9: drive-off characteristics according to the APPs.....	48
Table 3.10: Variation of the drive-off profiles for study 2.....	49
Table 3.11 Evaluation criteria for the experienced drive-off	50
Table 3.12: MANOVA Multivariate Tests (Wilks-Lambda).....	52
Table 3.13: ANOVA for investigating the significance of response time and APP	53
Table 3.14: Pairwise comparisons for identifying the EDTs of response time	54
Table 3.15: Variation of the engine speed curves for study 3.....	55
Table 3.16 Evaluation criteria for the experienced drive-off.....	55
Table 3.17: MANOVA Multivariate Tests (Wilks-Lambda).....	58
Table 3.18: ANOVA for investigating the significance of engine speed flare	58
Table 3.19: Pairwise comparisons for identifying the EDTs of engine speed flare	59
Table 3.20: EDT ranges for the influence factors.....	60
Table 4.1: The component parameters and properties for the vehicle simulation model	65
Table 4.2: Average cumulative absolute velocity error for both vehicle operation modes.....	95
Table 4.3: variation of the battery SOC during WLTC driving simulation	99
Table 5.1: Characteristic values of drive-offs with and without EM support according to APPs	106
Table 5.2: Subjective evaluation of the drive-off dynamics using the evaluation models.....	107
Table 5.3: Thermal load and temperature in the clutch during drive-offs with different APPs..	109
Table 5.4: Fuel consumption improvement during drive-offs considering energy recuperation	114
Table 5.5: Subjective and ecological evaluations of the drive-offs in the mild hybrid powertrain	119
Table 5.6: Heat generation in the clutch C1 and clutch C2 for gear shifting from 2 nd to 7 th	121

Nomenclature

Acronyms/Abbreviations

A-ECMS	Adaptive Equivalent Consumption Minimization Strategy
ANOVA	ANalysis Of VAriance
APP	Accelerator Pedal Position
ASR	Advanced Slip Ratio
ATF	Automatic Transmission Fluid
BEV	Battery-Electric Vehicle
BSFC	Brake-Specific Fuel Consumption
CoF	Coefficient Of Friction
CoG	Center of Gravity
DCT	Dual-Clutch Transmission
DFG	Deutsche ForschungsGemeinschaft
DMF	Dual Mass Flywheel
DP	Dynamic Programming
ECMS	Equivalent Consumption Minimization Strategy
EDT	Evaluation Difference Threshold
EM	Electric Motor
EMS	Energy Management System
FCI	Fuel Consumption Improvement
FHEV	Full Hybrid Electric Vehicle
HEV	Hybrid Electric Vehicle
HMI	Human-Machine Interface
ICE	Internal Combustion Engine
IMS	Institute of Mechatronic Systems in mechanical engineering
JND	Just Noticeable Difference
KMO	Kaiser-Meyer-Olkin
LUT	LookUp Table
MHEV	Mild Hybrid Electric Vehicle
MLE	Maximum Likelihood Estimation
P	Parallel hybrid
PCA	Principal Component Analysis

PHEV	Plug-in Hybrid Electric Vehicle
PI	Proportional-Integral
PMP	Pontryagin Minimum Principle
PMR	Power-to-Mass Ratio
SI	Spark-Ignition
SOC	State Of Charge
VR	Virtual Reality
WLTC	Worldwide harmonized Light-duty Test Cycle

Latin Symbols

A_f	Frontal projection area of the vehicle
A_T	Contact area of the friction oil
a	Coefficients of the clutch degradation model
a_p	Exponential coefficient in the penalty function of the control strategy
a_{Corr}	Correction acceleration for compensation of the vehicle speed deviation
a_{Ctrl}	Vehicle control acceleration
a_{des}	Desired acceleration
a_{PI}	Correction acceleration from the PI controller
a_{ToA}	Time of arrival-based acceleration from the concept of “Time of Arrive”
B	Stiffness factor in Magic Formula
b	Coefficients of the clutch degradation model
C	Form factor in Magic Formula
$C1$	Instantaneous cost in the EMS control strategy
$C2$	Traction power error cost in the EMS control strategy
$C3$	Actuator constraint cost in the EMS control strategy
$C4$	Engine torque jerk cost in the EMS control strategy
C_{aero}	Aerodynamic drag coefficient
C_λ	Longitudinal slip stiffness
c	Coefficients of the clutch degradation model
c_{fric}	Heat capacity of the steel plates in the clutch
D	Peak factor in Magic Formula
D_{Cs}	Viscose damping coefficient of the ATF
$D_{Vis, Clu}$	Effective damping coefficient in the clutch

$D_{\text{Vis, Diff}}$	Effective damping coefficient in the differential
d_{vir}	Cumulative distance from the concept of “Time of Arrive”
E	Curvature factor in Magic Formula
E	Total dissipation energy
F	Actuator force acting on the clutch plates
F_{aero}	Aerodynamic resistance
F_{grade}	Road slope force
F_{inertia}	Inertial resistance of the vehicle
F_{roll}	Rolling resistance from all the wheels
F_{roll}	Rolling resistance
F_{trac}	Traction force
$F_{\text{Wh, f}}$	Vertical force on the front wheels
$F_{\text{Wh, r}}$	Vertical force on the rear wheels
$F_{\text{Wheel, z}}$	Vertical force on the wheel
G	Admissible operation states of the actuators
g	Gravitational acceleration
h_{CoG}	Height of the vehicle's CoG
h_{fuel}	Fuel lower heat value
I	Current for the charge or discharge of the battery
$i_{\text{Diff, x}}$	Gear ratios for the differential
$i_{\text{FD, x}}$	Final drive gear ratio
$i_{\text{Gear, x}}$	Gear ratios for the transmission
$J_{\text{Clu, in, x}}$	Inertia of the clutch input side
$J_{\text{Clu, out, x}}$	Inertia of the clutch output side
J_{Cs}	Inertia of the engine crankshaft
J_{Equ}	Equivalent inertia
J_{Wheel}	Wheel inertia
k_I	Integral coefficient of the PI controller
k_P	Proportional coefficient of the PI controller
L_{Tire}	Relaxation length of dynamic traction force
l_f	Distance from the front axle to CoG,
l_r	Distance from the rear axle to CoG
m_{fric}	Mass of the steel plates in the clutch

\dot{m}_{fuel}	Fuel mass flow
Nu	Nusselt number for forced heat convection
P	Probability for dependent variable
Pr	Prandtl number for calculation of the Nusselt number
p_i	Coefficients of the clutch degradation model
p	Penalty function of the control strategy
Q_{Batt}	Battery capacity of the battery
\dot{Q}_{In}	Incoming heat flow in the clutch
\dot{Q}_{Out}	Cooling heat flow in the clutch
R_{Batt}	Internal resistance of the battery
Re	Reynolds number for calculation of the Nusselt number
r_{dyn}	Dynamic radius of the wheel
r_{in}	Mean friction radius of the clutch friction plates
T_0	Initial temperature of the steel plates in the clutch
T_{Brake}	Brake torque on brake discs
$T_{\text{Cl, des}}$	Desired clutch torque
$T_{\text{Cl, fdbk}}$	Feedback torque from the clutch
$T_{\text{Clu, in, x}}$	Clutch input and output shaft torque
$T_{\text{Clu, out, x}}$	Clutch input and output shaft torque
$T_{\text{DCT, out}}$	DCT output torque
T_{EM}	Electric motor's output torque
$T_{\text{EM, Cand}}$	EM torque candidate in the control strategy
$T_{\text{Fric, x}}$	Friction torque in the odd or even clutch
$T_{\text{Gear, x}}$	Torque of the inter shaft
T_{ICE}	Engine output torque
$T_{\text{ICE, Cand}}$	ICE torque candidate in the control strategy
T_{L}	Load torque acting on the clutch secondary side
T_{Oil}	Temperature of the friction oil
T_{roll}	Rolling resistance torque
T_{Req}	Requested drive torque in the ICE
$T_{\text{Stat, max}}$	Maximum static torque in the clutch
$T_{\text{Stat, x}}$	Static torque in the odd or even clutch
T_{Surf}	Surface temperature of the steel plates in the clutch

$T_{Syn,x}$	Synchronizer torque
T_{Wheel}	Drive torque from differential
t	Time
t_n	Time point n
$t_{ToA}(t)$	Time to arrive from the concept of “Time of Arrive”
V_{Batt}	Battery voltage
V_{EM}	DC output voltage of the battery
v_{des}	Desired vehicle speed
v_{veh}	Vehicle velocity
\bar{v}_m	Minimum margin velocity
W_{chem}	Chemical energy consumed by ICE
W_{elec}	Electrical energy consumed by EM
W_{input}	Energy input in the propulsion unit
$W_{kinetic}$	Vehicle’s kinetic energy
W_{output}	Energy output of the powertrain
x	Operation states of the actuators
x_i	Independent variable
Y	Dependent variable
z	Systematic component of the regression model
z_x	Friction surfaces number


Greek Symbols

α_T	Heat transfer coefficient
λ	Equivalence factor in the control strategy
β_i	Coefficient of the
Δt	Simulation step size
δ	Road slope angle
$\Delta\mu^*$	Difference in the arithmetic mean value of the reinforced CoF
$\Delta\omega_{Clu, Threshold}$	Speed interval limit for detecting zero speed of the clutch
$\Delta\omega_{Clu,x}(t)$	Sliding speed between the clutch input and output plates
Δv_{ACA}	Average cumulative absolute velocity error
η_{Batt}	Battery efficiency
η_{DCT}	DCT efficiency

$\eta_{EM}(t)$	Combined efficiency of EM and inverter
η_m	Safety coefficient to prevent marginal instability in ASR calculation
$\eta_{overall}$	Overall energy efficiency
λ_0	Initial equivalence factor in the control strategy
λ_{ASR}	Advanced slip ratio
μ	Coefficient of friction
μ^*	Reinforced coefficient of friction
$\bar{\mu}_H^*$	Mean value of the reinforced CoFs at the high sliding speed ranges
$\bar{\mu}_L^*$	Mean value of the reinforced CoFs at the low sliding speed ranges
μ_{roll}	Rolling resistance coefficient
μ_s	Static friction coefficient
μ_{Tire}	Longitudinal friction coefficient
μ_{vis}	Viscous friction coefficient
μ_x	Dynamic friction coefficient for odd or even friction plates
ρ_{air}	Air density
τ_m	Marginal time constant of the explicit Euler method
τ_{Tire}	Variable time constant
$\overline{\omega}_{Clu,H}$	Mean value of the sliding speeds at high sliding speed ranges
$\omega_{Clu,in}(t)$	Clutch input plate speed
$\overline{\omega}_{Clu,L}$	Mean value of the sliding speeds at low sliding speed ranges
$\omega_{Cl,Odd/Even}(t)$	Speed of the odd or even clutch input shaft
$\omega_{Clu,out,x}(t)$	Clutch output plate speed
$\omega_{EM}(t)$	Electric motor speed
ω_{ICE}	Engine speed
$\omega_{Wheel}(t)$	Wheel speed

Subscripts

0	Initial value
ACA	Average cumulative absolute value
ASR	Advanced slip ratio
Batt	Battery
Clu	Clutch
DCT	Dual-clutch transmission



EM	Electric motor
H	High sliding speed ranges
ICE	Internal combustion engine
L	Low sliding speed ranges
m	Marginal
roll	Rolling resistance
s	Static
vis	Viscous
Wh	Wheel
x	Index for odd or even clutch

1 Introduction

The automotive industry stands at the threshold of a transformative era, driven by the urgent need to mitigate environmental impact and reduce fossil fuel dependency. Hybrid powertrains have become an essential solution with global interest and have gained an expanding market share since the early 2010s based on the studies [1] and [2]. Among these, mild hybrid powertrains have garnered significant attention due to their role in bridging the gap between traditional internal combustion engines and full-hybrid vehicles. Their cost-effectiveness and scalability make them attractive for manufacturers transitioning to electrification. This technology offers the groundwork for scaling up electrification efforts and guiding the development of more advanced hybrid systems. Additionally, their potential to optimize fuel efficiency, reduce emissions, and improve vehicle performance, according to [3], [4] and [5], has attracted substantial research interest.

Regarding energy efficiency and vehicle dynamics, the drive-off procedure is a critical phase characterized by the transition from standstill to motion. Traditional drive-off procedure relies mainly on the internal combustion engine and conventional clutch engagement, leading to suboptimal energy utilization, increased wear on mechanical components, and aging of the clutch system components [6], [7], [8], [9], [10], [11], [12], [13]. Integrating an electric motor into this phase presents a compelling avenue for enhancing energy efficiency, extending the lifetime of critical powertrain elements, and improving the driving experience [5]. Moreover, these aspects are closely linked to driving style, resulting in diverse loads on the powertrain, different fuel consumption, and distinct driving dynamics [14], [15], [16], [17]. Therefore, investigating the drive-off procedure in a mild hybrid powertrain, considering drive-off dynamics, becomes imperative. The current work focuses on this area and merges ecological evaluation aspects with varying drive-off dynamics assessed through subjective impressions.

1.1 Motivation

The drive-off procedure significantly impacts a vehicle's performance, fuel consumption, and user experience. Examining the benefits and limitations of the drive-off procedure can provide insights into the complex relationship between technology, engineering, and user experience. The outcomes can advance the theoretical understanding and practical implementation of the drive-off procedure, provide a holistic approach for evaluation of the drive-off procedure, and gain the functional knowledge for a unitive calibration of the powertrain.

In alignment with the technical development, contemporary powertrain designs are increasingly characterized by a spectrum of electrification levels. In this landscape, mild hybrids emerge as a practical transition to powertrain electrification. They also introduce some challenges. Mild

hybrids, characterized by a smaller electric motor (EM) that supports the internal combustion engine (ICE), demand calibrated precision to gain their benefits effectively. By concentrating on mild hybrids, it is possible to address the fundamentals for powertrain calibration to maximize efficiency gains within the constraints of limited electric power support and to research the benefits of the lifetime enhancement of the drive-off element during its operating cycle.


Furthermore, it is interesting to investigate the complicated interaction between the EM and the ICE during the drive-off procedure. By optimizing this synergy, it can achieve not only improved energy efficiency but also a satisfying driving experience. In pursuit of this purpose, the subjective evaluation of the drive-off procedure has to be involved. In this position, the definitions for the driving style and driving mode are first introduced. The study [18] clarified these definitions and investigated the methods to classify the subjective driving style with the help of machine learning methods.

Subjective driving style refers to the manner in which an individual driver operates a vehicle. It is characterized by personal preferences, habits, comfort levels, etc. It involves factors such as acceleration aggressiveness, braking behavior, steering inputs, and overall driving attitude. Subjective driving style is highly influenced by individual personality traits, mood, and driving experiences. It is difficult to objectively quantify since it involves personal interpretations and behaviors that are not directly measurable.

Objective driving style refers to quantifiable and measurable aspects of how a vehicle is operated. It includes parameters such as acceleration rate, braking force, steering angle, speed changes, and other driving dynamics that can be captured through sensors, data loggers, and vehicle instrumentation. Unlike subjective driving style, objective driving style focuses on tangible measurements that can be analyzed and compared across different drivers or driving scenarios. This information is crucial for understanding vehicle behavior, optimizing fuel efficiency, and enhancing safety.

Driving modes refer to predefined settings or configurations that modify a vehicle's performance characteristics based on specific conditions or desired outcomes. These modes can change aspects like throttle response, suspension stiffness, transmission shift points, and engine power output. For example, a vehicle might offer modes like "Eco," "Sport," or "Comfort," each suited to different driving preferences or conditions. Driving modes allow drivers to adapt their vehicles to suit their needs, whether it is maximizing fuel efficiency, enhancing performance, or optimizing comfort. Specific calibration settings are employed to differentiate between driving modes. These settings are established during the calibration process. The calibration engineer strives to determine the appropriate parameter configuration for each driving mode, aiming to achieve the optimal alignment with the intended objective driving style.

In the following, the motivation of this work is described with aspects of the role of the drive-off procedure, functional knowledge for the Calibration Process, the user experience, and the bridge



effect of the mild hybrid powertrain.

Role of the drive-off procedure

The drive-off procedure, often regarded as a transition from standstill to motion, carries profound implications for vehicle characteristics. This procedure also has a significant influence on the customer's evaluation of the vehicle. As the automotive landscape evolves, a comprehensive understanding of the drive-off procedure becomes essential. Exploring it allows to unlock hidden potential for energy optimization, emissions reduction, and enhanced customer evaluation regarding driving dynamics.

Functional knowledge for the calibration process

As modern powertrains become increasingly complex, traditional manual calibration methods demand significant time, expertise, and human resources [19]. The intricacies of optimizing the drive-off procedure and powertrain dynamics require numerous iterations and careful adjustments. However, the availability of skilled calibration engineers is limited, and the traditional manual calibration process can lead to inefficiencies and delays. In this context, automating the calibration process emerges as an imperative solution to address these challenges, enabling a more streamlined and efficient calibration process [19]. It needs functional knowledge about the subjective evaluation of the drive-off procedure.

By focusing on the subjective evaluation of the drive-off procedure, this work delves into the driver's perspective. It serves as a vital bridge between objective calibration parameters and the human-centric dimensions of vehicle dynamics and uncovers how the driver's impression connects with the vehicle's behavior during the transition from standstill to motion. Through the research of subjective evaluation, this work can illuminate the direction for an effective calibration process and guide the development of automated calibration algorithms that consider not only technical performance but also the emotional and cognitive dimensions of driving. By infusing automation with the essence of human judgment and preference, the calibration process becomes a uniform approach, ensuring that the drive-off procedure aligns with drivers' expectations.

User experience

At the intersection of engineering and human interaction lies the user experience – an intangible yet vital component of powertrain design. The drive-off procedure is an important assessment maneuver of this interaction due to its frequent occurrence, where a well-calibrated powertrain can elevate the driving experience from mundane to impressive and determine comfort and driving pleasure. Regarding the vehicle dynamics characteristics, the user experience encompasses subjective evaluation of diverse aspects such as comfort, sportiness, smoothness, and satisfaction. This work aims to investigate the subjective evaluation in the context of the drive-off dynamics and to objectivate the subjective evaluation of the drive-off procedure in order to quantify and measure

subjective perceptions. In this way, researchers and engineers can develop a more structured and data-driven approach to optimizing the drive-off procedure. It enables a quantitative understanding of how different calibration settings affect drivers' subjective impressions. The calibration engineer can transform subjective driver preferences into calibrated settings for various driving modes. Objectivating these preferences ensures that each driving mode's behavior is precisely tuned to match the driver's intended experience. It is important to enhance the vehicle's performance and user satisfaction by aligning the calibration process with the perceptions and preferences of drivers.

Bridge effect of the mild hybrid powertrain

Mild hybrid powertrains serve as a bridge between traditional powertrains with ICE and full-hybrid powertrains. It integrates a small electric motor and a relatively modest battery system into the vehicle, enabling functions such as regenerative braking, engine start-stop, and limited electric-only propulsion. This technology offers partial electrification of the powertrain, serving as a springboard for more comprehensive electrification strategies, such as plug-in hybrid electric vehicles. It is meaningful to recognize the bridge effect of mild hybrid powertrains, leveraging their unique characteristics to illuminate the potential benefits and challenges associated with the drive-off procedure. Through this, it is possible to gain deeper insights into the interaction between electric and conventional power sources.

1.2 Research objectives

According to the previous statements, this work introduces an overall evaluation of the drive-off procedure within the context of a mild hybrid powertrain.

The evaluative framework is visually depicted in Figure 1.1, including the subjective and ecological aspects related to the drive-off procedure. A vehicle model with a mild hybrid powertrain is built with the help of Matlab/Simulink® to simulate these procedures. By employing the accelerator pedal position (APP) as an input, the simulated vehicle can be driven off with diverse acceleration profiles, distinguishing from the maximum acceleration and the mean jerk, also called the acceleration build-up, which is expressed as the mean value of the first-time derivative of acceleration [20]. These Profiles can be evaluated according to the subjective evaluation criteria, such as comfort, sportiness, and jerkiness. The ratings of these criteria are estimated by using objectivation models. Furthermore, each drive-off profile presents a fuel consumption and a thermal load in the drive-off element, which are considered the ecological criteria.

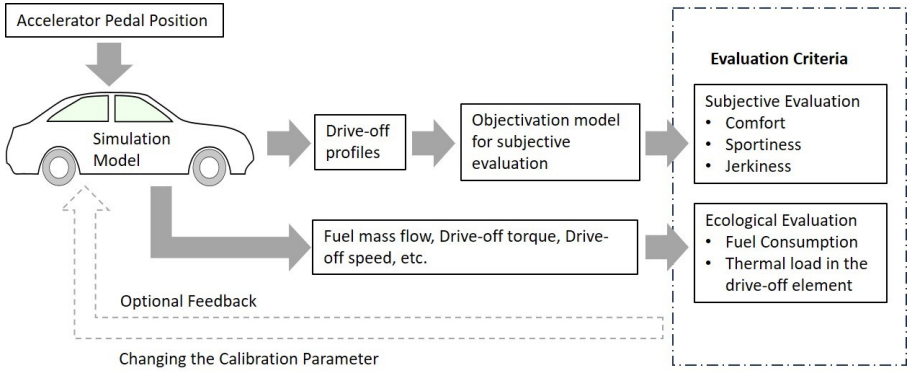



Figure 1.1: Illustration of the subjective and ecological evaluation of the drive-off procedures in a mild hybrid powertrain

This methodology starts with objectivating the subjective evaluation criteria. It enables the quantification of subjective perceptions regarding drive-off dynamics and the illustration of its distinctive attributes. Within the scope of this work, subjective evaluations are quantified within a controlled laboratory environment, whereby external factors such as weather conditions are disregarded. With the help of these objectivated subjective evaluation measures, the drive-off dynamics can be evaluated with mathematical methods without performing further test subject studies. Concurrently, an ecological investigation of the drive-off procedures is conducted by considering various APPs that objectively represent different driving styles. It focuses on the fuel consumption and thermal load reduction in the drive-off element. In the context of the mild-hybrid powertrain, special focus is given to exploring these advantages through the use of an EM. This work seeks to contribute to the overarching goals of evaluating the drive-off procedure within the context of a mild hybrid powertrain, considering a subjective aspect with the help of the objectivation model and an ecological aspect regarding fuel consumption and thermal load.

The outcome extends to calibration engineering. It facilitates the calibration process by considering the impact of alterations in drive-off dynamics on the aforementioned ecological facets. Furthermore, the potential for applying this approach to different driving modes with adjusted calibration parameters is illustrated through the optional feedback. Notably, this investigation maintains a specific focus on a powertrain calibrated to prioritize a comfortable driving experience. Subsequently, the following section outlines the summarized research objectives and constraints.

Research objectives:

Investigation of the subjective evaluation: The subjective evaluation represents in this work the evaluation of subjective driving style. Objectivating the subjective evaluation in this context



involves translating these perceptions and preferences into quantifiable measurements. For instance, a driver might subjectively prefer a smooth and gradual acceleration. By objectivating this preference, it becomes quantified as a specific acceleration rate or an acceleration value. In this context, the following two objectives are formulated:

- **Finding the evaluation difference threshold (EDT):** The EDT describes how much the stimulus intensity must be changed in order to generate a variation of an evaluation [21]. The EDT is generally larger than the Just Noticeable Difference (JND) from general psychophysics since a small change in vestibular perception does not necessarily cause a different evaluation of a drive-off behavior. Based on the literature research, there are hardly any studies that examine the EDT for the drive-off procedure to determine the variation of an evaluation according to subjective evaluation criteria. This research, however, places primary emphasis on the exploration of EDTs of influence factors for drive-off procedures.
- **Objectivation of the subjective evaluation:** This facet of the study aims to translate qualitative-subjective evaluations into quantifiable parameters, thereby facilitating a systematic and objective assessment of perceptual changes through the drive-off procedure.

Investigation of the ecological evaluation: By examining drive-off dynamics and utilizing ecological evaluation criteria such as fuel consumption and thermal load in the drive-off element, researchers and engineers can gain insights into the efficiency, durability, and overall performance of the vehicle during this critical phase of operation. This information is vital for optimizing powertrain calibration, improving fuel efficiency, and ensuring the lifetime of the drive-off element in the drivetrain. The following two objectives regarding the ecological evaluation criteria are investigated in this work:

- **Fuel consumption:** The investigation deals with the quantification of fuel consumption, particularly focusing on the influence of the electric motor's support during the drive-off procedure, shedding light on the interplay between electrification and energy efficiency according to different driving-off dynamics.
- **Thermal load in the drive-off element:** This work performs an investigation into the changing of the drive-off element's thermal load, strategically employed as a pivotal ecological evaluation criterion. This choice is motivated by the significant reduction in thermal load caused by using EM during the drive-off procedure. The aim of the work is to investigate the effects of the different drive-off dynamics on the thermal load in the drive-off element and the influence of the EM support on the development of the thermal load change.

Constraints:

In the realm of laboratory measurements for subjective evaluations, the process is involved in complex psychophysical aspects. This work conducts measurements while adhering to specific constraints, ensuring consistent conditions and excluding external influences, such as weather conditions. However, it's important to acknowledge that the awareness of the environment might influence participant behavior. Moreover, several variables can also impact the results, including equipment accuracy, psychological factors, and ethical considerations. While laboratory settings provide control and test replicability, they may not fully replicate the complexities of real-world driving scenarios. For this topic, the study [22] offers well-founded research results. Therefore, the findings of this work should be interpreted with the awareness of these limitations, recognizing that laboratory conditions may not include the full spectrum of multifaceted driving conditions.


Another constraint in this work is related to the drive-off component and the powertrain configuration. It refers to the dedicated examination of a specific type of drive-off element, the wet friction dual-clutch system. This component is integrated into a test vehicle propelled by an ICE and has a maximum torque transfer capacity of 400 Nm. The research concentrates exclusively on a mild hybrid configuration, which uses a compact EM with a maximum power of 15 kW and a maximum torque of 25.3 Nm. This focus allows for a detailed examination of a specific level of electrification magnitude within the powertrain configuration.

Furthermore, the simulation model used in the work represents a comfort-oriented powertrain calibration. The simulation model is designed to reflect this calibration with a focus on parameters and configurations that prioritize smooth and pleasant driving dynamics. By concentrating on this specific calibration, the study delves into the powertrain behavior in the context of comfortable drive-offs, offering insights into the interaction between the driving behavior and the vehicle's propulsion system.

Lastly, the research adopts a specific control strategy based on the Adaptive Equivalent Consumption Minimization Strategy (A-ECMS) to manage the interplay between the ICE and EM. This strategy governs load point upshifting or downshifting for the ICE, enabling processes such as battery charging and collaborative driving with the EM. Although various alternative control strategies are available, this work employs the A-ECMS without conducting a comparative analysis with other control methods because it is out of the research scope.

1.3 Structure of the content

In this work, the content is organized to guide readers through the exploration of drive-off procedures in a mild hybrid powertrain regarding the subjective and ecological evaluations. The work begins with an introduction in Chapter 1, where the motivation behind the research is described,



followed by an introduction of the research objectives. Chapter 2, Fundamentals and State of the Art, forms the cornerstone of this work. It delves into the fundamentals and current research state for each topic related to this work.

Chapter 3 introduces the investigation of the subjective evaluation through test subject studies. Various factors are explored in the studies according to different evaluation criteria for the drive-off behavior.

In Chapter 4, vehicle modeling is detailed with insight into powertrain component modeling, covering propulsion units, DCT modeling, wheel dynamics, and vehicle dynamics modeling. The control module subsection defines the algorithms and strategies for managing the simulation.

Chapter 5 presents the results of the research in the scope of subjective and ecological evaluations of the drive-off procedure.

The work provides a conclusion and perspectives in Chapter 6. The conclusion section introduces the essence of the research and summarizes key takeaways, while perspectives offer an outlook into the future, providing considerations for future research.

2 Fundamentals and state of the art

Within the domain of automotive engineering, the evaluation of driving dynamics often involves subjective and ecological dimensions. These facets collectively illuminate the multifaceted characteristics of a vehicle and the implications of the driver's behavior. This chapter serves as an introduction to key topics relevant to this work. Section 2.1 defines the drive-off procedure, outlines its scope, and presents relevant definitions related to drive-off behavior. Sections 2.2 and 2.3 introduce the mild hybrid powertrain and the drive-off element being studied, respectively. Section 2.4 begins by introducing the perception of motion and discussing subjective evaluation and objectivation methods, concluding with an introduction to the driving simulator utilized. Section 2.5 delves into ecological evaluation within the realm of driving dynamics research and provides a general overview of this area. The concluding section of this chapter highlights the research gap and underscores the practical applicability of the work.

2.1 Definition and evaluation of the drive-off procedure

Definition of the drive-off procedure

A drive-off procedure, also named as vehicle start-up or vehicle launch [23], in the context of a vehicle typically refers to the initial phase of vehicle movement when it transitions from a stationary position, such as when starting from a complete stop or standstill, and beginning to move forward [24]. This phase involves accelerating the vehicle and is usually characterized by the engine or motor providing the necessary power to overcome inertia and resistance. Drive-off procedures are critical in understanding the performance, energy consumption, and driving experience of a vehicle, especially in the context of HEVs, where the coordination between the ICE and EM plays a significant role.

The definition of the end of a drive-off procedure is hardly found in the literature. The studies [20] and [23] focused on the research of the drive-off procedure. However, there is no clear definition of the end of this procedure. The time period under consideration always begins at the time point when the driver starts the operation of the vehicle and ends shortly after the synchronization of the clutch. This work is oriented to the following definition of the drive-off procedure: "In a drive-off procedure of the vehicle with a DCT, a predefined speed curve between engine and transmission speed is usually set until the clutch has reached speed equality based on the maximal speed difference [25]". It indicates that the drive-off procedure ends at the time point when the clutch output plate speed is synchronized with the engine speed. Namely, the clutch is locked up.

Evaluation of the drive-off procedure

The evaluation of the drive-off dynamics is often investigated within the context of the calibration process. In a drive-off calibration, the fundamental principle driving this calibration is to strike a delicate balance between ensuring both driving comfort and dynamic performance under the consideration of an appropriate reaction of the vehicle without acceleration inconsistencies during clutch engagement throughout the entire lifetime of the clutch and under all driving conditions [26]. While striving for this optimal balance, certain constraints may arise in the context of transmission calibration. However, these constraints are permissible to be executed without compromising the overall drive-off experience and damage to the components. To achieve this, the embedded software solution is widely used, which includes control parameters to influence driving behavior [19]. The calibration engineer typically needs to optimize these parameters through an iterative process [27].

In the drive-off procedure, one phase significantly influences the above-mentioned aspects: the vehicle's performance, energy consumption, and driving experience. It is the synchronization phase of the clutch. The drive-off control strategy is essential to achieve a desired drive-off behavior, in which the engine and clutch output plate speeds interaction must be considered. The behavior of engine speed significantly impacts the driver's perception during the drive-off, primarily by influencing the vehicle's acoustics with a speed flare [28]. Speed flare can directly impact driving comfort and is generally not desirable in drive-off control. Consequently, enhancing the comfort aspect of drive-off behavior involves ensuring that the engine speed consistently increases [27] und [28].

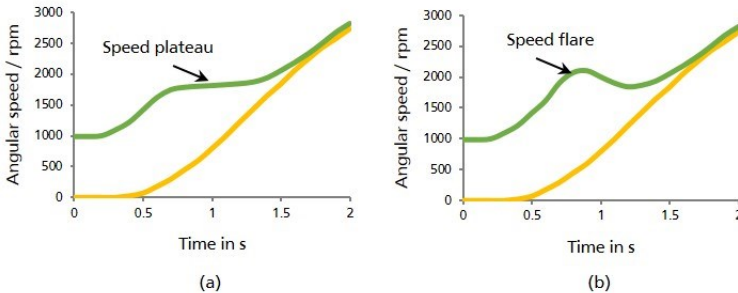



Figure 2.1: Engine speed (green) and clutch output plate speed (orange) during a drive-off procedure, (a): Drive-off with a consistently increasing engine speed, (b): Drive-off with a flare in engine speed

Figure 2.1 illustrates the interaction between engine and clutch output plate speed during a drive-off, depicting one scenario with a consistently increasing engine speed and another with a flare in engine speed. A speed plateau refers to a phase where the engine speed stabilizes temporarily



before continuing to increase. This behavior is typically seen when the engine speed is briefly maintained at a constant level to achieve smoother drive-off behavior. A speed flare occurs when the engine speed overshoots the predefined constant plateau level during speed synchronization.

The study [23] proposed an algorithm to control the drive-off procedure with a focus on the engine and clutch output plate speed interaction. The rate of clutch synchronization is controlled by feeding back the clutch torque to control the engine speed. In this work, a similar strategy, provided by an industrial research partner, is utilized to control the drive-off procedure. Further introduction is placed in Section 4.4. For fine-tuning the clutch torque transmission and engine speed behavior, the calibration process plays an essential role, either for comfort or sporty drive-off.

Additionally, for the purpose of achieving a comfortable impression regarding driving dynamics, the emphasis is placed on crafting a drive-off that offers a solely increasing longitudinal acceleration profile. It ensures a harmonious and gradual build-up of acceleration, thereby contributing to an overall sense of comfort during drive-off. The calibration also takes into account the dynamic aspects of the drive-off procedure. It recognizes the significance of quick response times and the achievement of high longitudinal acceleration values, which contribute to a sense of sporty driving [29]. For having a dynamic driving experience, a rapid torque build-up from the ICE is desired, which also results in a high build-up of acceleration. According to the studies [30], [31], [32], the range of acceleration for slow driving in city traffic typically falls between 0.8 m/s^2 and 2 m/s^2 , for normal driving between 1.5 m/s^2 and 3 m/s^2 , and for sporty driving between 2.5 m/s^2 and 4.5 m/s^2 . Another study [33] defined driving styles as safe, normal, aggressive, and dangerous, with corresponding acceleration ranges of 0 m/s^2 to 1.5 m/s^2 , 1.5 m/s^2 to 3.5 m/s^2 , 3.5 m/s^2 to 7 m/s^2 , and 7 m/s^2 to 12 m/s^2 . However, there is limited documentation in the literature regarding the ranges for different driving styles based on mean jerks.

Study [20] evaluates drive-off behavior with various factors according to agility, comfort, and dosing capability. Based on this study, the following definitions are introduced to evaluate or describe a drive-off procedure.

Drive-off comfort includes all aspects related to the comfort and amenities of the driving experience. In the context of this work, it primarily focuses on the driving dynamics related to the drive-off behavior, such as jerkiness and acoustic impression caused by engine speed variation.

Drive-off dynamics is often related to the sportiness of the vehicle and refers to how quickly a vehicle responds to driver input and its ability to achieve high longitudinal acceleration values. In essence, drive-off dynamics represents the vehicle's ability to swiftly accelerate in response to APP, with a focus on response time and achieving high acceleration. For describing this performance, the acceleration build-up is an important factor, which is introduced below.

Drive-off agility is used to describe the vehicle's driving performance impression. Specifically, it

aims to classify the subjective initial acceleration behavior in terms of a "sluggish," "neutral," or "sporty" vehicle impression. In this context, the response time plays an important role.

Drive-off dosing capability describes the controllability of the vehicle with respect to driver-executable control options during an acceleration process. Since there is no controllability evaluation for vehicle reactions in this work, it will not be involved further.

Maximum acceleration represents the first local maximum of the acceleration during a drive-off procedure.

Mean jerk serves as a descriptor for the acceleration profile and characterizes the range between the beginning of acceleration and reaching the maximum value. To calculate this, a regression line is calculated in a range between 15% and 85% of maximum acceleration. The slope of the linear regression function corresponds to the value of the mean jerk.

Acceleration build-up is used synonymously with the mean jerk in this work.

Response Time refers to the duration between a sudden input on the accelerator pedal and the initial response, which describes the first noticeable acceleration response from the vehicle. It is defined as reaching an acceleration of 15% of the maximum value in this work.

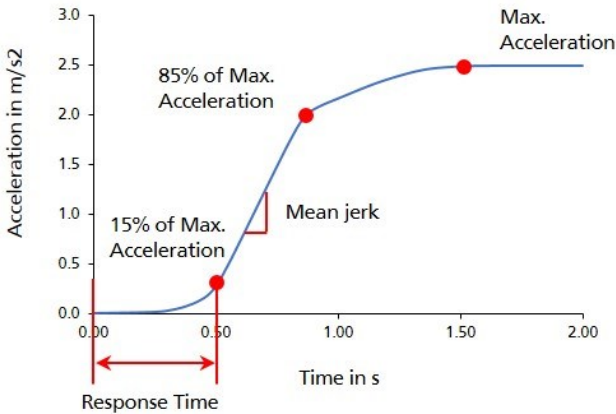


Figure 2.2: Exemplary illustration of an acceleration profile of a drive-off




Figure 2.2 shows an exemplary drive-off acceleration profile with the labeling of the main characteristics. To evaluate a drive-off behavior simulated later with the vehicle model, it is necessary to transfer subjective impressions into objective measurements. For this purpose, the test subject studies are conducted with the help of the driving simulator. The investigation of subjective evaluation of the drive-off behavior is introduced in Chapter 3.

2.2 The mild hybrid powertrain

This section provides an introduction to the hybrid powertrain regarding the classification and the control strategy that regulates the operation. The configuration of the mild hybrid powertrain being studied is illustrated, including the key components that constitute the core of the powertrain.

Classification

The hybrid powertrain can be categorized according to the degree of hybridization. The degree of hybridization depends upon the power supplied by EM. For this reason, hybrid powertrains can be divided into micro, mild, and full hybrid, which generally provide 3 to 5 kW, 7 to 25 kW, and 30 to 50 kW, according to [34] and [35]. The power range for these categories differs slightly in the literature. Moreover, plug-in hybrids combine an engine with a high-power electric motor and a large rechargeable battery.

Based on energy flow from the propulsion units to the wheels, the hybrid powertrain can be divided into series configuration, parallel configuration, and series-parallel configuration [34], [36], [37]. In a series configuration, the mechanical energy produced by the ICE undergoes a transformation process within a generator. This transformation results in the conversion of mechanical energy into electrical energy, which is then used to power another EM for propelling the vehicle. Notably, the electrical energy generated by the generator can also be stored within an electrochemical energy storage system, such as a battery. In a parallel hybrid configuration, the ICE and the EM are connected in parallel along the drivetrain and mechanically coupled to the drive wheels. Such concepts involve not only the two propulsion motors and energy storage but also one or more transmissions or clutches. Both propulsion systems can be used individually or simultaneously to drive the vehicle. Due to power addition, both motors can be designed with relatively low power without compromising performance during acceleration or on gradients. Another but highly complicated concept is the series-parallel configuration. In this configuration, a portion of the internal combustion engine's power is mechanically transmitted to the drive wheels through a gearbox. The remaining power is converted into electrical energy, which is then reconverted into mechanical power and delivered to the wheels. The advantage of this system lies in the decoupling of the engine's operating point from the vehicle's state. Consequently, it becomes possible to operate the ICE with better efficiency. This configuration allows the operating point to shift both on the hyperbola of constant power and in the load direction within the engine's characteristic map.

Parallel configurations, due to their reduced weight, size, and cost, are widely spread. This configuration presents a better perspective of development and is becoming mainstream [38], [39], [40]. In a parallel hybrid (P-hybrid), only one EM is required in a parallel hybrid setup, and it can be integrated at various positions within the conventional drivetrain. The characterization of a parallel hybrid is determined by the installation position of EM with the nomenclature Px. These are briefly described as below according to [5] and [41]:

1. P0: The EM is normally connected to the crankshaft at the front of the engine via a belt or chain.
2. P1: The EM is connected to the crankshaft at the rear of the engine.
3. P2: The EM is connected to the transmission input between the engine and transmission by a clutch to disconnect the engine.
4. P2.5: The EM is integrated into the input shaft of the transmission, typically via an intermediate gear.
5. P3: The EM is mounted between the transmission and the axle.
6. P4: The EM is a separately driven axle.

In addition to the primary parallel hybrid configurations (P0, P1, P2, P2.5, P3, and P4), various hybrid combinations can be created by integrating two EMs into the vehicle. For example, the P12 hybrid configuration is a combination of the P1 and P2 hybrid configurations, while the P14 hybrid configuration blends elements of the P1 and P4 hybrids. This approach allows for the incorporation of the advantages offered by each configuration but at a higher cost.

The P2.5 hybrid concept being investigated integrates a dual-clutch transmission (DCT) as its fundamental framework. Behind the dual-clutch is an EM, which is mechanically linked to the transmission's second input shaft through an intermediate gear. Figure 2.3 illustrates its schematic configuration, including the ICE, EM, power electronics, battery, clutch, transmission, and the output shaft to the drive wheels. The EM is connected to the battery through power electronics. This configuration is utilized as a study case in this work.

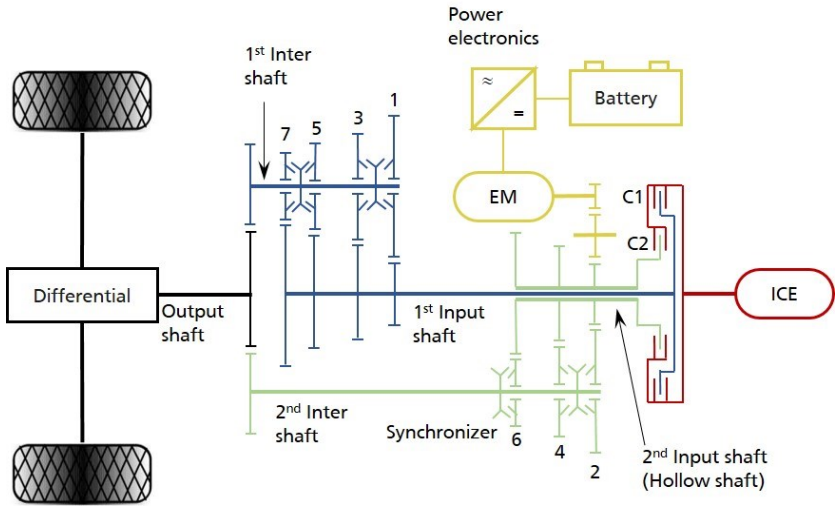



Figure 2.3: P2.5 hybrid configuration with an integrated EM connected mechanically to the second input shaft of the transmission via an intermediate gear, C1 and C2 represent the Clutches 1 and 2

Control strategy

In a 48 V-hybrid powertrain, the control strategy is important in managing energy consumption and coordinating torque distribution between the EM and the ICE. This is often referred to as the Energy Management System (EMS), which aims to minimize fuel consumption by optimizing torque distribution while considering various constraints. These constraints may arise from component limitations, such as maximum voltage or torque capacity, as well as system-level requirements.

Existing approaches for implementing an EMS can be categorized as offline or online methods. Offline approaches often involve global optimization-based EMS, typically relying on techniques like Dynamic Programming (DP) or the Pontryagin Minimum Principle (PMP) to find the global optimum for power distribution. However, they demand significant computational resources and prior knowledge of specific driving cycles [42], [43]. To reduce computational demands, global optimization-based EMS is usually used in backward modeling approaches for dynamic systems. Nevertheless, these backward simulation models tend to oversimplify the transient and dynamic properties of the system. It potentially results in doubt on the declared global optimum [44], [45].

Some methods focus on instantaneous optimization, aiming to minimize a local cost function like Equivalent Consumption Minimization Strategies (ECMS). It is widely employed in forward-facing models to reduce instantaneous fuel consumption and optimize power distribution between the



ICE and EM while managing the state of charge (SOC) of the battery [46], [47]. The literature [47] has demonstrated ECMS as an effective solution for HEV energy management problems. ECMS revolves around the concept of converting electricity consumption into equivalent fuel consumption, enabling the calculation of minimum total consumption. The control variable, known as the equivalence factor or co-state, plays a crucial role in ECMS. The references [48] and [49] propose several methods to determine an optimal value. Once the equivalence factor is determined, ECMS can lead to a local optimum due to the lack of knowledge about future driving behavior [50]. Thus, this method cannot be used for an online control strategy.

The literature [47] proposed an Adaptive Equivalent Consumption Minimization Strategy (A-ECMS), which regulates the equivalence factor using a PI controller based on the deviation between the actual SOC and the desired SOC. This deviation is continuously considered and minimized throughout the driving cycle, making A-ECMS suitable for online control without prior knowledge of the driving cycle. The literature investigated the online adaptability of this method with two case studies.

2.3 The wet friction dual-clutches

In this work, the drive-off element refers to a wet friction dual-clutch, which has gained remarkable attention in recent automotive technology. It is known for its low cost, precision, and durability. It has become an important factor in improving performance and driving comfort. This section delves into the introduction of this clutch system, explaining its mechanics, operation, degradation mechanisms, and lifetime prediction methods.

2.3.1 Understanding wet friction dual-clutches

A wet friction dual-clutch, often referred to as a wet-running dual-clutch, represents a specialized type of clutch mechanism used predominantly in dual-clutch transmissions (DCTs). The term "wet" comes from the fact that this clutch operates within an environment immersed in transmission fluid or oil, distinguishing it from dry clutches that function in a dry environment. The following introduction is based on [25], [51] and [52]. Further information on the design and construction of the various types of clutch systems and their differences can be found in [25].

Fundamental mechanics and operation

Understanding these fundamental mechanics and operation phases is crucial to understanding the behavior and performance of wet friction clutches in various automotive applications. Wet friction clutches operate on the principle of friction generated within lubricated contact surfaces. These clutches are lubricated by an automatic transmission fluid (ATF), serving dual purposes as a cooling agent and lubricant. This ATF, while ensuring smoother operation and extended clutch life,

leads to adaptation of the friction characteristics of the wet clutch and the slope of the coefficient of friction (CoF) versus sliding speed, which is often referred to as the μ - v curve. A positive slope is beneficial in terms of avoiding shudder, a self-induced vibration due to the negative slope of the μ - v curve [51].

The wet friction dual clutch being investigated includes multiple plates, including steel plates and friction plates. The steel plates, also called separator plates, are rigid and flat steel components, typically made from high-strength steel. Their primary function is to transfer torque and power between the engine and the transmission. They are highly regarded for their durability and ability to endure the high levels of heat generated during clutch engagement. The friction plates are also known as clutch plates. They consist of steel-core plates with friction material on both sides with specially designed grooves. The friction materials are responsible for generating the necessary friction for realizing clutch engagement. The grooves on these plates contribute to improving heat dissipation. Figure 2.4 illustrates a wet friction dual-clutch as an example cited from [25], which has a comparable mechanical structure to the clutch under investigated in this work.

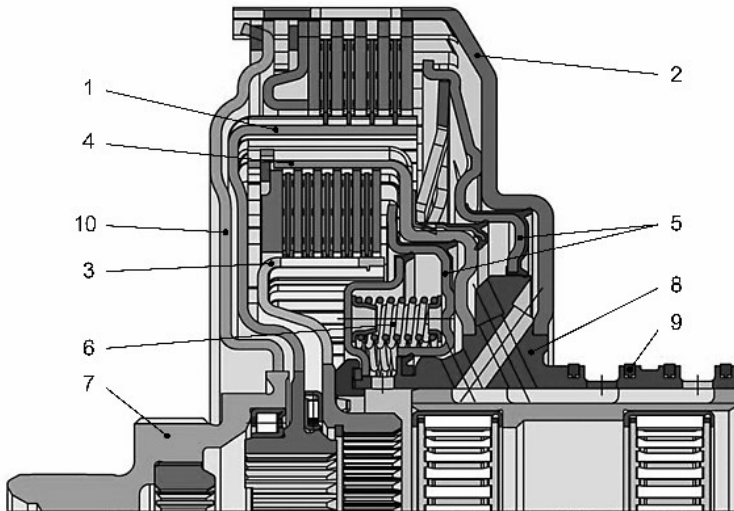


Figure 2.4: Wet friction dual-clutch of VW (BorgWarner) [25]. 1 Inner plate carrier of the outer clutch; 2 Outer plate carrier of the outer clutch; 3 Inner plate carrier of the inner clutch; 4 Outer plate carrier of inner clutch; 5 Piston; 6 Compression spring; 7 Input hub; 8 Drum; 9 Sealing ring; 10 Driving plate

In applications demanding high-power transmission, wet friction clutches are designed with multiple friction and separator plates. This configuration, termed a multidisc wet friction clutch, comprises friction plates attached to the input hub via inner plate carriers and separator plates secured to the outer plate carriers connected to the drum using lugs.

Wet friction clutches function as mechatronic systems, often integrated with electro-mechanical-hydraulic actuators for engagement and disengagement. These actuators consist of essential components, including a piston, a return spring constantly under compression, and a hydraulic group featuring a control valve and oil pump. The piston and return spring are located within the clutch assembly. The pressurized ATF, regulated by the valve, exerts force on the piston to engage the clutch. Once this pressure exceeds a certain threshold value, overcoming resistance from the spring and friction within the drum, the piston initiates movement and pushes the friction and separator plates together. Disengaging the clutch involves releasing pressurized ATF, enabling the return spring to restore the piston to its initial position.

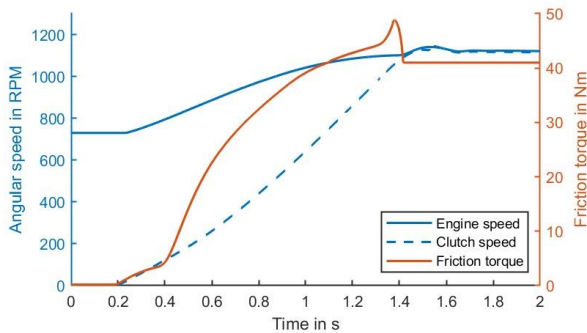


Figure 2.5: An exemplary illustration of a complete duty cycle of a wet friction clutch

The duty cycle of wet friction clutches can be categorized into three phases, an illustration of a complete duty cycle is shown in Figure 2.5:

Filling phase ($0 \text{ s} < t < 0.2 \text{ s}$): The actuator comes into play, swiftly pushing the piston until it makes contact with the neighboring plate.

Engagement phase ($0.2 \text{ s} < t < 1.4 \text{ s}$): A gradual increase in ATF pressure initiates gentle contact between the friction and separator plates. This gradual contact results in a slow rise in the transmitted friction torque M_{fric} . Simultaneously, the speed difference between the engine crankshaft speed and the clutch output plate speed decreases until it reaches zero. This phase generates heat due to friction, leading to an increase in ATF temperature.

Fully engaged phase ($t > 1.4 \text{ s}$): Also known as the post-lockup phase, the clutch is fully engaged,

there is no speed difference in the clutch system, the actuator is operated with a high ATF pressure to maintain the lockup state of the clutch.

2.3.2 Degradation mechanisms

The investigation of influence factors on wet friction clutch performance has been the subject of extensive research over the years. Most studies have primarily focused on three aspects: the degradation of friction materials, the condition of the automotive transmission fluid (ATF), and the operating conditions. The interaction between the friction material and ATF degradation shows a complex process, according to [52], which introduces this effect for the degradation mechanisms of wet friction clutches in Figure 2.6. It shows that the operation conditions have influence on the system temperature, which plays an important role in different degradation processes. High temperatures, for instance, accelerate mechanical wear and can lead to the carbonization of the friction materials. This generates more debris particles in the ATF. These particles, in turn, affect the ATF's characteristics. Additionally, external environmental factors such as water also play a role in the degradation process [10].

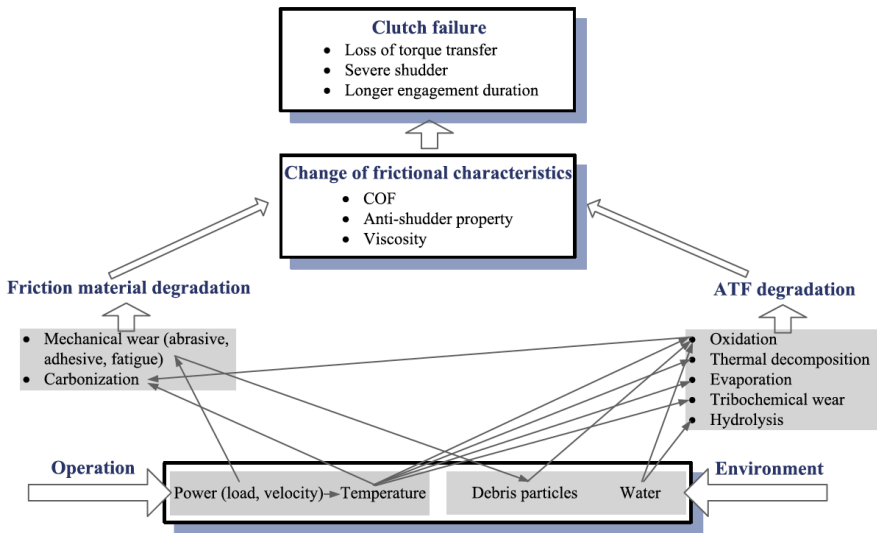



Figure 2.6: interaction among the clutch degradation mechanisms [52]



In essence, the interplay of temperature, environmental elements, and operational factors results in a parallel degradation of both the friction material and the ATF degradation. This intricate relationship underscores the importance of considering multiple factors when studying the degradation mechanisms of wet clutch systems. In the following, the friction material degradation, the ATF degradation, and the influence of operating conditions are introduced.

Friction material degradation

Mechanical wear and thermal degradation stand out as central degradation mechanisms affecting friction materials. The thermal degradation is closely related to the carbonization of the friction materials. The studies [6], [7], [8], [9] have concentrated their efforts in this domain, providing valuable insights into these processes. This particular aspect falls outside the scope of the present work. Therefore, no further details on this topic are provided within this work.


ATF degradation

The degradation of ATF can be attributed to various influence factors, including the oxidation of additives, tribochemical wear, thermal decomposition, and alterations in viscosity. These factors collectively contribute to ATF aging. The oxidation of lubricants is influenced by two key factors: the temperature of the lubricant and the presence of catalysts. Thermal degradation of the lubricant can take place at elevated temperatures, even in the absence of oxygen. It's worth noting that temperature plays a role in various chemical reactions, such as tribochemical reactions that occur at the friction interface [51]. The thermal degradation resulting from the dissipation energy during shifting affects cumulatively the ATF aging. It's essential to note that oil aging exerts a multifaceted impact on friction behavior, as documented in [10], [11], [12], [13].

Operating conditions

Operating temperature plays a prominent role in influencing clutch performance. The study [53] explored the relationship between oil temperature and the CoF. Using a wet clutch test rig that is capable of operating under varied conditions, including drive torque and inertia, the study examined the effects of oil temperature and energy levels during sliding, controlled by start sliding speed. Notably, oil temperature significantly influences changes in CoF, affecting both dynamic and static friction coefficients. Experimental tests conducted in another study [54], using a clutch test rig at different oil temperatures, yielded similar findings. Both investigations [11, 12] concluded that as oil temperature increases, there is a slight decrease in both dynamic and static friction coefficients.

Furthermore, it's crucial to acknowledge that CoF variations are not only time-dependent but also contingent on operational conditions such as sliding speed, drive torque, inertia, force rate, temperature, and lubricant flow [55], [56]. The well-established Stribeck curve illustrates CoF fluctuations concerning sliding speed. This dependency is further explored with experimental



verification in the study [9].

2.3.3 Lifetime prediction

The state of the art underscores the friction characteristics of wet clutch systems, which are influenced by a multitude of factors. Due to the complex interaction of these factors, providing a quantitative description of how the CoF changes over time in conjunction with all these influencing factors is a major challenge.

Typically, investigations in this domain involve simplified test environments. For example, in the study [9], a test rig known as "SAE#II" was employed. This test utilized only a single pair of friction plates and subjected them to a simplified test cycle comprising a certain rotation speed of an electric motor and an actuation force applied as a jump function. The results revealed a gradual increase in vibration amplitudes with the number of test cycles.


The study [57] identified torsional vibrations attributed to a negative CoF-slope versus sliding speed. This observation was made possible by using a scanning force microscope, which precisely measures the CoF-slope.

Additionally, a novel aspect is introduced, the lifetime of the drive-off element, which has a strong correlation with the thermal load according to [58] and [59]. The rate of degradation in the friction materials is influenced by the dissipation energy during shifting. This influence has been established through measurements of samples obtained from the continuous slip test conducted on the full-pack machine [58]. Furthermore, the study [59] has confirmed a reduction in the CoF in relation to the dissipation energy during shifting, which is observed during experiments conducted on the test bench.

The current work presents the findings of a study conducted through experimental analyses in Section 4.3.2, incorporating endurance experiments conducted on a powertrain test bench. The testing environment closely replicates actual driving conditions. The test bench offers a platform to test the entire transmission system, accounting for the intricate interplay between hardware and software, as well as the interactions among individual components, all over a representative runtime. Importantly, the sensors employed for signal measurements are identical to those used in the series products.

The endurance measurements have revealed changes in the CoF-slope that correlate with variations in vibration amplitudes. Furthermore, these CoF-slope changes, which are linked to dissipation energy changes, have been confirmed. These findings align with the statement made in the existing literature with more realistic experimental data.

Based on these results, a regression model is introduced to simulate the degradation process of the clutch. This model offers the capability to estimate clutch degradation during operation and utilize



this information in vehicle operation or incorporate clutch degradation into vehicle simulation models. With the current CoF-slope state and energy dissipation as a foundation, this model also enables the prediction of the remaining useful life of the clutch through extrapolation. The analysis and development of this model are introduced in Section 4.3.2 and published in [60].

2.4 Subjective evaluation of the driving dynamics

This section provides the basic knowledge for understanding the subjective evaluation regarding driving dynamics and describes firstly the definition of the subjective and objective evaluation approaches and the meaning of the objectivation approach. Section 2.4.1 starts with the human perception of motion. After this, the current research about the subjective evaluation of the driving dynamics and the perception threshold for linear motion and acceleration is introduced. Section 2.4.3 provides information about the state of the art and the methods used for objectivation of the subjective evaluation. Following this, the driving simulator used in this work is described. These subsections offer the fundamental knowledge for understanding the subsequent investigation in Chapter 3.


The subjective evaluation of the driving dynamics describes the qualitative assessment of a driver's experiential engagement with a vehicle's dynamic attributes. It refers to the assessment and judgment of a vehicle's performance and handling characteristics by individuals, typically drivers or test participants, based on their personal experiences, perceptions, and feelings. This evaluation is rooted in the realm of human perception and emotional response and delves into the interplay between vehicle behavior and human senses, which also provides insights into the psychological and sensory dimensions of interaction with vehicles.

The objective evaluation of driving dynamics focuses on the quantitative analysis of a vehicle's dynamic performance within the realm governed by empirical data and quantifiable metrics. This involves measurements of parameters such as acceleration, braking, cornering, and stability. Objectivity is maintained by the elimination of personal interpretations, resulting in a comprehensive and repeatable framework for analyzing the behavior and performance of vehicles.

The objectivation approach serves as a strategic bridge that unifies the subjective and objective evaluation. Objectivation involves the translation of subjective driver perceptions into quantifiable data points through instrumentation, data acquisition methodologies, and analytical tools. This approach aims to make the ethereal realm of human perception tangible and measurable and to enable an empirical correlation with objectively measurable vehicle characteristics.

2.4.1 Perception of motion

Motion refers to the change in an object's position concerning a reference point or another object.



It is characterized by the temporal displacement of an object. Motion can be described in terms of speed (how fast an object moves) and direction (the path it follows). There are various types of motion, including linear motion, circular motion, oscillatory motion, and rotational motion.

Perception of motion refers to how humans and animals perceive and interpret the movement of objects or their surroundings. It encompasses the visual, auditory, vestibular, and tactile signals that our senses receive and process to understand movement. Motion perception is essential for various aspects of daily life, such as navigation, object tracking, and spatial awareness.

In the context of this work, the emphasis is placed on researching the sensory modality responsible for perceiving acceleration and velocity during the drive-off procedure utilizing a driving simulator. Within the framework of the driving dynamics research, In the context of vehicle dynamics research, the vestibular system as the primary sensory system is at the center of the investigation. The following information on the functioning of this system is based on sources in the literature on perceptual psychology [61], [62], [63].

Vestibular perception, also known as the sense of balance, is a sensory perception used to obtain information about motion and orientation. It provides spatial orientation and balance during movement. The perception of motion and acceleration is primarily generated by the vestibular organs (balance organs). The vestibular organ is located in the petrous part of the temporal bone and is part of the inner ear, which combines two functions: hearing and the sense of balance. The vestibular organ serves a pivotal role in influencing reflex responses. Additionally, it plays a crucial part in computational processes required for higher-order vestibular functions. These functions encompass self-motion perception and spatial orientation. It transmits information about the force of gravity to the brain, providing information about changes in body posture or position, as well as rotational and linear accelerations.

The perception of motion is related to the object recognition process, which is a multimodal perception. It refers to the interaction and integration of various sensory systems, including the vestibular, auditory, visual, and haptic senses. The integration of multimodal sensory stimuli provides humans with the ability to achieve an enhanced understanding of acceleration during a driving maneuver, as one can simultaneously perceive the movement of objects on the road, engine sounds, and the driving force at the back. In multimodal perception, the perception from one sense is influenced and complemented by perception from another, as the perceived features are integrated into a coherent interpretation. Neurons receive inputs from the vestibular nerve and project directly to extraocular motoneurons. Simultaneously, the vestibular nuclei receive projections not only from afferent nerve input but also from various cortical, cerebellar, and other brainstem structures. This integration of vestibular nerve input from multiple modalities at the initial stage of central vestibular processing is known as multimodal perception.

2.4.2 State of the art of the subjective evaluation and perception threshold for linear motion and acceleration


During a subjective evaluation of the driving dynamics, drivers or participants provide qualitative feedback on aspects like ride comfort, handling, steering feel, acceleration responsiveness, braking performance, and overall driving experience. The assessments are often expressed by using descriptive terms like smooth, agile, comfortable, or sporty.

Subjective evaluations play an important role in the development and improvement of vehicles, as they help automotive engineers and designers understand how real drivers perceive and interact with a vehicle. This feedback informs decisions related to vehicle design, suspension tuning, powertrain calibration, and other factors to optimize the driving experience based on user preferences.

State of the art of subjective evaluation

The study [64] researched the subjective perception and evaluation of driving dynamics in a driving simulator, aiming to study the subjectively comfortable feedback for the rolling and yawing vehicle motion with consideration of road unevenness. The study [65] generated a series of external yaw and roll moment disturbances, varying in amplitudes and frequencies, during a high-speed stability simulation test in a driving simulator. These tests involve both regular and experienced test drivers. Based on their responses to these external disturbances, this study identified the crucial quantities that influence the driver's perception of vehicle stability. The study [66] analyzed the various subjective evaluation indicators related to braking performance from different companies. The objective was to categorize these indicators systematically in order to describe the subjective assessment of the brake system and to identify the indicators that significantly influence the driver's perception.

Kraft investigated the subjective evaluation of drive-off dynamics in the study [22] by using the driving simulator introduced in Section 2.4.4. Two test subject studies were conducted. The first study examined the influence of virtual reality design on the evaluation of drive-off behavior. Three test groups were formed, differing in the type of stimuli presented (immersive virtual reality vs. simplified virtual reality) and whether test subjects actively controlled the vehicle or it was automated (active vs. passive driving). In total, nine application variants of the drive-off behavior were evaluated, defined by the pedal position and torque gradient of the electric motors. The evaluation was based on the criteria of sportiness, comfort, and responsiveness. The results indicate that the evaluations of the application variants do not exhibit significant differences between immersive and simplified virtual reality. Only differences in the evaluation of the responsiveness criterion were observed between active and passive driving. The presence, as measured by the IPQ questionnaire introduced in [67] cited by [22], showed a significant difference between active and passive driving in terms of involvement. There were no significant differences in the other



subscales of the IPQ questionnaire among the three test groups. It can be concluded that the presented visual, acoustic, and haptic stimuli do not have a significant impact on the evaluation of drive-off behavior under the investigated conditions. In the second study, the usability of the driving simulator for the application of a drive-off procedure was investigated. The test subjects first experienced a drive-off procedure in a test vehicle with a focus on acceleration characteristics. Subsequently, they adjusted the drive torque gradient on the driving simulator to replicate the drive-off character they experienced in the test vehicle. According to the subjective evaluation of the test subjects, driving simulators are well-suited for the conducted application task. This underscores the significant potential of dynamic driving simulators in the context of powertrain applications.

Perception threshold for acceleration and jerk

In the study conducted by Kingma [68], the perception thresholds for accelerations and velocities in longitudinal and lateral directions were identified. The conclusion was that the perception threshold concerning acceleration relies on the excitation profile or driving profile, while the perception threshold concerning velocity remains unaffected. Furthermore, investigations conducted in [69] and [70] examined the impact of jerk on the perception threshold of linear motion. The findings suggest that jerk influences the subjective impression of linear motion, and the perception threshold is a function of jerk and acceleration. The study [69] conducted an experiment within a flight simulator and presented accelerations in a trapezoidal profile. The maximum acceleration and jerk values were derived from this profile. However, it should be noted that acceleration was only investigated up to a value of 1 m/s^2 and jerk up to a value of 3 m/s^3 . These values are notably smaller than those commonly encountered during vehicle acceleration processes. The study [71] identified the perception threshold for acceleration (0.1 m/s^2) and jerk (1 m/s^3) through experimentation with a specialized vehicle.

In the literature research, inconsistent values for perception thresholds for the maximum longitudinal acceleration and jerk (mean gradient of acceleration) can be found. The threshold values are identified in different environments. Table 2.1 summarizes perception thresholds for acceleration and jerk.

There is a consensus in the literature that the threshold levels vary depending on the test environment, evaluation method, and test profiles. Therefore, the literature research in the context of longitudinal motion has been conducted and focused as much as possible on a vehicle or similar environment. According to [72] and [73], speed and engine noise do not significantly influence the threshold levels of acceleration and jerk.

Table 2.1: Perception threshold for acceleration and jerk

Author	Year	Environment	Type	Threshold
Rockwell & Snider [74]	1965	Real Vehicle	Absolute	0.15 m/s ²
Howard [75]	1986	Laboratory Study	Absolute	0.06 – 0.1 m/s ²
Kingma [68]	2005	Laboratory Study	Absolute	0.088 m/s ²
Reid & Nahnon cited by Baumgartner & Ronellenfitsch [76]	(1985) 2017	Flight Simulator	Absolute	0.1 – 0.17 m/s ²
Ernst & Rockwell cited by Henderson [77]	(1966) 1987	Real Vehicle	Relative	At 55 km/h: 0.12 m/s ² At 90 km/h: 0.11 m/s ²
Müller cited by Erler [78]	(2016) 2019	Real Vehicle	Relative	0.07 – 0.13 m/s ² until 80 km/h
Müller & Hajek [71]	2013	Real Vehicle	Relative	0.09 m/s ² 1 m/s ³ for jerk

Literature research further shows that the studies mainly focus on human perception with a focus on the just noticeable difference (JND). Studies employing difference thresholds to assess drive-offs are not well-documented. However, the JND does not necessarily correspond to threshold values that lead to significantly different evaluations of drive-off behavior, as slight changes in vestibular perception do not inherently result in a different evaluation.

2.4.3 Objectivation of the subjective evaluation

The objectivation approach holds pivotal significance in driving dynamics evaluation. By making subjective impressions accessible to empirical analysis, it enriches the empirical evaluation paradigm with insights that are deeply rooted in the experiential aspects of driving. This methodological synergy promotes a comprehensive understanding of vehicle behavior that is connected with the perceptual facets valued by drivers. Simultaneously, it engages with the precision of objective assessment methods. Ultimately, the objectivation approach leads to a more holistic and comprehensive understanding of driving dynamics.

State of the art

Research on the objectivation of subjective evaluations in the field of automotive engineering is widespread in the literature. However, it primarily focuses on the correlation of subjective evaluation and objective measurements in the context of aspects such as ride comfort or vehicle handling [79], [80], [81], [82], [83], [84], [85], [86]. For instance, the study [79] conducted a literature review on the objective assessment of vehicle ride comfort, but it did not delve into the methods for objectivating subjective evaluations. The study [80] conducted by Kim researched ride comfort regarding driver-perceived vibrations and established correlations between the subjective evaluations and measured vibration signals from sensors placed on different body positions. The objective measurements at the hip had the strongest correlation with subjective evaluations.

The studies [81] and [82] concentrated on establishing correlations between objective and subjective evaluations of vehicle ride comfort across different vehicle and road types. Maier [83] did research in his doctoral work to develop a method for objectivating subjective perceptions of vibrations excited by drive trains during engine start, engine stop, and idling. Measurement points are positioned on the seat, steering wheel, and foot space. This study proposed an analysis process for objectivation of the subjective perception based on correlation analysis. The study [84] considered both ride comfort and vehicle handling and focused on correlation analysis between objective and subjective evaluations. The studies [85] and [86] specifically examined the correlation between subjective and objective evaluations of handling, with a focus on steering-related indicators like steering response and yawing response for subjective evaluations, as well as average steering angle and yaw velocity for objective evaluations. Both studies employed regression analysis to complete the correlation analysis.

In 2010, Dirk [20] published the research results in the doctoral research for developing a method to evaluate the drive-off procedure of the vehicle with the consideration of the accelerator pedal position, respective for partial load and full load drive-offs. The primary objective of this research was to develop an objective assessment method for vehicle drive-off behavior regarding comfort, drivability, and agility impressions. Multiple test subject studies were conducted to analyze these aspects, considering various types of drive-off conditions and vehicle concepts. For partial load drive-off via the accelerator pedal, a target range was established for the dose ability gradient based on mean jerk and mean response time. Furthermore, it was also found that the accelerator pedal's angle plays a crucial role in achieving optimal drive-off behavior. In the case of full load drive-off with both accelerator and clutch pedals, additional variables were identified as relevant, namely the clutch pedal force profiles and optimal clutch behavior.

There remains a notable gap in the literature concerning the objectivation of subjective evaluations related to driving dynamics, particularly in the context of subjective evaluations of drive-off behavior, an area that received limited research attention.

Logistic regression

Due to the diverse research aspects of the subjective evaluation, this work conducted the investigation focusing on the drive-off dynamics in the longitudinal direction. According to Weber's Law, the difference threshold ΔS between two stimuli is proportional to the size of the reference stimulus S , specifically $\Delta S = k \cdot S$. Here, k represents the Weber constant, which varies for different sensory modalities [87]. This law illustrates the non-linear behavior where the discriminability between two stimuli decreases as the intensity of the reference stimulus increases. Physicist and philosopher Gustav Theodor Fechner extended Weber's Law by proposing that the sensation strength E is logarithmically dependent on the stimulus intensity [87]. Based on this, logistic regression is employed in this work to objectivate the subjective evaluation gained by test subject studies. The following introduction to the logistic regression is based on [88]. The logistic regression belongs to the class of structural testing procedures. It is a variant of regression analysis with the distinction that the dependent variable Y is a categorical variable, the subjective evaluation for the evaluation criteria in this work. Since the evaluation is often uncertain, the probabilities for the outcome of Y are predicted. Because of the nonlinearity, the estimation of the parameter in the regression model is based on Maximum Likelihood Estimation (MLE) and differs from the method of least squares used in linear regression analysis. The MLE principle determines the estimated values for the unknown parameters in such a way that the realized data attain maximum plausibility (Likelihood). Unlike linear regression, the estimated curve is not a straight line. Instead, it is a logistic function. It has a symmetrical "S-shape", and approaches asymptotes at $Y = 0$ and $Y = 1$, which represents the probability P of the outcome of Y .

For the probability applies:

$$P(Y = 0) = 1 - P(Y = 1) \quad (2.1)$$

and vice versa. For the design of the logistic regression model, the logistic function is used, from which the name results:

$$P(x) = \frac{1}{1 + e^{-z}} \quad (2.2)$$

with

$$z = \beta_0 + \beta_1 \cdot x_1 + \beta_2 \cdot x_2 \dots + \beta_k \cdot x_k$$

This linear combination is called the systematic component of the model. The model is identical to linear regression analysis in this respect and represents a linear regression model of the independent variables x_i with coefficient β_i , for $i = 0, \dots, k$. The choice of the independent variables is dependent on the test subject study design.

2.4.4 Longitudinal dynamic driving simulator

The driving simulator at the Institute of Mechatronic Systems in Mechanical Engineering (IMS) at

the Technical University of Darmstadt was developed to investigate human perceptions of vestibular, visual, and auditory stimuli during longitudinal vehicle maneuvers. Its primary goal is to enable early examination of drivetrain concepts before hardware is available. In the following, more details about the driving simulator are introduced to help understand the test environment. The information is based on [22], [78], and [89]. A side view and a front view of the driving simulator are shown in Figure 2.7 cited from [22].

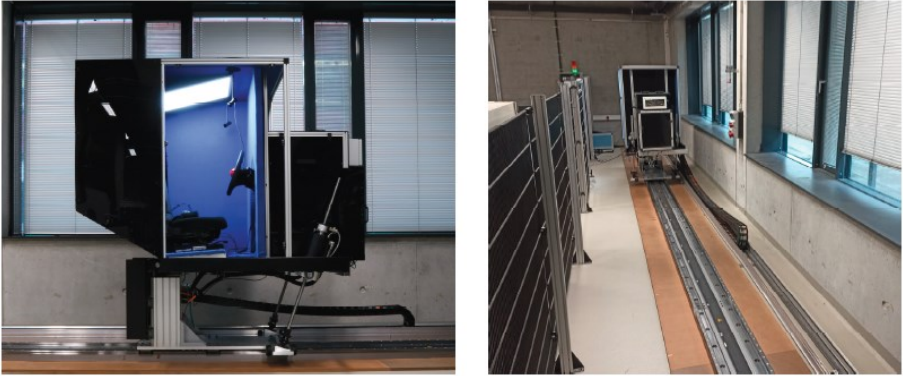


Figure 2.7: Longitudinal dynamic driving simulator in side view (left) and front view (right) [22]

Motion system

The driving simulator is capable of simulating accelerations through a combined translational and rotational motion of the driver's cabin. The translational motion system has a 10-meter linear rail, along which the entire platform is propelled by a linear actuator. It allows a maximum speed of 5 m/s. Due to the direct drive and a low overall mass of 460 kg the system is well-suited for the presentation of jerky maneuvers with a jerk up to 130 m/s^3 [89]. The rotary motion system includes a lifting actuator positioned at the rear of the platform to adjust the rear point of the driver's cabin vertically. Additionally, two hollow spindle motors are situated at the front of the platform to facilitate the rotation of the driver's cabin around the transverse axis. The rotation point is positioned at the driver's head, where the vestibular organ is located. This utilizes gravitational force to create the sensation of acceleration [90], [91]. In order to create a realistic linear self-acceleration perception through tilt coordination, it is necessary to maintain the tilt rate and its change rate below the threshold of human detection. Various acceptable perception thresholds have been reported in the literature, ranging from $3 \text{ }^\circ/\text{s}$ to $6 \text{ }^\circ/\text{s}$ with associated accelerations up to $8 \text{ }^\circ/\text{s}^2$ [92], [93]. A summarized specification of the motion system can be found in Table 2.2 [78].

Table 2.2: Actuator and platform specifications [78]

Actuator Specifications	Linear Motion	Rotation Rear	Rotation Front
Nom. Force	3000 N	6880 N	1666 N
Nom. Speed	4.9 m/s	0.25 m/s	1.25 m/s
Max. Force	4000 N	16000 N	2848 N
Max. Travel	10 m	0.15 m	1 m
Sensor Type	SinCos	Resolver	SSI/SinCos
Platform Specifications	Longitudinal	Rotational	
Max. Workspace	± 5 m	$\pm 25^\circ$	
Max. Velocity	± 5 m/s	$> \pm 6^\circ/\text{s}$	
Max. Acceleration	± 8 m/s ²	$> \pm 6^\circ/\text{s}^2$	

Human-machine interface

The Human-machine interface (HMI) in the context of a driving simulator refers to the technology or interface through which the simulator user engages with and manages the simulator while also receiving feedback. The primary objective of the HMI within a driving simulator is to create a realistic and immersive driving experience while allowing the driver to control and interact with the simulated environment. This interface serves as a pivotal instrument for investigating vehicle dynamics and the reactions of the driver, facilitating research and experimentation in a controlled and safe situation. The used driving simulator contains the following HMI functions:

- Steering and vehicle controls:** The simulator provides a realistic steering wheel, pedals, and other controls similar to those found in actual vehicles. These controls allow the driver (simulator user) to interact with the simulated vehicle, including steering, accelerating, braking, and shifting gears. However, the steering only has an influence on the motion of the virtual vehicle. The physical simulator platform does not show any corresponding lateral movement to the steering wheel angle.
- Sound and audio feedback:** Realistic audio feedback, including engine sounds, tire screeches, and road noise, is presented via in-ear headphones with a noise-canceling function. It provides auditory cues about the vehicle's behavior to enhance the immersion level and suppresses the external noise simultaneously. The auditory software can also synthesize the engine sound according to the engine speed curve.

- **Visual environment:** The virtual reality (VR) technology provides a highly detailed and immersive visual representation of the road, surroundings, and the vehicle's interior through a VR Headset, the Oculus Rift CV1. In the test subject studies for this work, participants sit in a Mercedes-Benz A-Class with a detailed interior and drive on a country road with different referenced objects, as shown in Figure 2.8 right.
- **Vibration feedback:** The vibration-shakers are mounted under the vehicle's seat and on the pedals. It is designed to generate vibrations and haptic feedback, aiming to provide users with a more realistic and engaging experience by adding haptic feedback to complement visual and auditory cues.

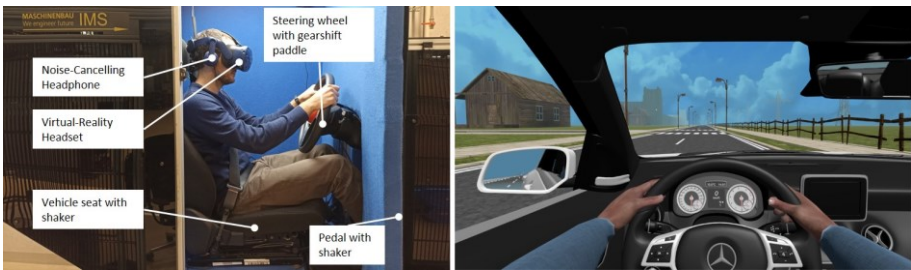


Figure 2.8: HMI in the driving simulator [22] (left) and the visual environment displayed in the VR Headset (right)

With the help of this dynamic driving simulator, various longitudinal acceleration profiles can be replicated, allowing for targeted investigations into human perception and longitudinal motion under reproducible and adjustable experimental conditions [94]. Further information about the design, components, and technical details of the driving simulator can be found in references [22], [78], and [89].

2.5 Ecological evaluation of the driving dynamics

The ecological evaluation of driving dynamics refers to an assessment or analysis of how a vehicle's performance and behavior impact the environment. It involves various facets such as energy efficiency, emissions, resource utilization, and lifetime of the components. The goal is to understand the ecological or environmental implications of a vehicle's driving characteristics and performance. This evaluation can help identify how a vehicle's behavior affects its carbon footprint, fuel efficiency, and overall sustainability. It is an important aspect of modern vehicle development, especially as the intention to create more eco-friendly and sustainable transport solutions is growing.

2.5.1 State of the art of the ecological evaluation


Numerous studies in the literature have examined the ecological assessment of driving dynamics, particularly concerning energy efficiency and emissions. Consequently, the overview of the current state of research in this field is limited with a specific focus on hybrid electric vehicles (HEVs), including mild and full hybrid electric vehicles (MHEVs/FHEVs). The plug-in hybrid electric vehicles (PHEVs) and battery-electric vehicles (BEVs) are excluded.

According to the research in [95], hybrid vehicles demonstrate a substantial improvement in fuel economy, with potential gains of up to 68 % observed in urban traffic conditions. In comparison, when considering highway driving cycles, the fuel economy improvement is only around 10 %. The study [96] corroborates these findings, reporting a slightly lower improvement of approximately 50 % for low and moderate speeds when using hybrid vehicles. Furthermore, this study highlights that not only the vehicle characteristics but also the driving behavior and the speed have a significant influence on fuel consumption.

Consistent findings are reported in [14], [15], [16], [17], with the most recent study [17] offering a comprehensive review of recent research on the sensitivity of energy consumption in hybrid powertrains to various driving styles. As presented in [14] and [17], a general analytical approach involves scaling standard driving cycles using constant factors to manipulate their characteristics. The results consistently illustrate that an aggressive or sporty driving style notably impacts fuel consumption, leading to increases ranging from 25 % to 68 % when compared to a more conservative, mild driving behavior, particularly evident in low-speed urban driving cycles.

48 V mild hybrid powertrains represent a notable advancement in automotive technology, as they offer enhancements in fuel efficiency, reduced CO₂ emissions, enhanced energy recovery, and improved drivability while incurring limited additional costs compared to traditional powertrains [5], [97].

The study [5] analyzed the 48 V mild hybrid powertrain across various parameters, including recuperation potential, powertrain efficiency, and overall performance. This investigation covered P1, P2, P3, and P4 topologies. The utilization of a dedicated 48 V battery provides flexibility for implementing control and operational functions, enabling efficient start-stop functionality in a wide range of driving scenarios with fewer constraints than micro-hybrid vehicles. Depending on the chosen hybrid topology, fuel consumption improvements can range from 4 % to 15 %. These diverse hybrid topologies were further examined in [98] to ascertain fuel consumption enhancements concerning different electrical power levels and driving cycles. It was found that P2 and P3 topologies consistently achieved a notable average fuel consumption reduction of 19 % compared to conventional powertrains, while P0 and P1 topologies exhibited improvements of only 4 %. The study [38] researched the performance of a vehicle with a mild hybrid powertrain for various urban driving conditions. It found that the low average speed, acceleration, and deceleration



throughout the driving implies a low rate of battery energy consumption per kilometer.

The study [99] explored the mild hybrid powertrain's impact on CO₂ emissions. The results indicated that the P1 topology led to a substantial reduction of up to 10 % in urban driving scenarios, while the P2 topology, featuring an electric motor with a power of 25 kW, delivered even more significant reductions of up to 25 %. Nevertheless, the CO₂ reduction achieved by both topologies on the highway was less pronounced, declining by less than 5% due to increased air drag resistance and reduced recuperation potential.


In general, the fuel consumption of HEVs is more susceptible to variations in driving styles compared to conventional vehicles. This heightened sensitivity stems from the significant role played by control strategy in the energy management system (EMS) in these vehicles. This system governs when and how the ICE adjusts its torque, as well as the extent of energy recuperation during braking. Both of these factors have a substantial impact on the State of Charge (SOC) of the vehicle's battery and, consequently, its overall fuel consumption.

The effectiveness of energy recuperation during braking is influenced by various factors, including vehicle mass, battery charging power, and the electric motor's (EM) power. As an example, the study [38] proposed a control strategy for maximizing the performance of heavyweight mild hybrid vehicles and found that the component size of the vehicle should be optimized according to speed and acceleration constraints. A recuperative braking control strategy outlined in [100] for an electric bus achieved a recuperation rate of 17.4 % in a simulation environment. Meanwhile, studies like [101] and [102] have explored the recuperation performance of full hybrid electric passenger vehicles in urban traffic conditions, reporting energy recovery rates of approximately 30% and 40%, respectively. These findings underscore the importance of efficient energy management and recuperation systems in optimizing the fuel economy of HEVs, including MHEVs, under diverse driving scenarios.

2.5.2 Ecological evaluation objectives

The existing research in the literature primarily focuses on hybrid powertrain topologies such as P1, P2, P3, and P4, examining aspects like fuel consumption or CO₂ emissions over entire driving cycles or in urban traffic. However, there is a lack of analysis on specific driving phases, particularly the drive-off procedure, during which the ICE operates at low efficiency and the drive-off element experiences significant load.

To address this research gap, previous work, as described in [103], has delved into the thermal load generated during the drive-off phase and the associated fuel consumption in mild hybrid powertrains. This investigation places particular emphasis on the drive-off procedures, which represent comfortable and sporty driving styles. To achieve this, the low-speed phase of the standard and scaled standard Worldwide harmonized Light-duty Test Cycle (WLTC) are employed. The



primary objectives of this investigation are twofold: first, to assess fuel consumption, and second, to evaluate the thermal load experienced by drive-off elements.

In the current work, both of these aspects are further utilized as ecological evaluation objectives because of their sensitivity to drive-off dynamics and the limited existing research with consideration of drive-off elements. It provides an intuitive assessment of the drive-off procedure in relation to drive-off dynamics. The thermal load is limited to encompass only the frictional heat generated by the slipping of the clutch during synchronization. Other sources of heat, such as those produced by the EM or from gear meshing, are not considered within this scope.

2.6 Research gap and usability

The research in this work addresses gaps in the field of automotive engineering with a focus on the drive-off procedure in the mild hybrid powertrain. It offers usability and contributes to knowledge in the evaluation and calibration of drive-off behavior.

Research gap

The primary research gap revolves around the limited research on drive-off behavior evaluation in vehicles. This encompasses a wide range of subjective assessments, including comfort, dynamic, and controllability during the drive-off phase. Insufficient research in this domain hinders the development of a nuanced understanding of drive-off behavior, which is essential for enhancing the overall driving experience.

Furthermore, there is a disconnection between subjective evaluations of drive-off behavior and the calibration process with regard to the ecological evaluation. The integration of these subjective assessments into the calibration workflow remains underdeveloped. This gap presents a considerable challenge for calibration engineers aiming to fine-tune drive-off characteristics according to user preferences and ecological aspects. This challenge becomes even more pronounced in the context of reduced vehicle development cycles driven by the rapid digitalization and electrification of powertrains.

Research usability

This research provides practical usability by addressing these gaps. It seeks to bridge the gap between subjective drive-off behavior evaluations and the calibration process, enhancing the effectiveness of vehicle calibration to align with driver preferences. It also aims to contribute to the development of knowledge for designing the control strategies and drive-off elements of the mild hybrid powertrains, considering factors like clutch lifetime and downsizing possibilities. In this way, it promotes the development of more efficient and eco-friendly mild hybrid systems. These contributions not only offer valuable insights into the hybrid powertrain but also the advancement

of knowledge in this field. They have the potential to influence the future of automotive engineering by promoting more eco-friendly practices without compromising the driving experience.

3 Investigation of the subjective evaluation

The primary objectives of this work are to determine the impact of key factors on the perceived impression during drive-off. To achieve these objectives, the following research questions are formulated:

- Do the influence factors have a significant impact on the evaluation of the drive-offs?
- What are the EDTs for each influence factor?

Based on the drive-off characteristics described in Section 2.1, the evaluation of drive-off behavior considers influence factors of maximum acceleration, mean jerk, response time, acceleration pedal position, and engine speed changes in speed plateau and flare. This evaluation encompasses aspects related to sportiness, jerkiness, agility, comfort, and acceptability. This work divides the factors into three separate studies to manage the complexity arising from an increasing number of influence factors in a test subject study.

In this chapter, all of these test subject studies are introduced. Each study begins with the design of the study and concludes with the subsequent analysis of the collected data and the discussion of the results.

3.1 Test subject study 1 – Investigation of the maximum acceleration and mean jerk

Based on the description in Section 2.1, it is presumed that the maximum acceleration has an impact on the evaluation of sportiness. Higher acceleration should lead to a sportier impression. As aforementioned, a dynamic driving impression is also based on the high acceleration rate within a certain response time. It indicates that a high mean jerk is desired for sporty driving. Additionally, the mean jerk directly influences the comfort evaluation with the aspect of jerkiness. Based on these presumptions, following hypotheses are formulated:

- H1: Maximum acceleration and mean jerk have an interaction effect for evaluating the drive-off behavior.
- H2: Maximum acceleration has a significant effect on sportiness, comfort, and jerkiness during drive-off.
- H3: Mean jerk has a significant effect on sportiness, comfort and jerkiness during drive-off.

An interaction effect between two factors, often referred to as a two-way interaction, occurs in statistical analysis when the effect of one factor (independent variable) on an evaluation criterion

(dependent variable) is not consistent across different levels of another factor. In other words, it means that the impact of one factor on the evaluation criterion depends on the specific conditions or levels of the other factor.

3.1.1 Design of the study

Definition of the drive-off profiles

To design the drive-off profiles, the maximum acceleration and mean jerk ranges in which both factors vary should first be determined. For this purpose, the drive-offs are carried out in a test vehicle with comfort driving mode in accordance with the APPs, varying in an interval from 10 % to 100 %. The analysis of the recorded data reveals a range of the maximum acceleration between 1 m/s² and 5 m/s² and a range of the mean jerk between 3 m/s³ and 10 m/s³.

Based on this knowledge, a range of 2.5 m/s² to 3.5 m/s² for acceleration and a range of 5 m/s³ to 9 m/s³ for mean jerk are selected. Both factors are varied across three levels each, resulting in a total of nine different driving profiles, as shown in Figure 3.1. Using a larger range or more levels would lead to longer testing periods, which can potentially induce driving simulator sickness [104], a variant of motion sickness (Kinetosis). This discomfort is often explained by Reason's sensor conflict theory [105], e.g., a conflict between virtual stimuli and vestibular stimuli. Further influence can be time differences in the stimulus presentation [106].

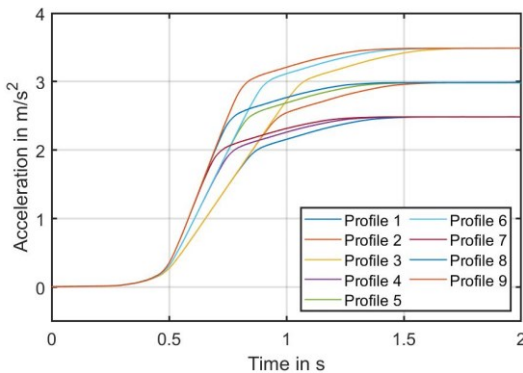


Figure 3.1: Drive-off profiles for the test subject study 1

To generate these profiles, one profile is extracted from the drive-off measured in the test vehicle and then adjusted to achieve the desired maximum acceleration and mean jerk values. The characteristics of the drive-off profiles are summarized in Table 3.1.

Table 3.1: Variation of the drive-off profiles for study 1

Drive-off Profiles	Mean Jerk	Max. Acceleration
1.	5 m/s ³	2.5 m/s ²
2.	5 m/s ³	3 m/s ²
3.	5 m/s ³	3.5 m/s ²
4.	7 m/s ³	2.5 m/s ²
5.	7 m/s ³	3 m/s ²
6.	7 m/s ³	3.5 m/s ²
7.	9 m/s ³	2.5 m/s ²
8.	9 m/s ³	3 m/s ²
9.	9 m/s ³	3.5 m/s ²

Study procedure

The study is conducted in German and consists of four phases that are conducted one after the other. These are:

1. Introduction, providing an overview of the study's content and purpose, instructions for test subjects. It also includes a brief statement about the study and assures test subjects of anonymity and confidentiality.
2. Pre-questionnaire, including questions that check physiological prerequisites and collect demographic information and other background details about the test subjects. It helps establish context, categorize test subjects, and analyze their characteristics or experiences.
3. Acclimatization phase, the test subjects acclimatize themselves with the driving simulator and familiarize themselves with the driving dynamics.
4. Test Phase, all nine drive-offs are presented to the subjects in a stochastic order. After each driving profile, they are asked to rate the experienced drive-off behavior on a scale of 1 to 5 based on the criteria of sportiness, jerkiness, and comfort.
5. Post-questionnaire, including questions presented to test subjects after they've completed the test phase. It includes follow-up questions related to the test experience and the evaluation of the driving simulator.

In the acclimatization phase, the test subjects are introduced to the fact that they are on a country road and stopped at a traffic light. When the light turns green, they start driving to reach a final speed of approximately 50 km/h. During this drive, they have to focus on the initial acceleration

phase, specifically from 0 km/h to 35 km/h. Initially, they will experience two drive-off scenarios as a reference for the subsequent evaluation. One of the two drive-off scenarios is very smooth, with a jerk of 3 m/s^3 and an acceleration of 2.5 m/s^2 , while another is an aggressive drive-off, see the ninth drive-off profile in Table 3.1. Afterward, they will be asked to assess each drive-off behavior according to Table 3.2, which is also used for the test phase.

Table 3.2: Evaluation criteria for the experienced drive-off

I perceived the drive-off behavior as...						
	1	2	3	4	5	
unsporty	O	O	O	O	O	sporty
fluent	O	O	O	O	O	jerky
uncomfortable	O	O	O	O	O	comfortable

In the acclimatization and test phases, the vehicle accelerates always to reach a target speed of approximately 50 km/h, so that the test subjects cannot easily establish the acceleration based on the final speed and focus on the subjective evaluation. Then, the vehicle starts braking and drives backward to the initial position. During the acceleration and deceleration, the vehicle drives autonomously. The test subjects do not have an interaction with the acceleration and braking pedals. This design is based on the statement of Kraft in his study [22] that there are no differences in the evaluation of the drive-off dynamics when the test subjects drive actively or passively in a driving simulator.

The corresponding questionnaire can be found in Appendix A.

3.1.2 Results of the test subject studies

Methodology

This study involves two factors (independent variables), and represents a multifactorial problem. The analysis includes testing the main effect of each factor and the interaction effect between them using MANOVA and ANOVA with repeated measures. One crucial prerequisite for employing repeated-measures analysis of variance, particularly when dealing with factors with more than two levels, is the sphericity, which necessitates equal variance among multiple groups. It is fulfilled by using the Mauchly test.

Another prerequisite involves the normal distribution of evaluation ratings (dependent variables) for each factor. Although the evaluation data is not strictly a normal distribution that is tested with the Shapiro-Wilk-Test, it is noteworthy that, as suggested by studies [107] and [108], the analysis of variance remains robust even when this prerequisite is violated.

The analysis of variance aims to determine if there are statistically significant differences among the means of various groups. To investigate these differences further, post-hoc tests accompany

the ANOVA. These post-hoc tests provide insights into which specific mean values exhibit significant distinctions from one another. A significance level of 0.05 is consistently applied to all statistical tests throughout this work. If the calculated significance value is less than this level, a significant distinction is then detected. The results of this test study were published in [21].

Statistical analysis

A total of 23 test subjects participated in the study. All of the test subjects were students at the Technical University of Darmstadt. Among them, 20 were male, and 3 were female, 90 % of them were under the age of 30, with an average age of 27.5 years and a standard deviation of 6.8 years.

The three figures below display the descriptive statistics for each criterion's evaluation. In each figure, the height of the blue bar corresponds to the mean evaluation rating for each drive-off, while the black line atop each bar represents the standard deviation.

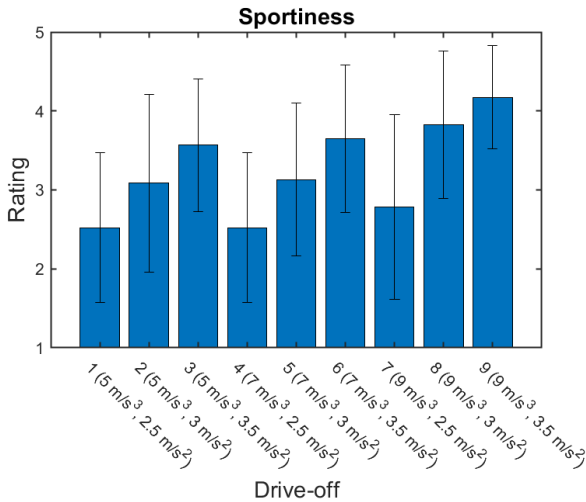


Figure 3.2: Descriptive statistics for drive-off evaluation according to sportiness in study 1

Figure 3.2 illustrates a discernible pattern in the evaluation of sportiness, indicating that increased acceleration is associated with higher sportiness ratings. When comparing drive-offs with varying mean jerk values but consistent acceleration (e.g., drive-offs 3, 6, and 9), a subtle increase in sportiness evaluation becomes apparent. A similar trend is observed in Figure 3.3 for the evaluation of jerkiness, while Figure 3.4 displays a contrasting trend regarding comfort evaluation. Here, higher factor levels correspond to lower comfort ratings, suggesting that greater driving dynamics lead to a reduction in perceived comfort.

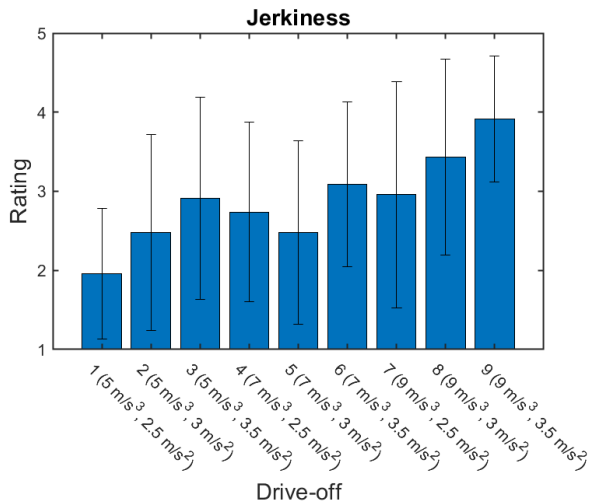


Figure 3.3: Descriptive statistics for drive-off evaluation according to jerkiness in study 1

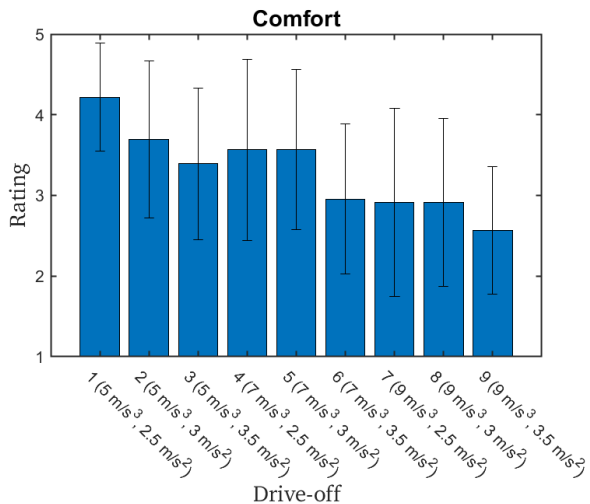


Figure 3.4: Descriptive statistics for drive-off evaluation according to comfort in study 1

In the following, further statistical analyses are conducted to examine the drive-off evaluations and the corresponding results are presented. First, the main and interaction effects of the factors are examined using Wilks-Lambda, a test statistic commonly applied in MANOVA, and then the EDTs in the ratings of sportiness, jerkiness, and comfort are identified. This will determine how much the jerk or maximum acceleration must be changed for the drive-off to be evaluated differently.

Table 3.3: MANOVA Multivariate Tests (Wilks-Lambda)

Factor	Significance (<i>p</i>-Value)
Max. acceleration	0.002
Mean jerk	<0.001
Max. acceleration * Mean jerk	0.342

The significance values (*p*-Values) in Table 3.3 indicate that both factors lead to significantly different evaluations of the drive-offs, as the significance values are less than 0.05. However, there is no interaction effect between the factors. The hypothesis H1 must be rejected. Therefore, the influences of both factors may be examined separately. To answer the research question and examine other hypotheses, a one-way repeated measures analysis of variance (ANOVA) and post-hoc tests are employed first to investigate the effect of the factor on each evaluation criterion and then identify the EDTs.

Table 3.4: ANOVA for investigating the significance of maximum acceleration and mean jerk

Factor	Criterion	Significance (<i>p</i>-Value)
Max. acceleration	Sportiness	<0.001
	Jerkiness	0.070
	Comfort	0.017
Mean jerk	Sportiness	<0.001
	Jerkiness	<0.001
	Comfort	<0.001

As shown in Table 3.4, the maximum acceleration has a significant impact on the sportiness and comfort evaluation criteria but not on jerkiness. In contrast, different jerk levels differ in terms of all considered criteria. Based on these results, the hypothesis formulated in H2 can be partially approved, and H3 can be fully approved.

In the next step, the EDTs for evaluating the drive-off behavior are analyzed using the calculated significances. For this purpose, the evaluations are examined through pairwise comparisons (post-hoc tests). However, adjustments for the significance need to be made to account for the increased

risk of Type I errors (false positives) that can occur when conducting multiple comparisons. With each additional comparison, there's a chance that a significant result might be found, even if there are no real differences in the population being tested. For this problem, the Bonferroni correction is applied in the analysis to calculate the p_{corr} -Values. It reduces the chances of making a Type I error.

According to Weber-Fechner Law [87] and [109], the ability to distinguish between two stimuli is not solely determined by the absolute difference between the stimuli but rather by the relative difference or the ratio of the differences. In other words, as the intensity of stimuli increases, the difference between them must also increase for a person to perceive a distinction. Human perception is known to be logarithmically dependent on stimulus intensity rather than linear. Based on the results in Table 3.5, the nonlinearity of human perception in evaluating sportiness can be observed because the difference between the low and medium acceleration levels is significant, while it is not between the medium and high levels.

Regarding the evaluation of sportiness, accelerations of 2.5 m/s^2 and 3 m/s^2 , as well as 2.5 m/s^2 and 3.5 m/s^2 , are significantly different. However, there is no significant difference in evaluations between accelerations of 3 m/s^2 and 3.5 m/s^2 . This suggests that the EDT for evaluating sportiness is less than 0.5 m/s^2 when acceleration is less than 3 m/s^2 , but it is greater than 0.5 m/s^2 as acceleration increases.

Table 3.5: Pairwise comparisons for identifying the EDTs of maximum acceleration

Criterion	Max. acceleration levels		Significance (p_{corr} -Value)
Sportiness	2.5 m/s^2	3 m/s^2	0.002
	2.5 m/s^2	3.5 m/s^2	<0.001
	3 m/s^2	3.5 m/s^2	0.216
Jerkiness	2.5 m/s^2	3 m/s^2	1.000
	2.5 m/s^2	3.5 m/s^2	0.151
	3 m/s^2	3.5 m/s^2	0.370
Comfort	2.5 m/s^2	3 m/s^2	0.815
	2.5 m/s^2	3.5 m/s^2	0.032
	3 m/s^2	3.5 m/s^2	0.115

Simultaneously, it can be observed that the EDT for evaluating comfort is greater than 0.5 m/s^2 but less than 1 m/s^2 , because the evaluations of two consecutive levels in pairwise comparisons are not significantly different, but there is a significant difference between 2.5 m/s^2 and 3.5 m/s^2 .

Table 3.6: Pairwise comparisons for identifying the EDTs of mean jerk

Criterion	Mean jerk levels		Significance (p_{corr} -Value)
Sportiness	5 m/s ³	7 m/s ³	1.000
	5 m/s ³	9 m/s ³	0.017
	7 m/s ³	9 m/s ³	<0.001
Jerkiness	5 m/s ³	7 m/s ³	0.283
	5 m/s ³	9 m/s ³	<0.001
	7 m/s ³	9 m/s ³	<0.001
Comfort	5 m/s ³	7 m/s ³	0.071
	5 m/s ³	9 m/s ³	<0.001
	7 m/s ³	9 m/s ³	0.008

In terms of assessing sportiness, jerkiness and comfort, jerk levels of 5 m/s³ and 9 m/s³, as well as 7 m/s³ and 9 m/s³, show significant differences. However, no significant differences in evaluations are observed between jerk levels of 5 m/s³ and 7 m/s³, the analysis results are shown in Table 3.6.

In the small jerk area (below 7 m/s³), the EDTs for the mean jerk, concerning all criteria (sportiness, jerkiness, and comfort), are greater than 2 m/s³. In contrast, in the large jerk area, these EDTs are less than 2 m/s³. These observations suggest that smaller differences in jerk are required to perceive distinctions in evaluations within the large jerk area compared to the small jerk area, illustrating the non-linear nature of human perception, particularly concerning sportiness, jerkiness, and comfort evaluations.

3.1.3 Objectivation of the subjective evaluation

In this section on objectivating the subjective evaluation, the regression model introduced in Section 2.4.3 is utilized. The factors of maximum acceleration and mean jerk are used as independent variables, x_{Acc} and x_{Jerk} , while the probability of the evaluation P_i for each criterion (Sportiness, Jerkiness, and Comfort) serves as the dependent variable. Binary logistic regression is often employed to examine the relationship between one or more independent variables and a dependent variable. It finds a logistic function according to Equation (2.2) that best fits the data. To apply this method, ordinal ratings must first be transformed into a nominal or binary form. During the familiarization phase, test subjects experienced both a gentle and a sporty acceleration profile. Ratings for the gentle profile mostly began at 2 on the scale, as test subjects didn't want to utilize the entire scale during their first experience. Consequently, they tended to assign ratings from 2 to 5 in subsequent trials. For the regression model, ratings from 1 to 3 are transformed into zero on the binary scale, while ratings of 4 and 5 are transformed into one. This results in a total of 207 binary data points (9 drive-off profiles and 23 participants) for each dependent variable available

for the regression model.

$$P_{\text{Sportiness}} = \frac{1}{1+e^{-z}} \text{ with } z = -9,978 + 0,301 \cdot x_{\text{Jerk}} + 2,503 \cdot x_{\text{Acc}} \quad (3.1)$$

$$P_{\text{Jerkiness}} = \frac{1}{1+e^{-z}} \text{ with } z = -7,181 + 0,404 \cdot x_{\text{Jerk}} + 1,215 \cdot x_{\text{Acc}} \quad (3.2)$$

$$P_{\text{Comfort}} = \frac{1}{1+e^{-z}} \text{ with } z = 8,293 - 0,591 \cdot x_{\text{Jerk}} - 1,472 \cdot x_{\text{Acc}} \quad (3.3)$$

To predict the evaluations for sportiness, jerkiness, and comfort, regression models are determined, as shown in Equations (3.1), (3.2), and (3.3). Figure 3.5 displays the characteristic maps of the regression models for the dependent variables.

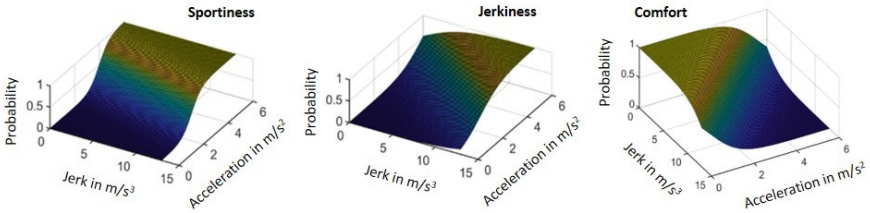


Figure 3.5: Regression models for evaluating drive-off dynamics

For each combination of mean jerk and maximum acceleration, the models provide a probability of a high rating (a value of one is associated with a rating of 100 %). A boundary between high and low ratings of the dependent variable is obtained by examining the intersection of the characteristic maps with the 50 % probability plane. By comparing the characteristic maps, it's also evident that comfort exhibits an opposite trend to jerkiness. The higher the mean jerk and maximum acceleration, the jerkier and less comfortable the drive-offs are perceived by the driver.

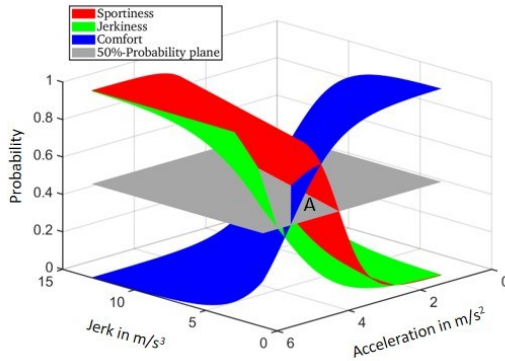


Figure 3.6: Division of the evaluation of the drive-off dynamics

As shown in Figure 3.6, the subjective evaluation of the drive-off dynamics can be divided into several regions using the characteristic map of each criterion and the 50 % probability plane (in gray). The blue area represents the comfort characteristic map, the red one represents the sportiness characteristic map, and the green area represents the jerkiness characteristic map. The region labeled with A which is bound by these three maps and located in the upper half of the diagram, represents combinations of mean jerk and maximum acceleration that result in sporty and comfortable drive-offs. When calibrating a sporty yet comfortable drive-off behavior, choosing a jerk-acceleration combination from this region is preferable. Drive-offs within this region are also rated as non-jerky. If sportiness needs to be further increased, comfort must be reduced, and jerkiness increased.

To validate the applicability of the proposed models, an additional test subject study is conducted using three distinct driving profiles. One of these profiles simulates an exceptionally smooth drive-off, featuring mean jerk and maximum acceleration values beyond the range considered in the regression models. This allows for assessing the accuracy of extrapolation of the models. The characteristic of these drive-off profiles is outlined in Table 3.7.

Table 3.7: Drive-off profiles for the validation of the regression models

Drive-off Profiles	Mean Jerk	Max. Acceleration
1.	3 m/s ³	2.5 m/s ²
2.	7 m/s ³	3.5 m/s ²
3.	9 m/s ³	3.5 m/s ²

In drive-off profile 1, 28 subjects participated, while driving profile 2 involved 30 test subjects, and driving profile 3 had 7 test subjects. Some of the subjects took part in both the test discussed

previously and the validation experiment. Table 3.8 presents a comparison between the experimental results (P_E) and the estimates (P_R) obtained from the regression models. The percentages indicate the probability of high scores (4 or 5 on the rating scale during the test or one on the binary scale) for each criterion.

Table 3.8: Results for validation of the regression models

Drive-off profiles	Sportiness		Jerkiness		Comfort	
	P_E	P_R	P_E	P_R	P_E	P_R
1.	3.6 %	5.6 %	7.1 %	5.1 %	75.0 %	94.5 %
2.	57.1 %	70.9 %	57.1 %	47.5 %	28.6 %	27.0 %
3.	86.7 %	81.6 %	53.3 %	67.0 %	23.3 %	10.2 %

Upon examining the results in Table 3.8, it becomes evident that the regression models correctly capture the overall rating tendencies. However, there are notable discrepancies between the experimental results and the model estimates, especially in the comfort rating for the first and third drive-off profiles, as well as the sportiness rating for the second drive-off profile. These differences can be attributed to the fact that the jerk-acceleration combinations in these regions of the maps have steep gradients. Consequently, small changes in input variables lead to significant variations in estimates. Furthermore, the assessments are influenced by the psychological state of the test subjects and their expectations regarding the drive-offs.

It's important to note that these derived characteristic maps should be used as a reference because different vehicle types may have varying expectations for drive-off behavior. Fine-tuning should be carried out based on individual requirements. Additionally, the test subjects in the simulator were passively involved, making the scenario similar to autonomous driving. When utilizing these characteristic maps for the calibration of an autonomous driving function, it's advisable to prioritize the regions below the 50 % probability plane, where the sporty and jerky driving experience is not noticeable. This approach helps mitigate safety concerns and reduce the perception of jitteriness. This recommendation is based on the study [110] that explored the impact of acceleration and jerk on the autonomous driving experience by examining the correlation of these factors with the heart rate and galvanic skin response. The results revealed that drivers are particularly sensitive to changes in acceleration, represented in this work by the mean jerk.

3.2 Test subject study 2 – Investigation of the response time

Study 2 follows a design and analysis principle comparable to that of study 1 due to the analogous structure between the two studies, both focusing on drive-off dynamics with two influence factors

each. It is carried out with identical study procedures and analysis methods. However, the test subjects are required to initiate the vehicle's acceleration by using the acceleration pedal. The vehicle exhibits different agility for distinct APPs. For this study, the following hypotheses are formulated:

- H1: Response time and APP have an interaction effect for evaluating the drive-off behavior.
- H2: Response time has a significant effect on sportiness, comfort, and agility during drive-off.
- H3: APP has a significant effect on sportiness, comfort, and agility during drive-off.

3.2.1 Design of the test subject studies

Definition of the Drive-off profiles

The drive-off data collected from the test vehicle, which is analyzed in study 1, reveals an average response time of approximately 500 ms. Based on this information, a range of 250 ms to 850 ms for the response time is selected, utilizing intervals of 300 ms to build three levels of this factor. The response time is illustrated in Figure 2.2.

Furthermore, the APP varies at three levels: 20 %, 40 %, and 60 %. This variation in APP aims to align with driver expectations regarding the vehicle response under different inputs of the acceleration pedal. Each APP corresponds to a specific drive-off characteristic with different maximum acceleration and mean jerk. Regarding the identified EDTs in study 1, the EDTs of 0.5 m/s^2 for maximum acceleration and 2 m/s^3 for mean jerk are taken into account in order to create distinct dynamic impressions for APPs. These variations are designed to simulate different vehicle dynamics to meet the expectations of the test subjects. Their characteristics are listed in Table 3.9.

Table 3.9: drive-off characteristics according to the APPs

APP	Max. Acceleration	Mean jerk
20 %	1 m/s^2	2 m/s^3
40 %	1.5 m/s^2	4 m/s^3
60 %	2 m/s^2	6 m/s^3

The combination of the response time and APP levels results in a total of nine distinct drive-off profiles for the test subject study. The characteristics of them are summarized in Table 3.10.

Table 3.10: Variation of the drive-off profiles for study 2

Drive-off Profiles	APP	Response time
1.	20 %	250 ms
2.	20 %	550 ms
3.	20 %	850 ms
4.	40 %	250 ms
5.	40 %	550 ms
6.	40 %	850 ms
7.	60 %	250 ms
8.	60 %	550 ms
9.	60 %	850 ms

Study procedure

This study has an identical procedure, as introduced for test subject study 1, including five phases: introduction, pre-questionnaire, acclimatization phase, test phase, and post-questionnaire. The questionnaire is designed to evaluate agility, sportiness, and comfort. The corresponding questionnaire can be found in Appendix B. Due to the similarity of the questionnaire to the study 1, only the different parts of the questionnaire are shown in the appendix.

During the acclimatization phase, the test subjects initially experience two drive-off scenarios to orient themselves for later evaluations. One of the two drive-off scenarios is very sluggish, with a response time of 850 ms under the APP of 20 %, while another is an agile drive-off with 250 ms under a 60 % APP.

The test subjects start this phase with an explanation text that they are on a country road, waiting at a traffic light. When the light turns green, they will begin driving, using 20 %, 40 %, or 60 % of the APP according to the test leader's decision. They should focus on the initial acceleration phase during this drive. The following acceleration, shifting, or braking phases should not be taken into consideration. Initially, they will experience two such acceleration phases as a reference for the subsequent evaluation. Afterward, they will be asked to assess the drive-off behavior based on the evaluation criteria in Table 3.11, which is also used for the test phase.

Table 3.11 Evaluation criteria for the experienced drive-off

I perceived the drive-off behavior as...						
	1	2	3	4	5	
sluggish	O	O	O	O	O	agile
unsporty	O	O	O	O	O	sporty
uncomfortable	O	O	O	O	O	comfortable

During the test phases, the test subjects experience the nine drive-offs in a random order. After each drive, they have the option to request a repeat or proceed to evaluate the drive-off behavior directly.

3.2.2 Results of the test subject studies

In this study, 31 test subjects participated, all of whom were students from the Department of Mechanical Engineering at the Technical University of Darmstadt. Among these participants, 26 were male, and 5 were female. The age range spanned from 15 to 35 years.

In the following sections, the analysis results of the drive-off evaluations are presented. For starting, descriptive statistics for each drive-off are provided. Subsequently, the examination of the main and interaction effects of the factors is conducted using Wilks-Lambda. Finally, the EDTs in the ratings for agility, sportiness, and comfort are identified through pairwise comparisons with Bonferroni correction. For the analysis, p -Values for the MANOVA and ANOVA and p_{corr} -Value for pairwise comparisons with Bonferroni correction are calculated. These values are used to assess significance by comparing them to a significance level of 0.05.

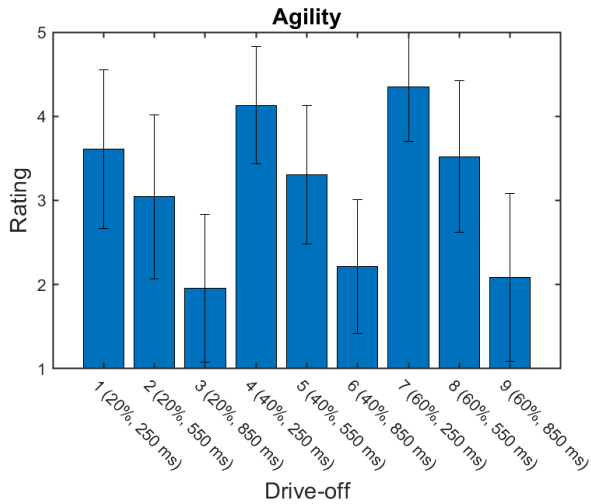


Figure 3.7: Descriptive statistics for drive-off evaluation according to agility in study 2

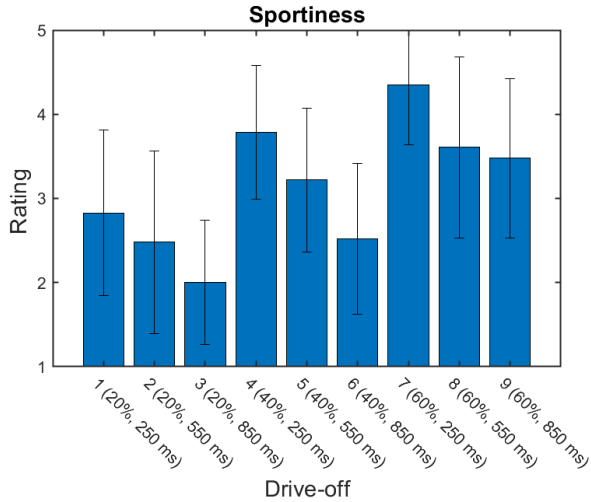


Figure 3.8: Descriptive statistics for drive-off evaluation according to sportiness in study 2

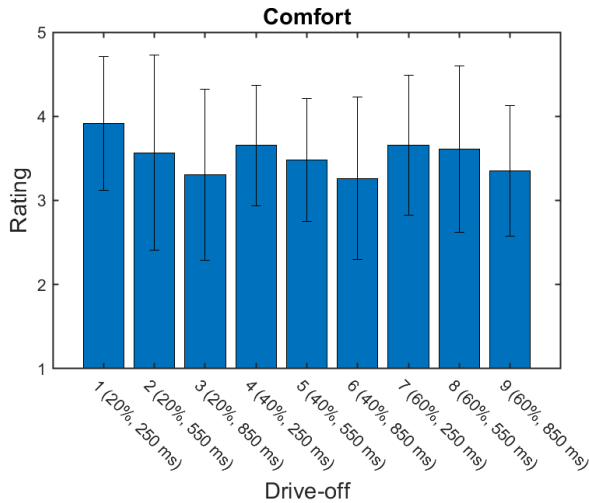


Figure 3.9: Descriptive statistics for drive-off evaluation according to comfort in study 2

Notably, evaluations for agility and sportiness exhibit changing tendencies, whether considering the same APP (e.g., comparing drive-offs 1, 2, and 3) or the same response time (e.g., comparing drive-offs 1, 4, and 7). However, evaluations for comfort across all drive-offs tend to have comparable mean values. A slight trend can be seen in that the rating decreases with increasing reaction time. To assess the influence of these factors, statistical tests are employed in the following analysis.

Table 3.12: MANOVA Multivariate Tests (Wilks-Lambda)

Factor	Significance (<i>p</i> -Value)
Response time	<0.001
APP	<0.001
Response time * APP	0.573

The significance values presented in Table 3.12 indicate that both factors have a statistically significant impact on the evaluations of the drive-offs, with significance values below 0.05. However, there is no observed interaction effect between these factors. The hypothesis H1 is rejected. Then, ANOVA is employed to investigate the influence of each factor on the evaluation criteria separately in order to examine the hypotheses H2 and H3. The results in Table 3.13 show the significant influence of response time on all evaluation criteria, while differing APP levels lead to significantly different evaluations of agility and sportiness only. Thus, the hypothesis H2 is approved, and H3 can be partially approved.

Although Kraft's study [22] shows that the interaction with the accelerator pedal does not affect the evaluation of drive-off behavior regarding sportiness. But this does not indicate a contradiction in the study results, as Kraft's study uses the unchanged values of the maximum acceleration and mean jerk to focus on the influence of interaction with the accelerator pedal without introducing the additional influence of these factors. In comparison, the APPs employed in the current test subject study are characterized by varying maximum acceleration and mean jerk. Thus, the impact of APPs in this work reflects the influence of the maximum acceleration and mean jerk, both of which are already investigated in the test subject study 1.

Table 3.13: ANOVA for investigating the significance of response time and APP

Factor	Criterion	Significance (<i>p</i> -Value)
Response time	Agility	<0.001
	Sportiness	<0.001
	Comfort	0.009
APP	Agility	<0.001
	Sportiness	<0.001
	Comfort	0.181

Despite the differences in APP levels, all drive-offs are featured with relatively small maximum acceleration (up to 2 m/s²) and mean jerk (up to 6 m/s³), providing a uniformly comfortable driving experience with no significant difference in the evaluation of the comfort criteria. It provides a consistent result to study 1, which can be verified with the comfort objectivation model, as shown in Figure 3.6.

To identify the EDTs of the response time while evaluating the drive-off behavior, pairwise comparisons (post-hoc tests) are conducted with Bonferroni correction for adjusting the *p*-Value with *p_{corr}*-Value.

In terms of evaluating agility and sportiness, it's notable that the 300 ms response time level leads to a significant difference across all groups. This suggests that the estimated EDT for response time concerning both criteria is less than 300 ms. Additionally, a significant difference between 250 ms and 850 ms is detected for comfort evaluation, but there are no significant differences between other levels. It implies that the EDT for comfort evaluation falls within the range of 300 ms to 600 ms. However, to pinpoint the precise EDTs, further studies are necessary.

Table 3.14: Pairwise comparisons for identifying the EDTs of response time

Criterion	Response time levels		Significance (p_{corr} -Value)
Agility	250 ms	550 ms	<0.001
	250 ms	850 ms	<0.001
	550 ms	850 ms	<0.001
Sportiness	250 ms	550 ms	<0.001
	250 ms	850 ms	<0.001
	550 ms	850 ms	0.009
Comfort	250 ms	550 ms	0.420
	250 ms	850 ms	0.002
	550 ms	850 ms	0.182

3.3 Test subject study 3 – Investigation of the engine speed changes

In this study, the analysis concentrates on the influence of the variation of the engine speed plateau and flare. Figure 2.1 demonstrates the engine speed curve with this variation as an example. With the prior knowledge from the literature, it is known that the engine sound has an influence on the evaluation of the driving comfort. The sportiness and acceptability serve as additional criteria.

For this study, the following hypotheses are formulated:

- H1: Engine speed plateau and Engine speed flare have an interaction effect for evaluating the drive-off behavior.
- H2: Engine speed plateau has a significant effect on sportiness, comfort, and acceptability during drive-off.
- H3: Engine speed flare has a significant effect on sportiness, comfort, and acceptability during drive-off.

3.3.1 Design of the test subject studies

Definition of the engine speed curve

Based on the drive-off data collected from the test vehicle, the engine speed plateau often occurs at 1500 RPM with medium APPs. To enhance the study duration, this study is also designed with three levels for each factor. In total, nine different engine speed curves are designed and shown in Table 3.15.

Table 3.15: Variation of the engine speed curves for study 3

Drive-off Profiles	Plateau	Flare
1.	1200 RPM	0 RPM
2.	1200 RPM	200 RPM
3.	1200 RPM	400 RPM
4.	1500 RPM	0 RPM
5.	1500 RPM	200 RPM
6.	1500 RPM	400 RPM
7.	1800 RPM	0 RPM
8.	1800 RPM	200 RPM
9.	1800 RPM	400 RPM

Study procedure

With a pre-test on the driving simulator, the test subjects were often disturbed by external noise resources, such as the rail and axle noise when the simulator moved. Therefore, this study is conducted without using the driving simulator but with the recorded video of the driving environment on the screen and the corresponding engine sound to be examined. The test subjects receive the video and evaluate the engine sound on their own computers allowing them to make the evaluation in their preferred environment and at their convenience.

This study also consists of five phases: introduction, pre-questionnaire, adjustment phase, test phase, and post-questionnaire. In the introduction, the study content and objectives are described, and the driving environment is presented. Before the test phase is started, an adjustment phase is necessary, during which the sound level adjustment is performed to ensure that all the test subjects experience the same engine sound level, which also has an influence on the evaluation, according to [111]. During the test phase, the drive-off animation is played with different engine sounds in a randomly arranged sequence. The test subject evaluates the engine sound directly after each drive-off according to the evaluation criteria between the rating 1 and 5, as shown in Table 3.16. Other phases are identical to the previous studies.

Table 3.16 Evaluation criteria for the experienced drive-off

I perceived the drive-off behavior according to the engine sound as...						
	1	2	3	4	5	
unsporty	O	O	O	O	O	sporty
uncomfortable	O	O	O	O	O	comfortable
unacceptable	O	O	O	O	O	acceptable

3.3.2 Results of the test subject studies

In this study, 27 test subjects participated. They were mainly students from the Department of Mechanical Engineering at the Technical University of Darmstadt. Among these participants, 23 were male, and 4 were female.

In the following sections, the descriptive statistics of the engine sound evaluations are presented. Figure 3.10 shows clearly that the evaluations have comparable evaluation ratings between all the variations of the engine speed. In comparison, the ratings for comfort and acceptability show a tendency that the evaluation rating decreases with increasing engine speed flare. The higher the flare, the lower the evaluation. It can be identified in Figure 3.11 and Figure 3.12. Furthermore, the rating for comfort shows an identical rating tendency with the rating of acceptability. It is, however, slightly lower on the scales. The evaluation for comfort arounds at the scale of 3 while the evaluation of acceptable arounds at 3.5. It indicates that the test subjects have a higher tolerance for acceptability.

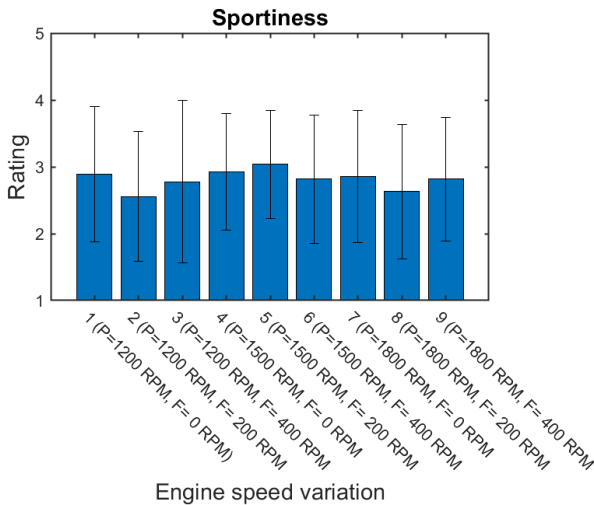


Figure 3.10: Descriptive statistics for engine speed evaluation according to sportiness in study 3

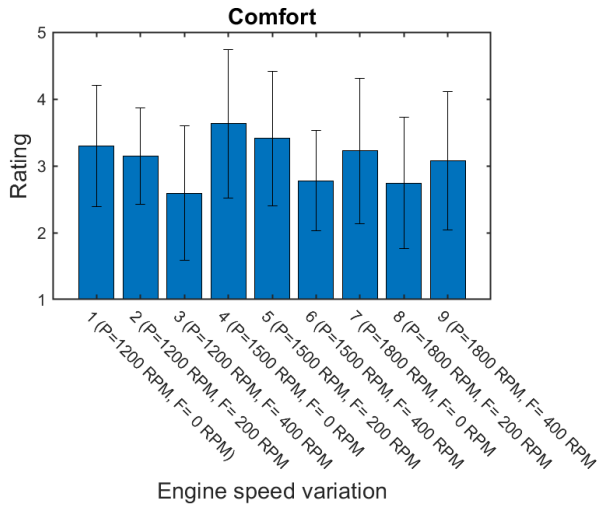


Figure 3.11: Descriptive statistics for engine speed evaluation according to comfort in study 3

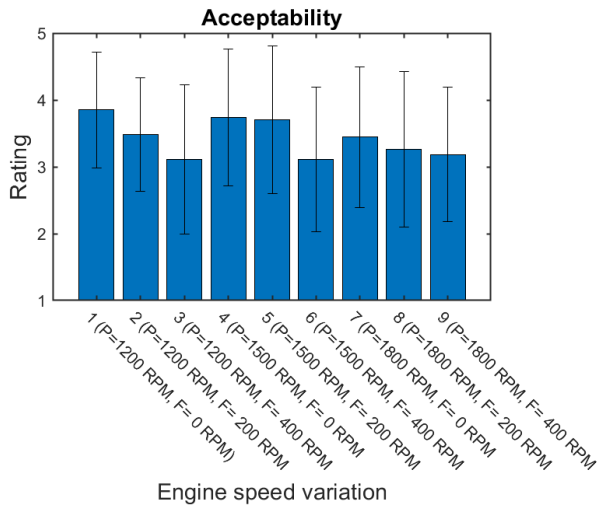


Figure 3.12: Descriptive statistics for engine speed evaluation according to acceptability in study 3

With the help of MANOVA, the significance values for examining the influence of the factors and the interaction effect between them are calculated and shown in Table 3.17. It is determined that

the engine speed flare has a significant influence on the evaluation by comparing the significance value with the significance level of 0.05. Conversely, the influence of the engine speed plateau and the interaction effect between the factors are not significant. This leads to the rejection of hypotheses H1 and H2.

Table 3.17: MANOVA Multivariate Tests (Wilks-Lambda)

Factor	Significance (<i>p</i>-Value)
Engine speed plateau	0.166
Engine speed flare	0.015
Engine speed plateau * Engine speed flare	0.264

In the following, the analysis focuses on the engine speed flare factor. The ANOVA is conducted to examine the influence of this factor on the ratings of the evaluation criteria in more detail. In Table 3.18, the *p*-Values for the evaluation criteria comfort and Acceptability are below the selected significance level of 0.05. It means a significant influence of the engine speed flare on these criteria. There is no significant difference in the evaluation of sportiness. The hypothesis H3 is then partially approved.

Table 3.18: ANOVA for investigating the significance of engine speed flare

Factor	Criterion	Significance (<i>p</i>-Value)
Engine speed flare	Sportiness	0.563
	Comfort	0.003
	Acceptability	0.013

To identify the EDTs of each factor while evaluating the engine speed behavior during drive-offs, pairwise comparisons (post-hoc tests) are conducted. The Bonferroni correction is performed to adjust the *p*-Value with p_{corr} -Value. A significance level of 0.05 is used to assess significance in all tests.

Table 3.19: Pairwise comparisons for identifying the EDTs of engine speed flare

Criterion	Engine flare levels		Significance (p_{corr} -Value)
Sportiness	0 RPM	200 RPM	1
	0 RPM	400 RPM	1
	200 RPM	400 RPM	1
Comfort	0 RPM	200 RPM	0.184
	0 RPM	400 RPM	0.001
	200 RPM	400 RPM	0.266
Acceptability	0 RPM	200 RPM	0.561
	0 RPM	400 RPM	0.002
	200 RPM	400 RPM	0.127

Regarding to the sportiness evaluation, the engine speed flare does not show significant influence. In terms of evaluating comfort and acceptability, it's notable that the test subject can perceive the difference in speed flare of 400 RPM. When comparing the engine speed flare difference of 200 RPM, there is not significant difference. It means that the EDTs for comfort and acceptability are greater than 200 RPM, but smaller than 400 RPM.

3.4 Conclusion for the results of the test subject studies and the limitations

With the help of these test subject studies, the driving dynamics and ride comfort-related influence factors are investigated in the context of the drive-off behavior. Using statistical tests, the significant influence of these factors on the evaluation criteria is examined and summarized below:

- Maximum acceleration has a significant effect on sportiness and comfort evaluation during drive-off but no effect on jerkiness.
- Mean jerk has a significant effect on sportiness, comfort, and jerkiness during drive-off.
- Response time has a significant effect on sportiness, comfort, and agility evaluation during drive-off.
- Engine speed flare has a significant effect on comfort, and acceptability evaluation during drive-off but no effect on sportiness.


Furthermore, the EDTs of these factors are determined to identify the necessary change that can result in a significantly different evaluation of the drive-off behavior. Based on the results presented, a range for the EDT of each factor is identified and shown in Table 3.20.

Table 3.20: EDT ranges for the influence factors

Criterion	Max. acceleration	EDT
Sportiness	<3 m/s ²	≤ 0.5 m/s ²
	>3 m/s ²	> 0.5 m/s ²
Jerkiness	Between all levels	No significance
Comfort	Between all levels	>0.5 m/s ² & ≤1 m/s ²
Criterion	Mean jerk	EDT
Sportiness	<7 m/s ³	>2 m/s ³
	>7 m/s ³	≤2 m/s ³
Jerkiness	<7 m/s ³	>2 m/s ³
	>7 m/s ³	≤2 m/s ³
Comfort	<7 m/s ³	>2 m/s ³
	>7 m/s ³	≤2 m/s ³
Criterion	Response time	EDT
Agility	Between all levels	<300 ms
Sportiness	Between all levels	<300 ms
Comfort	Between all levels	>300 ms & ≤600 ms
Criterion	Engine speed flare	EDT
Sportiness	Between all levels	No significance
Comfort	Between all levels	>200 RPM & ≤400 RPM
Acceptability	Between all levels	>200 RPM & ≤400 RPM

For maximum acceleration, the analysis suggests that differences in acceleration values of 0.5 m/s² can lead to significantly different sporty evaluations when the acceleration is below 3 m/s². When the acceleration increases beyond 3 m/s², only an acceleration difference greater than 0.5 m/s² can lead to different perceptions. The perception is more sensitive for evaluating the sportiness than evaluating the comfort. For mean jerk, the analysis indicates that differences in jerk values of greater than 2 m/s³ can be perceived as significant in the small jerk area (below 7 m/s³). However, in the large jerk area (above 7 m/s³), even small differences can become noticeable. This is valid for the evaluation of sportiness, comfort, and jerkiness.

It is noticeable that there is a difference in perception threshold tendency between the maximum acceleration and mean jerk. Maximum acceleration has a logarithmic tendency between the difference threshold of the perception and the stimulus intensity, where perception becomes less sensitive as acceleration increases. It matches the Weber-Fechner Law, which employs a



logarithmic psychophysical function, describing a decreasing sensitivity with increasing stimulus strength. On the other hand, jerk has an opposite tendency, where in the small jerk area, the perception is less sensitive, but in the large jerk area, it becomes more sensitive to small differences. Stevens's Power Law offers an explanation for the limited applicability of the Weber-Fechner Law to human perception. In comparison, Stevens's Power Law indicates an increasing slope for certain stimuli, signifying that the sensory organ becomes more sensitive as the stimulus strength grows [109].

Additionally, Table 3.20 also shows the EDT ranges for the response time and the engine speed flare. Compared to the comfort evaluation, the response time for the evaluation of agility and sportiness is more sensitive. The EDTs for these two criteria are below 300 ms. The EDTs of the engine speed flare are between 200 RPM and 400 RPM for comfort and acceptability evaluation. These findings are further considered in the powertrain modeling to orientate towards a comfortable calibration of the drive-off behavior.

There are several limitations to these test subject studies. Firstly, all studies are conducted either in the laboratory using a driving simulator or on a computer with synthetically generated engine sounds. It should be noted that the experimental conditions may not account for all influencing factors. This limitation is particularly relevant to the issue of presence and the degree of immersion in a simulated test environment. However, investigating these aspects is beyond the scope of this work. A study on this topic has been undertaken by Kraft in his doctoral thesis [22].

Another limitation relies on the challenge of accurately determining the EDTs. The EDT is referred to as a relative threshold, and its determination relies on comparing different factor levels. The increase in the number of factor levels leads to an exponential rise in the number of test signals, resulting in a longer test duration. Extended test duration is associated with an increased risk of driving simulator sickness and increased physical and mental demands, which directly influence the subjective perception of the drive-off behavior. To mitigate this, nine variations of the test signals are consistently used in all studies. Through this, the total test duration can be limited to 40 minutes, which is acceptable according to the post-questionnaire results. However, for a precise determination of the EDTs, additional experiments are required.

The third limitation of the test subject studies is related to the composition of the test samples. Most of the participants are students from the Technical University Darmstadt, aged between 20 and 35 years. This demographic specificity introduces a potential bias in terms of a sensitive sensory system, as individuals in this age range may have heightened sensitivity and a more acute ability to detect test signals compared to older individuals. This could impact the generalizability of the study findings to a broader population, particularly those with different age groups or sensory sensitivities.

4 Powertrain model for ecological evaluation

The simulation model is constructed based on the previously introduced P2.5 hybrid powertrain configuration outlined in Section 2.2. Building upon this foundation, the primary focus of the model centers around the longitudinal driving dynamics and the simulation of the drive-off procedure. Unlike PHEVs, MHEVs do not have an additional power source to charge the battery. Consequently, the battery in MHEVs must be recharged either by the ICE during driving or through recuperation during deceleration. To address this, the model must be able to follow driving cycles, such as the WLTC, for consideration of energy recuperation. In the following, an introduction is given, starting with the component modeling, followed by the thermal model and the degradation model for the clutch system, and the description of the control module. This chapter concludes with the analysis of the simulation correctness. The powertrain modeling and correctness analysis were based on the student work [112].

4.1 Foundational modeling principle

According to [47], the forward approach is typically employed in conventional simulators. In this method, the desired speed derived from driving cycle inputs is compared to the actual vehicle speed. Commands for braking or throttle are generated utilizing a driver model, such as based on a PID speed controller. These commands serve as inputs for the supervisor block, which determines the setpoints for various actuators (engine, electric machines, and braking torques). These actuators, in turn, produce the traction force necessary for the vehicle's movement. This force is applied to the vehicle dynamics model, determining the acceleration and the vehicle speed with consideration of road load information. Additionally, the forward approach simulates the vehicle dynamics accounting for powertrain limitations. This makes it suitable for testing the system's behavior under saturation conditions and for acceleration tests. However, it introduces deviations between the actual and desired driving cycles, which requires careful tuning of the driver model to minimize the deviation.

In contrast, the backward simulation functions differently. Here, no driver model is needed as the desired speed directly feeds into the simulation model. Backward simulation ensures precise adherence to predetermined driving cycles. Outputs of the model include engine torque and fuel consumption. The model calculates the traction force required based on velocity, payload, grade profiles, and vehicle characteristics. According to the traction force, the powertrain's necessary torque is determined. The torque/speed characteristics of different powertrain components are considered to establish engine operating conditions and, subsequently, fuel consumption. The backward approach assumes that the vehicle and powertrain can perfectly follow the speed profile, neglecting powertrain limitations. This can be problematic for evaluating demanding cycles that

may exceed the powertrain's capabilities.

A hybrid approach combines the advantages of both simulation approaches. It employs a forward simulation approach for the drive-off phase, and backward simulation instead of a driver model is used to simulate the post-drive-off phase in order to ensure that the resulting speed profile precisely matches the reference driving cycle. This hybrid approach offers a robust method for evaluating the drive-off behavior, considering both powertrain limitations and cycle accuracy. Figure 4.1 provides an illustrative overview of the P2.5 HEV model and its corresponding control module.

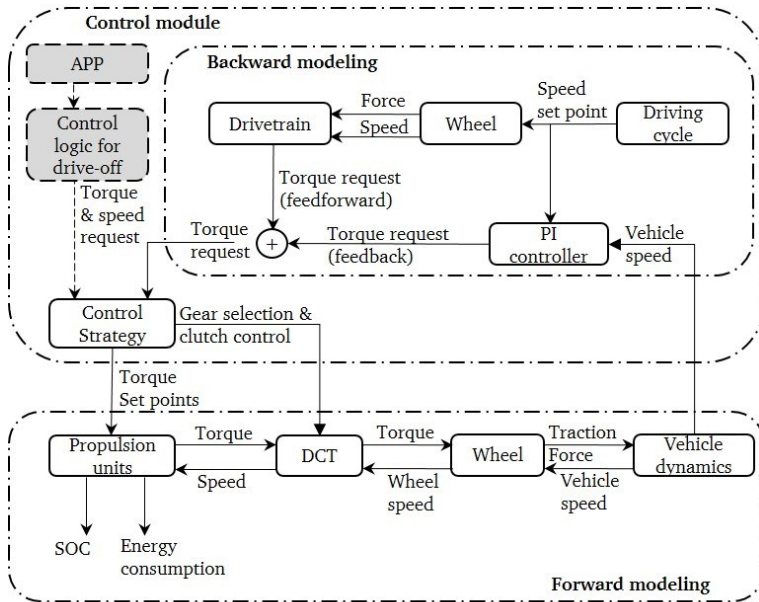



Figure 4.1: Overview of the P2.5 HEV model and control module, information flow for the drive-off procedure, and subsequent driving

During the drive-off phase, a drive-off control logic governs the procedure, determining torque and speed requests based on APP inputs. These requests are applied to the control strategy, which encompasses a clutch control logic that is responsible for gear selection and clutch actuator control and an EMS that computes torque set points for both the ICE and EM. The calculated torque set points are then channeled into a forward modeling approach, which replicates vehicle dynamics, power distribution, driving load, and energy consumption. This forward simulation provides detailed insights into drive components' behavior and limitations and calculates traction forces, which interact with the vehicle dynamics model. This dynamic system computes wheel torque and resultant vehicle acceleration.



In the post-drive-off phase, a backward simulation takes charge of ongoing vehicle operations. The vehicle's speed, derived from the vehicle dynamics model, feeds back into the backward simulation. Within this, the speed deviation between the target and current vehicle speed is determined. This deviation serves as input for a Proportional-Integral (PI) controller. The controller calculates an additional feedback torque, supplementing the torque request from the backward simulation, aimed at correcting the speed deviation in the subsequent time step. The refined torque request becomes the input for the control strategy, supplanting the outputs from the drive-off control logic. This iterative feedback mechanism guarantees the vehicle's precise adherence to the driving cycle. This backward simulation approach, which is consistent with a prior study [103] based on [47], ensures an accurate tracking of the driving cycle. The parameters and properties of the powertrain components are oriented towards a Mini Clubman from BMW and are listed in Table 4.1.

Table 4.1: The component parameters and properties for the vehicle simulation model

Parameters and properties		
ICE	Engine type	SI engine
	Max. engine torque	349 Nm
	Max. engine speed	7500 RPM
	Crankshaft inertia moment	0.1772 kgm ²
EM	Max. EM torque	25.3 Nm
	Max. EM speed	12000 RPM
	Max. power	15 kW
Battery	Total capacity	0.48 kWh
	Voltage	48 V
	Initial SOC	50 %
	Battery efficiency	0.98
Transmission	Transmission type	7-speed DCT
	Gear ratio with final drive ratio	$i_1 = 14.736$ $i_2 = 10.100$ $i_3 = 5.402$ $i_4 = 4.245$ $i_5 = 3.190$ $i_6 = 2.815$ $i_7 = 2.280$
	Gear ratio for EM	$i_{EM} = 2.8$
	Efficiency	0.95
Clutch	Mean friction radius	$r_{m, Odd} = 92.47$ mm $r_{m, Even} = 69.85$ mm
	Friction surfaces number	$z_{Odd} = 6$ $z_{Even} = 8$
	Heat capacity of steel plate	490 J/(kg*K)
	Heat capacity of friction oil	1570 J/(kg*K)
Vehicle	Mass	1620 kg
	Height of center of gravity	0.534 m
	Front axis to center of gravity	1.05 m
	Rear axis to center of gravity	1.68 m
	Air density	1.25 kg/m ³
	Frontal projection area	1.6 m ²
Aerodynamic drag coefficient	0.39	

4.2 Powertrain component modeling

The component modeling follows a kinematic chain within the powertrain, as illustrated in the forward modeling block of Figure 4.1. It begins with modeling the propulsion units, followed by the description of the DCT. The research in this work primarily focuses on the powertrain's performance. It does not delve into powertrain vibrations resulting from factors like compression/expansion torque and combustion torque during engine operation. Consequently, a Dual Mass Flywheel (DMF) between the engine and the clutch, typically used to reduce the impact of irregular engine torque on the remainder of the powertrain, is neglected in the simulation. Following the DCT modeling, the tire model and vehicle dynamics model are introduced.

4.2.1 Propulsion Units

An ICE, an EM including an inverter, and a battery are the main propulsion units that should be simulated. In a dynamic system, the static mapped modeling approach is widely used because of the simulation efficiency. The propulsion units mentioned above are implemented mainly through the lookup table-based models, which provide sufficient accuracy in performing efficiency analysis according to [113].

ICE modeling

The ICE model contains two main sub-models: a mapped spark-ignition (SI) engine model from the Matlab/Simulink® built-in library using lookup tables (LUTs) and a crankshaft dynamics model. To adapt the Simulink library data into the model, upscaling is performed to adjust the data to fit the desired torque and speed ranges for the simulation. The LUTs are implemented as a series of 2-D LUTs with inputs including the ICE command torque $T_{ICE,ctrl}$, and the actual engine speed $n_{ICE,act}$, the model generates outputs including the engine's actual output torque T_{ICE} and the fuel mass flow \dot{m}_{fuel} . The actual output torque of the ICE covers the engine drag torque due to friction losses and the maximum torque the engine can provide. Figure 4.2 illustrates the LUTs. To account for the response delay between the torque command and the engine output torque, a first-order delay block (PT1 block) is implemented after the model's actual torque output.

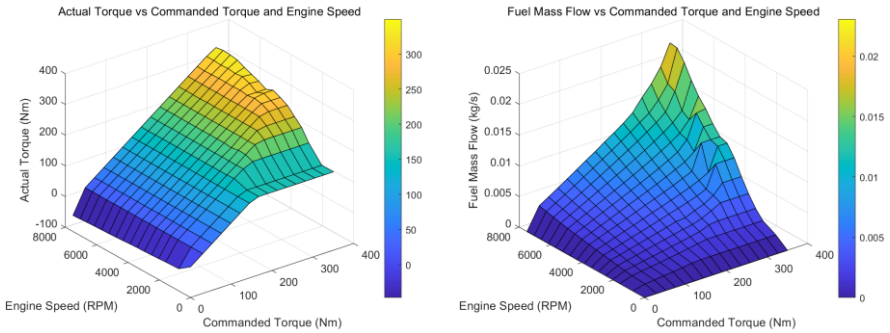


Figure 4.2: LUTs from the Simulink® library for the simulation of the engine torque and fuel mass flow

The brake-specific fuel consumption (BSFC) map is a measure of the fuel efficiency of an engine. It quantifies the rate of fuel consumption in relation to the power produced, usually expressed in units of with units of grams per kilowatt-hour (g/kWh). This map is a visual representation of fuel consumption rates across various operating conditions, determined by engine speed and torque. Figure 4.3 illustrates the BSFC map of the utilized ICE, offering insight into the engine's performance characteristics.

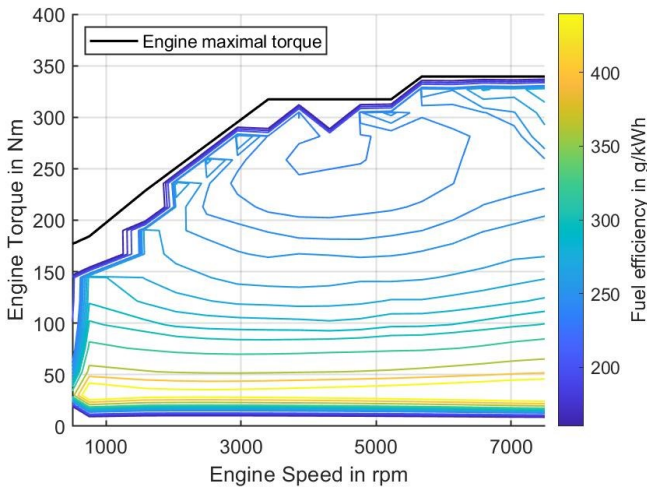


Figure 4.3: The brake-specific fuel consumption

This work simplifies the crankshaft by modeling it as a rigid shaft. This representation transforms it into a first-order dynamical system, effectively reducing computational complexity. Given the reference driving speed, the ICE rotation speed depends on the clutch-locked state. The viscous resistance, which is proportional to the engine speed, is also considered in this work. When the clutch is slipping or disengaged, the engine speed ω_{ICE} can be described as:

$$J_{Cs} \cdot \dot{\omega}_{ICE} = (T_{ICE} - T_{Cl, fdbk}) - D_{Cs} \cdot \omega_{ICE} \quad (4.1)$$

where J_{Cs} is crankshaft inertia, D_{Cs} is the viscose damping coefficient, T_{ICE} is the engine output torque and $T_{Cl, fdbk}$ is the feedback torque from the clutch.

When the clutch is engaged, the engine speed is the same as the clutch shaft speed $\omega_{Cl, Odd/Even}$:

$$\omega_{ICE} = \omega_{Cl, Odd/Even} \quad (4.2)$$

EM and battery modeling

The EM Efficiency map utilized in this work is derived by scaling the empirical data obtained from a test bench at IMS. An electric powertrain, including an EM and a 2-speed manual transmission, is mounted on this test bench to measure the efficiency of the motor and gearbox separately or in combination. The efficiency characteristics used in this work is illustrated in Figure 4.4 for understanding its performance. The black lines delineate the torque boundaries. The current in the EM, denoted as I_{EM} , can be calculated using Equation (4.3).

$$I_{EM} = \frac{T_{EM} \cdot \omega_{EM}}{V_{EM} \cdot \eta_{EM}^{\text{sign}(T_{EM})}} \quad (4.3)$$

where T_{EM} is the motor's output torque, ω_{EM} its speed, V_{EM} is the DC output voltage of the battery acting on the inverter of EM and η_{EM} is the combined efficiency of EM and inverter. A negative sign of the motor torque means that the electric motor works as a generator and the battery is charged.

The connection between the EM and the transmission's second input shaft is considered rigid and has a fixed ratio i_{EM} .

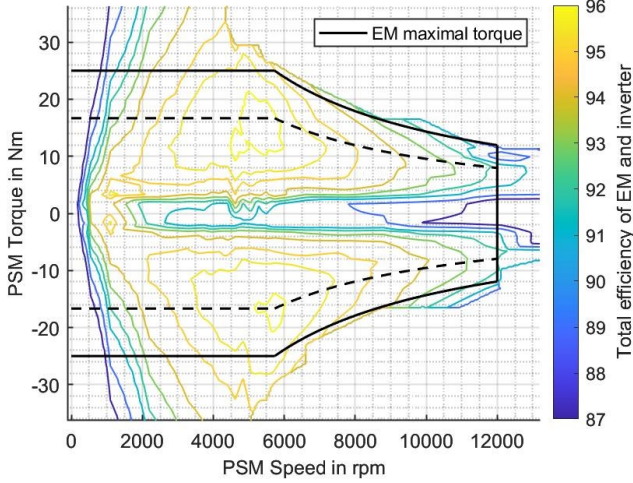


Figure 4.4: Efficiency map of EM including an inverter

The traction battery exhibits a time-varying characteristic with a complex nonlinear behavior, influenced by factors such as temperature, internal resistance, state of charge (SOC), and voltage [114]. For this work, the battery model is built based on the open circuit voltage curve and its internal resistance map, illustrated in Figure 4.5. The temperature influences on the battery performance are modeled with a LUT, as shown on the right side of Figure 4.5. It provides the possibility to set the working temperature at different levels. A detailed thermal model for the battery is not considered. The internal temperature of the battery is set at 300 Kelvin in this work. The current $I_{\text{Batt}}(t_n)$, voltage $V_{\text{Batt}}(t_n)$, and $\text{SOC}(t_n)$ can be described with the following equations:

$$I_{\text{Batt}}(t_n) = \frac{V_{\text{EM}}(t_n) \cdot J_{\text{EM}}(t_n) \cdot \text{sign}(I_{\text{EM}}(t_n))}{V_{\text{Batt}}(t_{n-1}) \cdot \eta_{\text{Batt}}} \quad (4.4)$$

$$V_{\text{Batt}}(t_n) = V_{\text{Batt,oc}}(t_n) - R_{\text{Batt}}(t_n) \cdot I_{\text{Batt}}(t_n) \quad (4.5)$$

$$\text{SOC}(t_n) = \frac{Q_{\text{Batt,init}} - \sum_{i=1}^n I_{\text{Batt}}(t_i) \cdot \Delta t}{Q_{\text{Batt}}} \quad (4.6)$$

Where Δt refers to the simulation step size, representing the time interval between two successive time points t_n and t_{n-1} . $V_{\text{Batt,oc}}(t_n)$ is the circuit voltage at time point t_n , $V_{\text{Batt}}(t_n)$ battery voltage, $R_{\text{Batt}}(t)$ internal resistance, Q_{Batt} battery capacity, and η_{Batt} its efficiency. The index *init* refers to the initial state of the battery capacity.

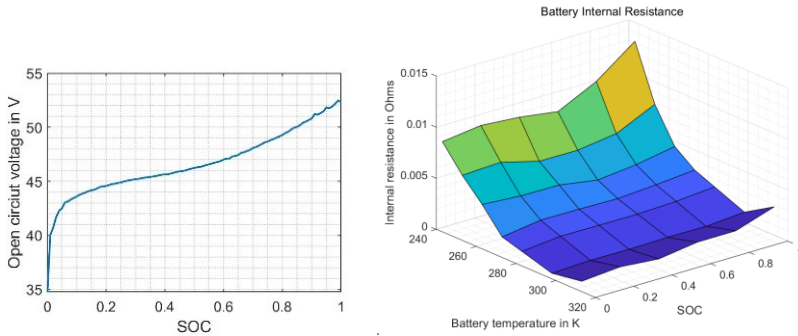


Figure 4.5: Open circuit voltage (left) and internal resistance of the battery model (right)

4.2.2 DCT Modeling

The simulated DCT consists of a dual-clutch system including inner and outer clutches, a gearbox (seven forward gear sets, one reverse gear), and synchronizers. Gear sets are taken into account in terms of gear ratios while modeling with a gearwheel model is omitted. The efficiency for each gear is maintained constant, and the transmission shafts are simulated as rigid. The viscous resistance is considered. The focus of this work lies on simulating the clutch behavior.

Clutch operating states and friction torque determination

This section focuses on the dynamics modeling according to the clutch operating states, i.e., the disengaged (unlocked), engaging (slipping), and engaged (locked) states. The engaged state refers to a clutch operating condition where the friction plates spin together as a unit. In this state, the clutch has only one rotational degree of freedom and does not have power losses due to friction. On the other hand, the engaging state represents a scenario where the friction plates slip with respect to each other. In this condition, the clutch has two rotational degrees of freedom. Power losses occur and are quantified as the product of the slip velocity and the kinetic friction torque. To determine the state changing between engaged and engaging states, the following switch conditions are employed:

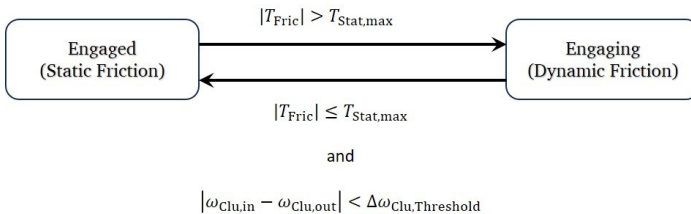


Figure 4.6: Switch condition for the clutch operating states

In order to change the state from engaging to engaged, the clutch input and output plate speed must be the same, and the transmitted friction torque T_{Fric} must be smaller than or equal to the static torque $T_{\text{Stat},x}$ in the clutch, which is calculated by using Equation (4.7).

$$T_{\text{Stat},x} = r_{m,x} \cdot z_x \cdot \mu_s \cdot F \quad (4.7)$$

If the friction torque exceeds the static torque, the clutch begins slipping. With respect to computational performance regarding zero velocity and the non-necessity to switch between engaged and engaging states, a Karnopp model is adopted [115]. In this model, the crankshaft speed ω_{ICE} is equal to the clutch input plate speed $\omega_{\text{Clu},\text{in},x}$, and the clutch input shaft speed is equal to the clutch output plate speed $\omega_{\text{Clu},\text{out},x}$. The strict condition of detecting zero speed difference is solved by defining an interval limit $\Delta\omega_{\text{Clu},\text{Threshold}}$. It is assumed that the output is maintained at zero when the speed difference is within the limit, as described in Equation (4.8). With a larger interval limit, the numerical stability increases, and the simulation becomes faster. However, it should not be chosen too large to maintain the simulation quality.

$$\text{if } |\omega_{\text{Clu},\text{in},x} - \omega_{\text{Clu},\text{out},x}| < \Delta\omega_{\text{Clu},\text{Threshold}}, \text{ then } \Delta\omega_{\text{Clu},x} = \omega_{\text{Clu},\text{in},x} - \omega_{\text{Clu},\text{out},x} = 0 \quad (4.8)$$

In the engaging state, the clutch represents a system with two degrees of freedom, as shown in Figure 4.7:

$$J_{\text{Clu},\text{in},x} \cdot \dot{\omega}_{\text{Clu},\text{in},x} = T_{\text{Clu},\text{in},x} - T_{\text{Fric},x} \quad (4.9)$$

$$J_{\text{Clu},\text{out},x} \cdot \dot{\omega}_{\text{Clu},\text{out},x} = T_{\text{Fric},x} - T_{\text{Clu},\text{out},x}$$

The clutch friction torque during engaging is calculated with:

$$T_{\text{Fric},x} = r_{m,x} \cdot z_x \cdot \mu_x \cdot F_x \cdot \text{sign}(\Delta\omega_{\text{Clu},x}) + \mu_{\text{vis}} \cdot \Delta\omega_{\text{Clu},x} \cdot r_{m,x} \quad (4.10)$$

where the μ_x is the dynamic friction coefficient for odd or even friction plates, μ_{vis} is the viscous friction coefficient, $\Delta\omega_{\text{Clu},x}$ is the sliding speed between the clutch input and output plates.

The estimation of CoF can be achieved through various friction models, such as the Stribeck model and LuGre model [116]. These models calculate the CoF, which is essential for estimating the friction torque. In this work, a characteristic map for CoF estimation is generated by using the durability testing data, which is introduced in Section 4.3.2.

In the engaged state, the clutch input plate speed $\omega_{Clu, in, x}$ is equal to the clutch output plate speed $\omega_{Clu, out, x}$. By using this condition in Equation (4.9), the friction torque can be derived. Considering the switch condition shown in Figure 4.6, the friction torque is formulated as follows:

$$T_{Fric, x} = \min \left(\frac{J_{Clu, in, x} \cdot T_{Clu, out, x} + J_{Clu, out, x} \cdot T_{Clu, in, x}}{J_{Clu, in, x} + J_{Clu, out, x}}, T_{Stat, x} \right) \quad (4.11)$$

where the index x refers to the odd or even clutch respectively, $J_{Clu, in, x}$ and $J_{Clu, out, x}$ refer to the inertia of the clutch input and output sides, $T_{Clu, in, x}$ and $T_{Clu, out, x}$ refer to the clutch input and output shaft torques. $r_{m, x}$ is the mean friction radius in the friction disc, z_x is the number of friction surfaces, μ_s represents the static friction coefficient, and F is the actuator force acting on the clutch discs.

When the clutch is disengaged, the transmitted friction torque T_{Fric} is zero.

Torque transfer

The following figure illustrates a reduced DCT model, aiming to show the torque flow within the transmission. The input torque for the clutch is generated by the engine, serving as the primary torque source that drives the entire drivetrain.

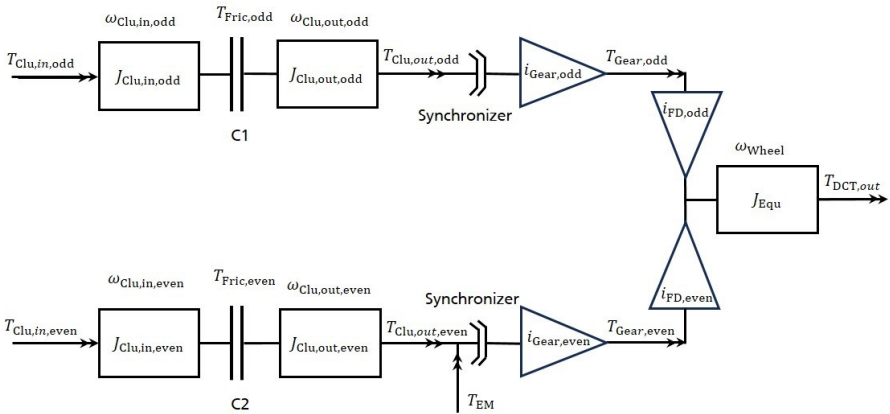


Figure 4.7: Torque transfer within the DCT

The DCT output torque $T_{\text{DCT, out}}(t)$ can be calculated as follows:

$$T_{\text{DCT, out}} = \eta_{\text{DCT}} \cdot (T_{\text{Gear, Odd}} \cdot i_{\text{FD, Odd}} + T_{\text{Gear, Even}} \cdot i_{\text{FD, Even}}) - D_{\text{Vis, Diff}} \cdot \omega_{\text{Wheel}} - J_{\text{Equ}} \cdot \dot{\omega}_{\text{Wheel}} \quad (4.12)$$

$$T_{\text{Gear, Odd}} = (T_{\text{Clu, in, odd}} - D_{\text{Vis, Clu}} \cdot \omega_{\text{Clu, out, odd}}) \cdot i_{\text{Gear, Odd}} \quad (4.13)$$

$$T_{\text{Gear, Even}} = (T_{\text{Clu, in, even}} - D_{\text{Vis, Clu}} \cdot \omega_{\text{Clu, out, even}} + T_{\text{EM}} \cdot i_{\text{EM}}) \cdot i_{\text{Gear, Even}} \quad (4.14)$$

where $T_{\text{Gear, x}}$ is the torque of the inter shaft, $D_{\text{Vis, Diff}}$ the effective damping coefficient in the differential, J_{Equ} the equivalent inertia consisting of the differential inertia and the reduced inertia of the gearbox on the differential, $i_{\text{FD, x}}$ the final drive gear ratio, $i_{\text{Gear, x}}$ the transmission gear ratio, ω_{Wheel} the wheel speed, and η_{DCT} the DCT efficiency defined as a constant.

Synchronizer

Similar to the clutch system, the synchronizer also uses a Karnopp model for zero velocity detection and the detection principle, as shown in Figure 4.6, for engaging and engaged operation states. It is simplified with a PID controller based on the speed deviation without modeling a dog clutch. In addition, it involves a reset function to determine whether the synchronizer is activated or not. The generated dynamic torque is saturated with a low value. The maximal transferable static torque is set very high in order to keep the synchronizer closed when the speed difference is within the interval limit. Once the synchronizer is engaged, it can be integrated into the inter shaft, as can be seen in Figure 2.3. The control sequence of the synchronizer and clutch is dependent on the shifting scenarios, such as upshifting or downshifting. During a drive-off procedure, the synchronizer remains engaged.

Hydraulic system

The hydraulic system is responsible for actuating the piston, which applies pressure on the clutch plates against a compression spring. This action generates a normal force on the contact surfaces of the clutch plates, enabling the generation of friction torque. The friction torque is essential for the synchronization of the clutch. In the simulation model, the hydraulic system is controlled by a PID controller, which uses the speed deviation between the clutch input plates and output plates as its input. This speed deviation serves as an error signal that the PID controller processes to adjust the hydraulic pressure applied to the piston. To simulate the response delay characteristic of the actual hydraulic system, a first-order delay element is deployed. This hydraulic system response is utilized to calibrate the vehicle's response time. Because the response time doesn't have a direct impact on the ecological evaluation criteria, the fuel consumption, and thermal load in the clutch. Therefore, this response time is maintained as a constant parameter. Based on the identified

EDTs from the test subject study 2, a drive-off response time of 250 ms is adopted in this work to represent the comfort reaction time of the vehicle.

Differential

The differential transfers torque from the gearbox subsystem to the wheel dynamics model, allowing rotation of wheels at different speeds. In the current P2.5 HEV model, the vehicle is a front-wheel drive, which indicates that the drive torque from the DCT is equally distributed between the two front wheels.

4.2.3 Wheel modeling

The wheel model provides a fundamental aspect for simulating vehicle dynamics and comprises four main parts: a wheel dynamics model, an advanced slip ratio (ASR) calculation, a rolling resistance calculation, and a tire model. Figure 4.8 shows the overview of the wheel model, including the signal flow.

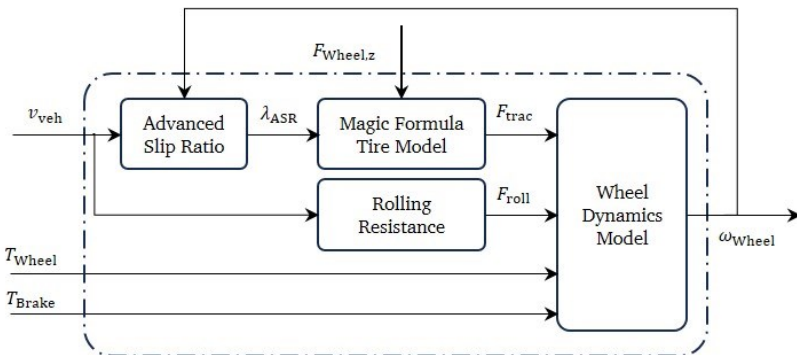


Figure 4.8: Overview of the wheel model [112]

The wheel dynamics model consolidates all torques acting on the half-axes, reconstructing the wheel speed generation process through dynamic modeling. In parallel, the tire model translates wheel motion into ground friction, driving the vehicle forward through the generated traction. The ASR is a slip rate calculation method for the Magic Formula tire model, and its deployment avoids numerical stiffness problems at large simulation step sizes [117].

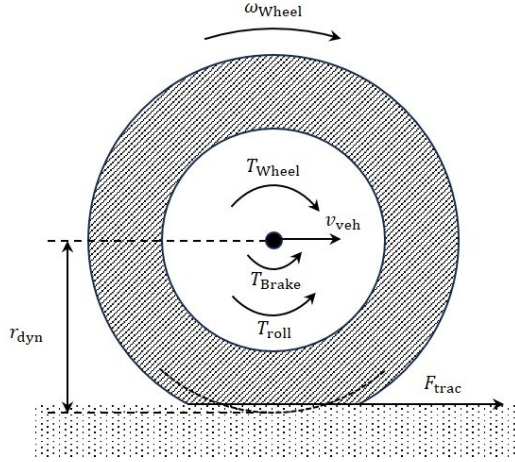


Figure 4.9: Schematic illustration of the wheel dynamics

For this work, a 1-DOF wheel model, which accounts for the rotation dynamics, is sufficient. This choice is due to the dominance of longitudinal dynamics during the drive-off procedure. Figure 4.9 shows a schematic representation of the wheel dynamics with force and torque acting on the wheel. The wheel rotation speed $\omega_{\text{Wheel}}(t)$ can be calculated by balancing the torque around the wheel rotation axis, as described in Equation (4.15).

$$\dot{\omega}_{\text{Wheel}} = \frac{T_{\text{Wheel}} - T_{\text{Brake}} - T_{\text{roll}} - r_{\text{dyn}} \cdot F_{\text{trac}}}{J_{\text{Wheel}}} \quad (4.15)$$

where J_{Wheel} is the wheel inertia, T_{Wheel} the drive torque from the differential, T_{Brake} the brake torque on brake discs, r_{dyn} the dynamic radius of the wheel, T_{roll} the rolling resistance torque and F_{trac} the traction force, which is calculated by the Magic Formula tire model.

The rolling resistance torque T_{roll} is mainly due to the deformation of the tire and the dissipation of energy through friction [118]. It can be calculated with Equation (4.16).

$$T_{\text{roll}} = F_{\text{roll}} \cdot r_{\text{dyn}} = \mu_{\text{roll}} \cdot F_{\text{Wheel},z} \cdot r_{\text{dyn}} \quad (4.16)$$

with

$$\mu_{\text{roll}} = a_{\text{roll}} + c_{\text{roll}} \cdot v_{\text{veh}}$$

where F_{roll} is the rolling resistance from all the wheels, which can be calculated with vertical force on the wheel $F_{\text{Wheel},z}$ and rolling resistance coefficient μ_{roll} . The vertical force is calculated in the vehicle dynamics model, and the rolling resistance coefficient is expressed as a polynomial function

depending on vehicle velocity v_{veh} and empirical coefficient a_{roll} and c_{roll} .

To ensure numerical stability and increase the computational efficiency of the simulation, this work deployed an ASR method that allows for stable simulations at a large time step based on [117]. The slip rate λ_{ASR} can be described with Equations (4.17) and (4.18). Thereby \bar{v}_m introduces a minimum margin velocity.

$$\lambda_{ASR} = \frac{r_{dyn} \cdot \omega_{Wh} - v_{veh}}{\max(|v_{veh}|, \eta_m \cdot \bar{v}_m)} \quad (4.17)$$

$$\bar{v}_m = \tau_m C_\lambda \left(\frac{r_{dyn}^2}{J_{Wh}} + \frac{1}{m_{veh}} \right) \quad (4.18)$$

where τ_m is the marginal time constant of the explicit Euler method related to the simulation step size, C_λ the longitudinal slip stiffness, m_{veh} the mass of the vehicle, and η_m a safety coefficient to prevent marginal instability.

The Magic Formula, also known as Pacejka tire model [119], is widely used for vehicle dynamics simulations. It is easy to implement and has a high computational efficiency. The Magic Formula has usually two parts: a static part that represents the static tire behavior and a dynamic part that simulates the transient tire behavior under dynamic loading variations [120]. To accurately simulate the construction of the tractive force on tires, this work employs a simplified Magic Formula based on references [119] and [121]. The suspension modeling of the wheels has been omitted to reduce the simulation complexity because this work does not investigate the vertical dynamics of the vehicle body. As a consequence, the camber angle from the Magic Formula is excluded. The specific Magic Formula employed in this work calculates the longitudinal friction coefficient $\mu_{Tire}(\lambda)$ from ASR λ_{ASR} . It can be represented as follows:

$$\mu_{Tire}(\lambda) = D \cdot \sin(C \cdot \arctan(B \cdot \lambda_{ASR} - E \cdot (B \cdot \lambda_{ASR} - \arctan(B \cdot \lambda_{ASR})))) \quad (4.19)$$

where parameter B is the stiffness factor, which influences the curve slope at the beginning; parameter C is the form factor, which is related to the form of approximation curve; parameter D is the peak factor, which determines the maximum value of curve; parameter E is the curvature factor, which influences the curvature around the curve maximum. The calculation of these factors can be found in Appendix C.

Given the longitudinal friction coefficient, the stationary longitudinal traction force $F_{trac,static}$ from the ground acting on the tire can be calculated as follows:

$$F_{trac,static} = \mu_{Tire} \cdot F_{Wheel,z} \quad (4.20)$$

The traction force for a dynamic process is not built-up immediately. It leads to the necessity to simulate the transient dynamics. The literature [120] and [122] recommended a consideration of a first order behavior. Therefore, a modified dynamic traction force model uses the PT1 block while introducing a variable time constant $\tau_{Tire}(\omega)$ to calculate the dynamic traction force F_{trac} :

$$\dot{F}_{trac} = -\frac{1}{\tau_{Tire}} \cdot F_{trac} + F_{trac,static} \quad (4.21)$$

with

$$\tau_{Tire} = \frac{L_{Tire}}{r_{dyn} \cdot \omega_{Wheel}}$$

where L_{Tire} is the wheel relaxation length of dynamic tractive force generation. In practical deployment, saturation is also necessary for τ_{Tire} to avoid numerical singularity.

4.2.4 Vehicle dynamics modeling

The vehicle dynamics model is a fundamental component used to convert various forces acting on a vehicle into its motion characteristics. In the context of this simulation, the focus is solely on longitudinal vehicle dynamics, and other aspects like lateral dynamics and suspension systems are omitted. This type of simplified longitudinal model is often referred to as a "bicycle model."

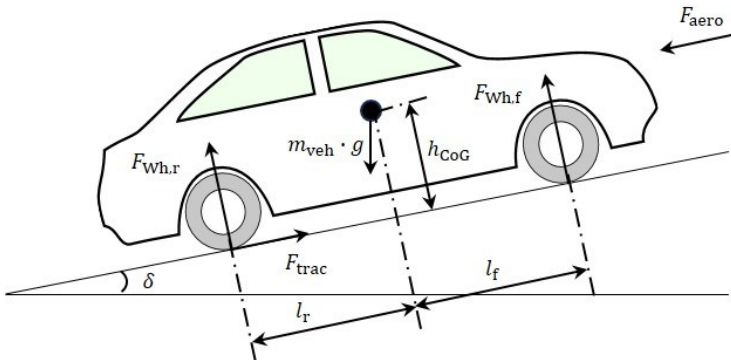


Figure 4.10: Forces acting on a vehicle

Within the vehicle dynamics model, two primary aspects are considered: the motion of the vehicle itself and the vertical forces applied to the wheels. When the vehicle is simplified as a point mass, the equation of its motion can be expressed as a force equilibrium acting on the center of gravity (CoG) as described in Equation (4.22).

$$\dot{v}_{\text{veh}} = \frac{1}{m_{\text{veh}}} \cdot (F_{\text{trac}} - F_{\text{aero}} - F_{\text{grade}}) \quad (4.22)$$

where m_{veh} is the overall vehicle mass, F_{aero} the aerodynamic resistance, and F_{grade} the road slope force.

Assume that the ambient air velocity is zero, the aerodynamic resistance F_{aero} in Equation (4.22) can be described as:

$$F_{\text{aero}} = \frac{1}{2} \cdot \rho_{\text{air}} \cdot A_f \cdot C_{\text{aero}} \cdot v_{\text{veh}}^2 \quad (4.23)$$

where ρ_{air} is the air density, A_f the frontal projection area of the vehicle, and C_{aero} the aerodynamic drag coefficient.

The road slope force F_{grade} is the component of gravity in longitudinal vehicle coordinates, which is expressed as:

$$F_{\text{grade}} = m_{\text{veh}} \cdot g \cdot \sin \delta \quad (4.24)$$

where g is the gravitational acceleration, and δ is the road slope angle. In standard driving simulations, the road slope angle is a parameter provided as part of the driving cycle data. However, for the context of this work, a value of zero is assigned to this parameter.

For determining the vertical forces acting on the front and rear wheels, the Equation (4.25) and (4.26) are formulated:

$$F_{\text{Wh},f} = \frac{1}{2 \cdot (l_f + l_r)} \cdot (l_r \cdot m_{\text{veh}} \cdot g \cdot \cos \delta - h_{\text{CoG}} \cdot (F_{\text{aero}} + \dots + m_{\text{veh}} \cdot g \cdot \sin \delta + m_{\text{veh}} \cdot \dot{v}_{\text{veh}})) \quad (4.25)$$

$$F_{\text{Wh},r} = \frac{1}{2 \cdot (l_f + l_r)} \cdot (l_f \cdot m_{\text{veh}} \cdot g \cdot \cos \delta + h_{\text{CoG}} \cdot (F_{\text{aero}} + \dots + m_{\text{veh}} \cdot g \cdot \sin \delta + m_{\text{veh}} \cdot \dot{v}_{\text{veh}})) \quad (4.26)$$

where $F_{\text{Wh},f}$ is the vertical force on the front wheels, $F_{\text{Wh},r}$ the vertical force on the rear wheels, h_{CoG} the height of the vehicle's CoG, l_f the distance from the front axle to CoG, and l_r the distance

from the rear axle to CoG.

4.3 Extended clutch modeling

In the last section, the modeling of powertrain dynamics has been presented based on the power flow. To analyze the thermal clutch load, a thermal model is built, which is capable of calculating the heat generation in the clutch and the temperature of the friction surface. In addition, a degradation model is developed for the clutch. It takes into account the sliding speed and the cumulative energy dissipation to determine the current health state by using the CoF-slope as an indicator. With the help of this model, the current CoF in the studied clutch system can also be estimated for the calculation of the friction torque in the clutch.

4.3.1 Thermal model for the clutch

The primary heat source during clutch slipping is friction, leading to a temperature increase in the component. This rise in temperature depends on the friction component properties and the cooling method. The investigated dual-clutch is known as a wet-running clutch. The term "wet" signifies that the clutches are immersed in oil, which is also known as friction oil in a clutch system. This lubrication not only helps in changing friction characteristics but also in cooling, especially during heavy usage or high-stress situations such as rapid acceleration. The friction component contains steel separator plates and friction plates made of steel cores covered with grooved friction materials. When the clutch is engaged, friction oil can flow through the grooves for cooling the friction materials. Forced heat convection is considered as the main cooling method with friction oil for the friction component, while heat conduction and heat radiation are not considered in this work.

The surface temperature T_{Surf} of the steel plates is computed to serve as a representative value for the temperature on the friction plates' surface within this work. This temperature can be calculated with Equation (4.27).

$$T_{\text{Surf}} = \int_{t_0}^t \frac{\dot{Q}_{\text{In}} - \dot{Q}_{\text{Out}}}{m_{\text{Fric}} \cdot c_{\text{Fric}}} dt + T_0 \quad (4.27)$$

\dot{Q}_{In} and \dot{Q}_{Out} represent the incoming and cooling heat flow, m_{Fric} the mass of the steel plates, c_{Fric} their specific heat capacity, and T_0 the initial temperature of the steel plates.

The incoming heat flow \dot{Q}_{In} is defined by the product of the transmitted frictional torque T_{Fric} and the slip speed $\Delta\omega_x$ as described in Equation (4.28).

$$\dot{Q}_{\text{In}} = T_{\text{Fric}} \cdot \Delta\omega_x \quad (4.28)$$

The cooling heat flow is described as follows:

$$\dot{Q}_{\text{Out}} = A_T \cdot (T_{\text{Surf}}(t_{n-1}) - T_{\text{Oil}}) \cdot \alpha_T \quad (4.29)$$

The contact area of the friction oil is denoted by A_T , with α_T representing the heat transfer coefficient, and T_{Oil} indicating the temperature of the friction oil. In this study, T_{Oil} is held constant at 85°C, representing a stationary operational temperature within the oil tank [25]. For an engaged or engaging clutch, heat absorption by the friction oil occurs through the grooves on the friction plates and along the outer surface of the friction plate pack. In the case of a disengaged clutch, the convection area extends to include the entire surfaces of both the friction and steel plates.

The oil flow rate is assumed to remain constant at 5 l/min, and the impact of centrifugal forces is disregarded. The heat transfer coefficient α_T encompasses the influence of the flowing medium's characteristics, such as flow velocity, flow form (laminar or turbulent), dynamic viscosity of the oil, and oil density. According to [123], α_T can be determined using the Nusselt number Nu for forced heat convection. This is a function of the Reynolds and Prandtl numbers, which are influenced by the characteristics of the friction oil and the geometric values of the contact surface between the oil and the friction components. As outlined in [123], the flow form of the friction oil is determined by the Reynolds and Prandtl numbers, Re and Pr . An approximation to calculate the Nusselt number for a mixed flow form, including both liminal and turbulence flow, is provided in Equations (4.30), (4.31) and (4.32), when the Reynolds number falls between 10 and 10^7 , and the Prandtl number between 0.6 and 2000. These specified ranges are applicable to the wet clutch cooling system employed in this work.

$$Nu = \sqrt{Nu_{\text{lam}}^2 + Nu_{\text{turb}}^2} \quad (4.30)$$

$$Nu_{\text{lam}} = 0.664 \cdot Re^{\frac{1}{2}} \cdot Pr^{\frac{1}{3}} \quad (4.31)$$

$$Nu_{\text{turb}} = \frac{0.037 \cdot Re^{0.8} \cdot Pr}{1 + 2.443 \cdot Re^{-0.1} \cdot (Pr^{\frac{2}{3}} - 1)} \quad (4.32)$$

where Nu_{lam} and Nu_{turb} are the Nusselt numbers for laminar and turbulence flow, respectively. It refers to theoretical modeling in this work. The parameters used in the above equations are taken from [123].

4.3.2 Degradation model for the clutch

This work explores the frictional behavior of the wet friction clutch being simulated through

comprehensive reality-close experimental measurements obtained with a series product of the sensors. Unlike the studies [9] and [57], which employed simplified conditions, this work utilizes an endurance experiment, considering system interactions, component interactions, and diverse driving scenarios for a more realistic assessment. The analysis detects that the changes in CoF-slope correlate with variations in vibration amplitude and the cumulative dissipation energy. It confirms the statements of the state of the art with the more reality-close experimental data. These results indicate that the CoF-slope changes can monitor the clutch health in realistic driving conditions using series product sensors.

Furthermore, a regression model is developed using the observed data to create a characteristic map. This map enables the estimation of CoF and simulation of clutch degradation during operation. It is integrated into the simulation model for determining the CoF according to the operation condition. Using this model, it is also possible to predict the remaining useful life of the clutch by extrapolating from the current CoF-slope and cumulative energy dissipation. In the following, the development of this degradation model is presented.

Endurance experiment

In the endurance experiment, a series product of a DCT is mounted on a powertrain test bench and operated under continuous loading, shifting cycles, temperature variations, and other stress factors that reflect real-world driving conditions. The test object experiences continuous operation over a large number of test cycles, which simulates various driving scenarios, including drive-off procedures, low-speed manoeuvres, and high-speed driving situations. Each test cycle spanned 1200 seconds, encapsulating a comprehensive range of real-world driving conditions. The endurance experiment consisted of more than 1300 test cycles. The cumulative frictional energy generated during these cycles was comparable to the frictional energy experienced by the clutch throughout its entire operational lifetime. The drive load is scaled up so that the comparable frictional energy can be generated within a shorter test duration. For this purpose, an amplification factor of 2 is used, which represents a doubled drive load generated in the powertrain. The traveled mileage during the experiment corresponds to half of the realistic driving. The purpose of the experiment is to evaluate the durability, reliability, and long-term performance of the transmission under various operating conditions. Figure 4.11 shows a part of the test cycle with an illustration of the shifting process. Due to the confidential agreement with the industrial research partner, the test cycle and test data are anonymized and nominalized for introduction.

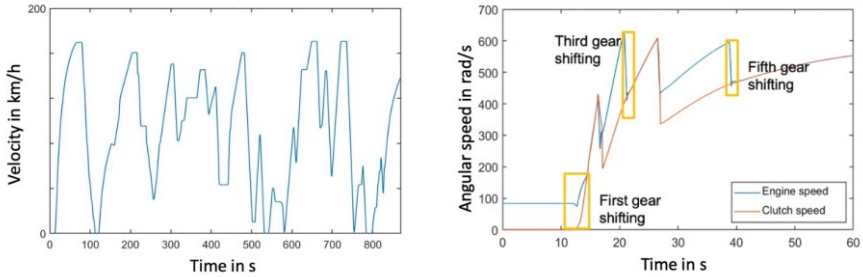


Figure 4.11: A part of a test cycle in the endurance experiment (left) and the shifting process at the start of the test cycle

Correlation between reinforced CoF-slope and peak amplitudes of sliding speed

As previously described in Section 2.3.2, the CoF is influenced by operational factors like drive torque and sliding speed during synchronization. To ensure consistency, the clutch's operating conditions are kept within a narrow range during the analysis of the CoF-slope development over time. Consequently, the analysis is conducted on drive-off procedures in the measurements, concentrating on engagements with the first gear shifting.

Measuring the frictional torque T_{Fric} poses challenges on the test bench. It is computed using another sensor signal, namely the load torque T_L acting on the clutch secondary side via a transmission ratio i_{Gear} . The actuation force $F(t)$ is determined using the hydraulic pressure P_{Hyd} that engages the clutch. A CoF multiplied with a gain K , defined as a reinforced CoF μ^* , can be derived as follows:

$$\mu^* = \mu \cdot K = \frac{T_{\text{Fric}}}{F(t)} = \frac{T_L}{i_{\text{Gear}} \cdot P_{\text{Hyd}} \cdot A} \quad (4.33)$$

with

$$K = r_m \cdot z$$

The drive-off procedure is observed every 2000 km throughout the entire endurance experiment. The gradient of the reinforced CoF can be calculated with Equation (4.34).

$$(\mu^*)' \cdot K = \frac{\Delta\mu^*}{\Delta\omega_{Clu}} = \frac{\overline{\mu^*}_{H} - \overline{\mu^*}_{L}}{\overline{\omega}_{Clu,H} - \overline{\omega}_{Clu,L}} \quad (4.34)$$

with

$$\left\{ \begin{array}{l} \overline{\mu^*}_{H} = \frac{1}{n} \sum_{i=1}^n \mu^*_{H,i} \\ \overline{\mu^*}_{L} = \frac{1}{n} \sum_{i=1}^n \mu^*_{L,i} \\ \overline{\omega}_{Clu,H} = \frac{1}{n} \sum_{i=1}^n \omega_{Clu,H,i} \\ \overline{\omega}_{Clu,L} = \frac{1}{n} \sum_{i=1}^n \omega_{Clu,L,i} \end{array} \right.$$

where $\Delta\omega_{Clu}$ represents the difference in the arithmetic mean value of the sliding speeds $\overline{\omega}_{Clu,H}$ and $\overline{\omega}_{Clu,L}$ at high and low sliding speed ranges, chosen from 40 to 60 rad/s and from 0 to 20 rad/s. The Latin letter n represents the sampling points in these speed ranges. The sampling frequency of the signal is 0.01 Hz. The symbols $\overline{\mu^*}_{H}$ and $\overline{\mu^*}_{L}$ represent the mean value of the reinforced CoFs at the chosen sliding speed ranges.

Since the denominator of Equation (4.34) is constant, the difference in the arithmetic mean value of the reinforced CoF $\Delta\mu^*$ signifies the change in the reinforced CoF-slope $(\mu^*)' \cdot K$ over time and the time point of transition from positive to negative slope. For the following analysis, this difference is computed for each observed drive-off procedure. Figure 4.12 shows the evolution of the reinforced CoF-slope over the test cycles.

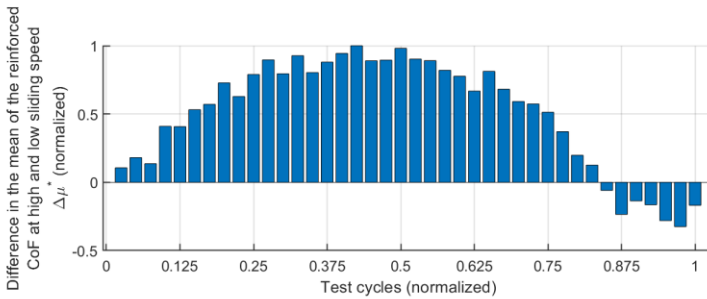


Figure 4.12: The changing of the reinforced CoF-slope over the test cycles represented by difference in the mean value of the reinforced CoF at high and low sliding speed

The reinforced CoF-slope increases due to the run-in procedure and subsequently decreases, indicating the degradation of the frictional surfaces. At about 80 % of the test cycles, the CoF-slope becomes negative. The validity of these findings is checked by observing the reinforced CoF-slope during gear shifts into the third, fifth, and seventh gears. All the transitions between positive and negative CoF-slope occur at this percentage of the test cycles.

To explore the relationship between vibration amplitude and the reinforced CoF-slope, peak amplitudes of the sliding speed of observed drive-off procedures were calculated and illustrated in Figure 4.13.

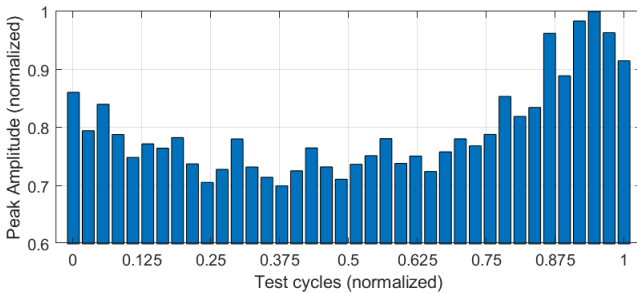


Figure 4.13: Peak amplitude of the sliding speed plotted over the test cycles

By comparing Figure 4.12 and Figure 4.13, the fluctuation in peak amplitudes corresponds directly to changes in the reinforced CoF-slope. Specifically, a higher reinforced CoF-slope indicates an enhanced damping effect within the clutch system, leading to a reduction in peak amplitudes. Conversely, after 60 % of the test cycles, peak amplitudes show an inverse relationship with the reinforced CoF-slope, becoming more pronounced as the CoF-slope becomes negative. This relationship is quantitatively expressed through a correlation coefficient of -0.89, signifying a strong negative correlation. This observation matches the fact that the vibration amplitude increases while the CoF-slope decreases. This demonstrates the reinforced CoF-slope changes as an indicator for monitoring clutch health under a realistic experimental environment.

Clutch degradation model

In the context of clutch degradation described in Section 2.3.3, dissipation energy is a crucial factor that influences the degradation rate of the friction materials. It can be calculated by integrating torque multiplied by sliding speed over sliding time. The total dissipation energy is the sum of energy dissipated during shifting and drive-off. A regression model considering this factor and sliding speed mathematically describes clutch degradation, as represented by Equation (4.35).

$$\mu^*(\Delta\omega_{\text{Clu}}) = a(E) \cdot \Delta\omega_{\text{Clu}}^2 + b(E) \cdot \Delta\omega_{\text{Clu}} + c(E) \quad (4.35)$$

with

$$a(E) = p_{a_1} \cdot E^5 + p_{a_2} \cdot E^4 + p_{a_3} \cdot E^3 + p_{a_4} \cdot E^2 + p_{a_5} \cdot E + p_{a_6}$$

$$b(E) = p_{b_1} \cdot E^5 + p_{b_2} \cdot E^4 + p_{b_3} \cdot E^3 + p_{b_4} \cdot E^2 + p_{b_5} \cdot E + p_{b_6}$$

$$c(E) = p_{c_1} \cdot E^5 + p_{c_2} \cdot E^4 + p_{c_3} \cdot E^3 + p_{c_4} \cdot E^2 + p_{c_5} \cdot E + p_{c_6}$$

where $a(E)$, $b(E)$, and $c(E)$ are the coefficients changing with the total dissipation energy E over time. The parameters p_i are the coefficients of the regression functions. The variable $c(E)$ corresponds to the reinforced static CoF.

The friction behavior, considering the degradation process, can be mathematically defined regarding the sliding speed and the cumulative dissipation energy, as shown in Figure 4.14. At each constant total dissipation energy, the cross-section describes the relationship between the reinforced CoF and the sliding speed, representing the friction behavior in one synchronization process. In contrast, the cross-section at a constant sliding speed illustrates changing in the reinforced static CoF, when sliding speed is zero, or reinforced dynamic CoF in relation to the cumulative dissipation energy. This transformation is characterized by changes in the parameters $a(E)$, $b(E)$, and $c(E)$. This model offers a mathematical representation of the frictional characteristics of the studied wet friction clutch, accounting for degradation process.

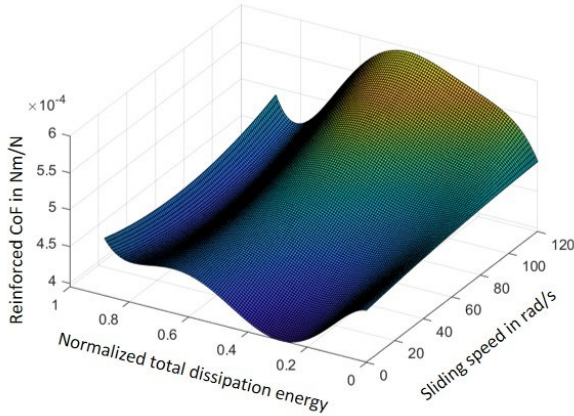


Figure 4.14: Characteristic diagram for the friction behavior of the clutch with consideration of the degradation process

4.4 Control module

4.4.1 Drive-off controller

The drive-off procedure refers to a phase during which a predefined speed curve is established for the engine speed. During this phase, the clutch synchronization process takes place, bringing both sides, the engine and the transmission, to equal rotational speeds. This synchronization is crucial to realize a transition of the vehicle from a stationary position to motion. As described in Section 2.1, the acoustic characteristics of the engine, influenced by engine speed behavior, impact the driver's perception of comfort during the drive-off procedure. To enhance this experience, it is essential to maintain a continuous increase in engine speed. For this purpose, the target engine speed is set as a step function from idle speed to a plateau, followed by a ramp function for raising the engine speed. Taking into account the findings from test subject study 3, it was observed that the speed plateau during the drive-off procedure has a minimal impact on the evaluation of the drive-off behavior. However, the instances of speed drop or flare significantly influence the evaluation. The design for this controller considers an EDT of 250 RPM for engine speed changes. This threshold serves as a saturation in the control system, ensuring that deviations in engine speed stay within this limitation.

In addition, the engine speed can be influenced by the clutch torque during the clutch slip phases [28], so a reduction in engine speed can only be achieved by either increasing the clutch torque over the engine torque or requesting engine intervention. However, requesting an engine intervention can lead to increased pollutant emissions [124]. Therefore, this work employs a reality-close controller for determining the desired drive torque and speed specifications of the ICE based on two characteristic maps provided by the industrial research partner. One map defines the desired engine speed based on the APP and the clutch input shaft speed, while the other map determines the desired drive torque according to the APP and engine speed. The engine speed is regulated by varying the clutch torque, which effectively imposes a load on the ICE. The desired clutch torque $T_{Cl, des}(t_n)$ is controlled by a P-controller, taking into account the ICE speed error $\omega_{ICE, err}(t_n)$, which is calculated based on the actual engine speed in last time step. The mathematical formulation for this control process is given as follows:

$$T_{Cl, des}(t_n) = T_{ICE, act}(t_n) - J_{ICE} \cdot \dot{\omega}_{Eng}(t_n) - k_{P, cl} \cdot \omega_{ICE, err}(t_n) \quad (4.36)$$

with

$$\omega_{ICE, err}(t_n) = \omega_{ICE, des}(t_n) - \omega_{ICE, act}(t_{n-1})$$

where $k_{P, cl}$ describes the proportional coefficient of the P controller.

A positive engine speed error results in a reduction of the desired clutch torque, and vice versa. To

prevent driving discomfort caused by rapid changes in driving torque, a rate limiter restricts the change rate of the clutch torque to 500 Nm/s. As a reference literature for understanding this controller, the study [23] can be involved.

4.4.2 Backward modeling for torque request estimation

This backward modeling constructs the requested on-wheel torque T_{ctrl} based on the vehicle control acceleration a_{ctrl} . Figure 4.15 shows the acceleration estimation in the modeling.

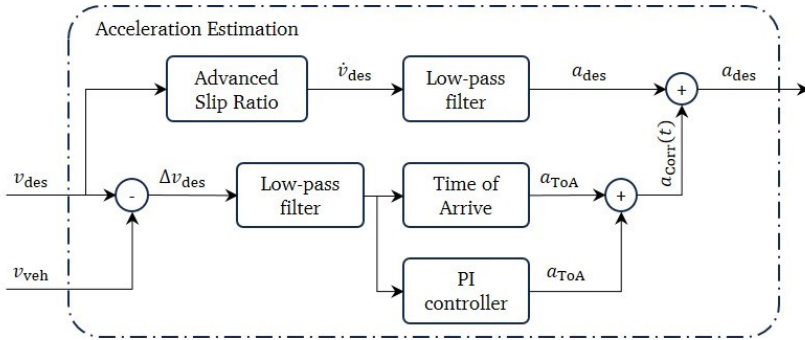


Figure 4.15: Acceleration estimation based on vehicle speed deviation

The essential idea for accurately following the driving cycle is to generate a correction acceleration a_{corr} for compensation of the vehicle speed deviation. This acceleration correction is added to the desired acceleration a_{des} , which can be estimated with the desired speed v_{des} derived from the driving cycle. The acceleration correction consists of a concept of “Time of Arrive” and a PI controller with the speed deviation as input, represented with a_{ToA} and a_{pi} , respectively. The low-pass filter reduces sudden changes in acceleration. Figure 4.16 illustrates the concept of “Time of Arrive”.

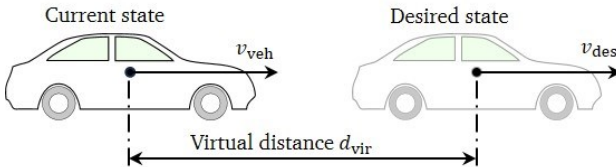


Figure 4.16: Schematic representation of the „Time of Arrive” concept

Assuming that there exists a virtual vehicle, whose velocity is consistent with v_{des} from the driving cycle. The cumulative distance d_{vir} between the virtual vehicle and the simulated vehicle can be expressed by integrating the speed difference Δv_{des} over time. The time to arrive t_{ToA} can be

calculated based on Δv_{des} and d_{vir} with Equation (4.37).

$$t_{\text{ToA}} = \frac{d_{\text{vir}}}{\Delta v_{\text{des}}} = \frac{\int_0^t \Delta v_{\text{des}}(t) dt}{v_{\text{des}} - v_{\text{veh}}} \quad (4.37)$$

Under the assumption that the vehicle is accelerating uniformly, the time of arrival-based acceleration a_{ToA} can be calculated from the following equation:

$$a_{\text{ToA}} = \frac{\Delta v_{\text{des}}}{t_{\text{ToA}}} = \frac{\Delta v_{\text{des}}^2}{d_{\text{vir}}} = \frac{\Delta v_{\text{des}}^2}{\int_0^t \Delta v_{\text{des}}(t) dt} \quad (4.38)$$

and the correction part from the PI controller is described in Equation (4.39).

$$a_{\text{PI}} = k_p \cdot \Delta v_{\text{des}} + k_i \cdot \int_0^t \Delta v_{\text{des}}(t) dt \quad (4.39)$$

Where k_p and k_i are the proportional and integral coefficients of the PI controller

The final output for the control acceleration is formulated as:

$$a_{\text{Ctrl}} = a_{\text{des}} + a_{\text{ToA}} + a_{\text{PI}} \quad (4.40)$$

The torque estimation process relies on the inverse model of the vehicle's longitudinal dynamics. The estimated torque applied to the wheel $T_{\text{Wheel,Ctrl}}$ is formulated as follows:

$$T_{\text{Wheel,Ctrl}} = r_{\text{dyn}} \cdot (F_{\text{inertia,ctrl}} + F_{\text{roll,ctrl}} + F_{\text{aero,ctrl}} + F_{\text{grade}}) \quad (4.41)$$

with

$$\begin{cases} F_{\text{inertia,Ctrl}} = m_{\text{veh}} \cdot a_{\text{Ctrl}} \\ F_{\text{roll,Ctrl}} = \mu_{\text{Roll}} \cdot m_{\text{veh}} \cdot g \cdot \cos\delta. \\ F_{\text{aero,Ctrl}} = \frac{1}{2} \cdot \rho_{\text{air}} \cdot A_f \cdot C_{\text{aero}} \cdot v_{\text{des}}^2 \\ F_{\text{grade}} = m_{\text{veh}} \cdot g \cdot \sin\delta. \end{cases}$$

where $F_{\text{inertia,ctrl}}$ is the inertial resistance corresponding to estimated acceleration a_{Ctrl} , $F_{\text{roll,ctrl}}$ is the estimated rolling resistance, $F_{\text{aero,ctrl}}$ is the estimated aerodynamic drag force and F_{grade} is the constant road slope force. All utilized parameters and variables are declared in Section 4.2.4 for the vehicle dynamics modeling. The estimated wheel torque serves as the input for the control strategy introduced in the following.

4.4.3 Control strategy for EMS

In this work, a hierarchical online EMS approach is employed, encompassing two components. Firstly, a rule-based DCT shifting logic is integrated, utilizing a predetermined shifting map and a control strategy aimed at optimizing power distribution between the ICE and EM. The DCT shifting logic firstly identifies the optimal gears in both sub-transmissions. Subsequently, based on the chosen gear, the control strategy establishes a locally optimal power distribution within a discrete optimization space, taking into account the current SOC.

DCT Shifting logic

The DCT shift logic operates based on rule-based principles. Its goal is to optimize the efficiency of the ICE according to the vehicle's motion state estimated in the backward modeling. In this approach, a shifting map, as depicted in Figure 4.17, is built by considering the engine's efficiency for each gear. The shifting logic chooses the most effective gear for various velocity and acceleration combinations. To prevent frequent shifting when driving nearby shifting thresholds, a watchdog timer oversees the time elapsed after shifting. The shift command can be executed after the previously engaged gear has been utilized for a specific duration of 1.2 seconds.

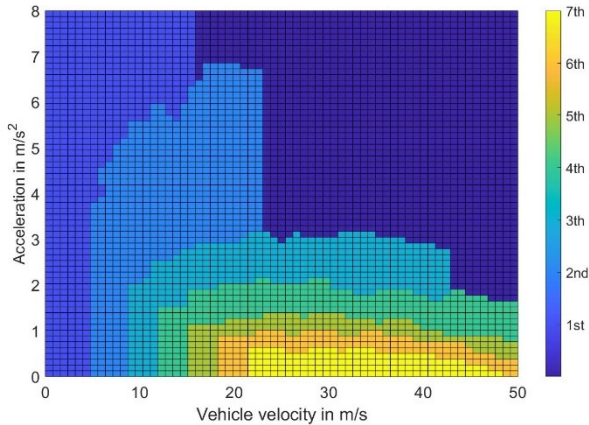


Figure 4.17: Gear shifting map, color bar shows the corresponding areas for each gear

For the braking scenarios, the gear selection depends entirely on the current vehicle velocity. Speed thresholds are utilized for gear shifting.

Control strategy

The EM enhances the ICE's efficiency by enabling operation at optimal points on its characteristic diagram during driving. This functionality, known as load point shifting, involves either upshifting

or downshifting. During upshifting, the ICE transfers the drive torque not only to the wheels but also to the EM via the differential and sub-transmission. In this case, the EM operates as a generator and charges the battery in generator mode. Conversely, in downshifting, the EM supports the ICE in propelling the vehicle to ensure the required torque. It is referred to as drive mode. For the load point shifting, the control strategy specifies the power distribution between the ICE and the EM, considering a predetermined target value for the SOC of the battery, and decides to switch from generator mode to drive mode or vice versa.

This work employs a control strategy based on the A-ECMS, a variant of the ECMS. In an ECMS, the global minimization problem is transferred to an instantaneous minimization problem, solvable at each moment by equating the use of stored electrical energy to using or saving a certain quantity of fuel consumption, also called instantaneous equivalent fuel consumption. This consumption is defined in Equation (4.42) involving an equivalence factor λ and a penalty function defined in Equation (4.43), known as the instantaneous cost function. The equivalence factor is a constant variable and influences the battery recharge performance. It signifies the conversion ratio of electrical power into chemical power. This factor varies with different boundary conditions of a simulation driving cycle and stands as a primary variable to achieve SOC neutrality after driving simulation. The penalty function ensures that SOC remains within acceptable limits.

$$C1(t_n) = \dot{m}_{\text{fuel}}(t_n) \cdot h_{\text{fuel}} + p(\text{SOC}) \cdot \lambda \cdot \frac{P_{\text{EM}}(t_n)}{(\eta_{\text{EM}}(t_n) \cdot \eta_{\text{batt}})^{\text{sign}(P_{\text{EM}}(t_n))}} \quad (4.42)$$

$$p(\text{SOC}) = 1 - \left(\frac{\text{SOC}(t_n) - \text{SOC}_{\text{target}}}{(\text{SOC}_{\text{max}} - \text{SOC}_{\text{min}})/2} \right)^{a_p} \quad (4.43)$$

where $C1(t_n)$ is the instantaneous cost, $\dot{m}_{\text{fuel}}(t_n)$ is the fuel mass flow of the operation point candidates in the engine consumption map, h_{fuel} is the fuel lower heat value, $p(\text{SOC})$ is the penalty function, which results in a low cost if $\text{SOC}(t_n) > \text{SOC}_{\text{target}}$, and the battery is more likely discharged. On the contrary, the EM works more likely as a generator when $\text{SOC}(t_n) < \text{SOC}_{\text{target}}$. It corresponds to a high cost of electrical energy, specifically when the current SOC is much smaller than the target SOC. a_p is an exponential coefficient. λ refers to the equivalence factor, which is a dimensionless conversion ratio.

Study [47] examined the online adaptability of the A-ECMS with two case studies. It is proved that the A-ECMS can be used as a control strategy applicable in practical settings, as opposed to ECMS, which is found to be unsuitable. This relies on the fact that A-ECMS regulates the equivalence factor λ based on the deviation of the actual SOC from the desired SOC by using a PI controller. The deviation between actual and desired SOC will be considered at each time instant and minimized at the end of the driving cycle. This strategy can be employed as an online control without prior knowledge of the driving cycle. It indicates that this work is performed based on a control

strategy that is useable in reality. The A-ECMS is formulated based on the general ECMS with feedback from SOC, as shown in Equation (4.44) and (4.45).

$$\lambda(t_n) = \lambda_0 + k_p \cdot \Delta SOC(t_n) + k_i \cdot \sum_{i=0}^n \Delta SOC(t_n) \quad (4.44)$$

$$\Delta SOC(t_n) = SOC_{\text{target}} - SOC(t_n) \quad (4.45)$$

By adding the additional costs to the cost function of the A-ECMS, a control strategy named Extended A-ECMS is implemented in this work. This strategy is the core of the EMS to solve the optimization problem of the determination of the torque distribution between the ICE and the EM. The additional costs can ensure the drivability and consider the powertrain constraints. To solve this optimization problem, a discrete static optimization space for the potential operating torque of the ICE and EM, respectively, is generated according to the desired operating speed. The requested drive torque $T_{\text{Req}}(t_n)$ is a sum of the ICE torque candidate $T_{\text{ICE,cand}}(t_n)$ and EM torque candidate $T_{\text{EM,cand}}(t_n)$. Each candidate of the operation torque point in the EM corresponds to a torque point candidate of the ICE. Every combination of both provides a cost. The combination providing the most favorable cost is chosen as the operation points for the ICE and the EM. According to the operating conditions of the ICE and EM, diverse operating scenarios can be realized, as described in the following. In this process, all energy flows in the powertrain are assumed to be steady-state.

$$T_{\text{Req}}(t_n) = T_{\text{ICE}}(t_n) + T_{\text{EM}}(t_n) \quad (4.46)$$

when

$$\begin{cases} T_{\text{ICE}}(t_n) > T_{\text{Req}}, & \text{Upshifting} \\ T_{\text{ICE}}(t_n) = T_{\text{Req}}, & \text{ICE only} \\ T_{\text{ICE}}(t_n) < T_{\text{Req}}, & \text{Downshifting} \\ T_{\text{ICE}}(t_n) = 0, & \text{EM only} \end{cases}$$

The Extended A-ECMS is formulated with Equation (4.47), defining a cost function $C(t_n)$, which needs to be minimized.

$$C(t_n) = C1(t_n) + p2 \cdot C2(t_n) + p3 \cdot C3(t_n) + p4 \cdot C4(t_n) \quad (4.47)$$

where $C1(t_n)$ is the energy consumption cost formulated by A-ECMS, $C2(t_n)$ is the traction power error cost, $C3(t_n)$ is the actuator constraint cost, $C4(t_n)$ is the engine torque jerk cost and p_x are the corresponding penalty coefficients. In the following, each term is explained in sequence.

The traction power error cost $C2(t_n)$ is added to the instantaneous cost to eliminate the power deviation between the desired and actual output so that the actual vehicle speed converges to the desired speed.

$$C2(t_n) = (T_{Wh, des}(t_n) \cdot 2 - T_{ICE, cand}(t_n) \cdot i_{Gear, x} - \dots) \quad (4.48)$$

$$T_{EM, cand}(t_n) \cdot i_{Even} \cdot i_{EM} \cdot \frac{v_{des}(t_n)}{r_{dyn}}$$

where $T_{Wh, des}(t_n)$ is the desired torque obtained from the backward-facing model, $v_{des}(t_n)$ the desired velocity, $i_{Gear, x}$ the gear ratio of the determined DCT gear, i_{Even} the gear ratio of the even gear used for the EM operation, i_{EM} is the gear ratio of the intermediate gear between EM and second input shaft, $T_{ICE, cand}(t_n)$ refers to the ICE torque candidate and $T_{EM, cand}(t_n)$ refers to the EM torque candidate.

The drivetrain constraint cost $C3(t_n)$ is a hard constraint that enforces all driving components (EM and ICE) to stay within feasible operation ranges to ensure drivability:

$$C3(t_n) = \begin{cases} 0, & \text{if } \begin{cases} \mathbf{G}_1(\mathbf{x}(t_n)) = \mathbf{x}(t_n) - \mathbf{x}_{max} > 0 \\ \mathbf{G}_1(\mathbf{x}(t_n)) = \mathbf{x}_{min} - \mathbf{x}(t_n) > 0 \end{cases} \\ 1, & \text{if } \begin{cases} \mathbf{G}_1(\mathbf{x}(t_n)) = \mathbf{x}(t_n) - \mathbf{x}_{max} \leq 0 \\ \mathbf{G}_1(\mathbf{x}(t_n)) = \mathbf{x}_{min} - \mathbf{x}(t_n) \leq 0 \end{cases} \end{cases} \quad (4.49)$$

where $\mathbf{x}(t_n)$ is the operation states at the time point t_n and $\mathbf{G}(\mathbf{x}(t_n))$ represents the admissible states denoted as below:

$$\begin{cases} \omega_{ICE, idle} \leq \omega_{ICE}(t_n) \leq \omega_{ICE, max} \\ -\omega_{EM, max} \leq \omega_{EM}(t_n) \leq \omega_{EM, max} \\ T_{ICE, min}(\omega_{ICE}) \leq T_{ICE, desired}(t_n) \leq T_{ICE, max}(\omega_{ICE}) \\ T_{EM, min}(\omega_{EM}) \leq T_{EM, desired}(t_n) \leq T_{EM, max}(\omega_{EM}) \\ I_{Chr, max} \leq I_{Batt}(t_n) \leq I_{Dischr, max} \end{cases} \quad (4.50)$$

where ω_x represents the permissible rotational speed range for the ICE or the EM, T_x the permissible torque range for both drives, respectively, and I_x the maximum current for the charge or discharge of the battery.

The jerk cost of the engine torque $C4(t_n)$ is added to take the drive comfort into account by comparing the current ICE torque candidates with the previous engine torque. A large change in the torque leads to a significantly increased cost. It is also a hard constraint for a maximum jerk included in this cost.

$$C4(t_n) = |T_{ICE, desired}(t_n) - T_{ICE}(t_{n-1})| \cdot \omega_{ICE}(t_n) \quad (4.51)$$

where $T_{ICE}(t_{n-1})$ is the ICE torque from the last time step.

Although, this control strategy has the capability to dynamically adjust the equivalence factor in real-time and maintain its value around the desired level. Still, individual parameterization is essential to ensure precise neutral SOC for different operating strategies. To achieve this, a shooting method is employed, iteratively changing parameters based on simulations with estimated values until SOC neutrality is achieved.

4.5 Analysis of the simulation results

In this section, the evaluation of the simulation results from the P2.5 HEV dynamics model and the validation of the model correctness are described. Section 4.5.1 provides a description of the test environment, i.e., the driving cycle for the model validation. Section 4.5.2 describes the evaluation criteria for the P2.5 HEV model. Section 4.5.3 analyzes the correctness of the vehicle model under the EMS control and compares the vehicle simulations with and without the EM support from a power distribution perspective. Section 4.5.4 discusses the performance of the control strategy in the EMS.

4.5.1 Driving cycle

The P2.5 HEV model is essentially a velocity-following model that requires a desired velocity as an input, providing a target for constructing the vehicle's motion. The driving cycle represents the vehicle driving state, which is defined as the time history of the vehicle velocity. The velocity profile of Worldwide harmonized Light vehicles Test Cycles (WLTC) has been developed by the UN ECE GRPE (Working Party on Pollution and Energy) group [125] and has several categories for light-duty vehicles with different power-to-mass ratio (PMR) [126]. The WLTC Class 3b used in this work is representative of the vehicles with a high PMR for the maximum speed higher than 120 km/h. Figure 4.18 illustrates the WLTC Class 3b speed profile. This driving cycle includes different driving speed scenarios: low, medium, high, and extra high speed. It represents a trip of 23266 m within 1800 seconds, including a stop duration of 242 seconds. The maximum velocity is 131.3 km/h. The maximum and minimum acceleration are 1.58 m/s^2 and -1.49 m/s^2 , respectively.

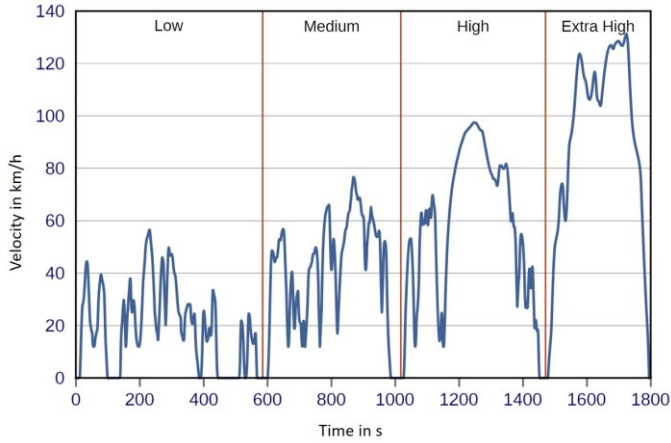


Figure 4.18: Velocity profile of the WLTC Class 3b [126]

4.5.2 Evaluation criteria

The validation and evaluation of the P2.5 HEV model with EMS consist of two main aspects, namely, simulation correctness and EMS performance. The simulation correctness is the foundation of the evaluation process. The EMS performance is essential for the power distribution in the P2.5 powertrain, which indicates the different hybrid operation modes described in Section 4.4.3. To illustrate the influence of EM on the powertrain performance, the analysis is conducted comparatively for the drivetrain operation with and without using EM, defined as the hybrid and conventional operation modes.

Another indicator for evaluating the feasibility is the velocity following performance, which can be measured by calculating the average cumulative absolute velocity error Δv_{ACA} with the following expression:

$$\Delta v_{ACA} = \frac{\int_0^{t_{end}} |v_{des}(\tau) - v_{veh}(\tau)| d\tau}{t_{end}} \quad (4.52)$$

where t_{end} is the simulation duration.

4.5.3 Correctness of the vehicle simulation model

The studied P2.5 HEV model is based on a conventional DCT powertrain. By deactivating the EM-related components, such as the EM, battery, and EMS, the HEV model can work in conventional operation modes. During the validation of the HEV model, the accuracy of the conventional

operation is also involved. The vehicle model's accuracy is firstly examined by comparing the desired vehicle velocity with the simulated vehicle velocity. Figure 4.19 depicts the desired velocities from the driving cycle, the velocity of HEV mode, and the velocity of the conventional mode, respectively.

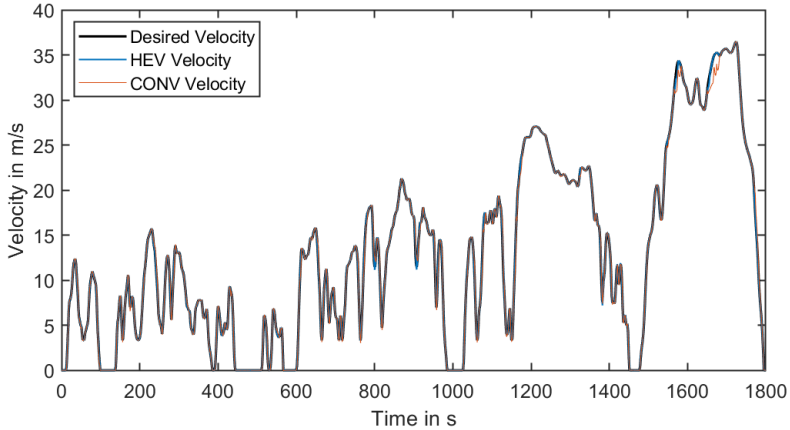


Figure 4.19: Comparison between desired velocity and simulated velocity from HEV and conventional vehicle.

The black speed curve, denoted as $v_{des}(t)$, highly aligns with the blue curve $v_{veh,HEV}(t)$ and the red curve $v_{veh,conv}(t)$. This observation indicates that the simulated velocity profiles of both the HEV model and the conventional vehicle model exhibit a high degree of consistency with the WLTC speed profile. Table 4.2 provides the average cumulative absolute velocity errors of both operations ($\Delta v_{ACA,HEV}$ and $\Delta v_{ACA,conv}$) with respect to the WLTC velocity profile.

Table 4.2: Average cumulative absolute velocity error for both vehicle operation modes

$\Delta v_{ACA,HEV}$	$\Delta v_{ACA,conv}$
0.04 m/s	0.29 m/s

It is evident that the errors of both the HEV and the conventional modes are relatively small. Hence, it validates the P2.5 HEV model for simulation of the dynamics required by the WLTC Class 3b.

In the following, the EMS effect on the power distribution is investigated by comparing the operation points for the propulsion units between the hybrid and the conventional operation mode. Figure 4.20 and Figure 4.21 show the operation point distributions according to torque and speed for both operation modes under the WLTC Class 3b. The ICE characteristic map is illustrated in

efficiency instead of brake-specific fuel consumption so that the ICE efficiency between both operation modes can be directly compared.

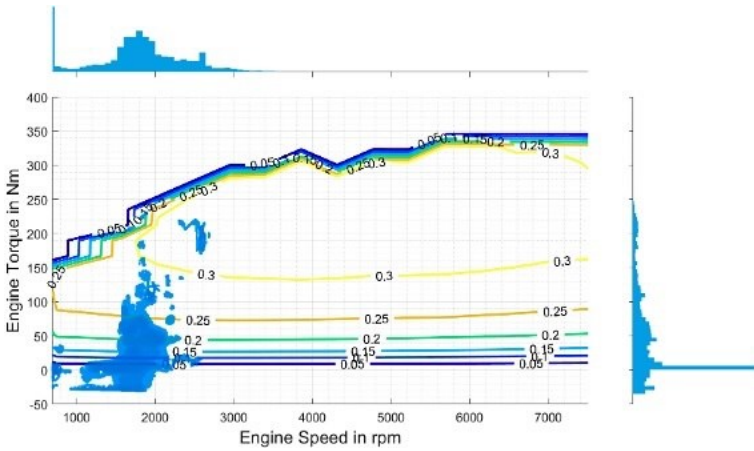


Figure 4.20: ICE operation points in the efficiency distribution diagram according to torque and speed in conventional operation mode

Operation points with high-frequency are highlighted in blue, with darker shades indicating a higher occurrence of these points. This indicates the engine speed and torque combinations that are most frequently reached during operation. The bar charts on the top and right sides of the distribution diagram display the frequency distribution of engine torque at different engine speeds and the distribution of engine speed at different torque levels, respectively. In the simulation results of the conventional mode (Figure 4.20), high-frequency operation points for the ICE are predominantly located in the low to medium torque range, spanning from 1000 RPM to 2500 RPM. Notably, only a small fraction of these high-frequency points is distributed within the medium torque range, specifically around 140 Nm, occurring at about 2000 RPM. These instances are associated with low-speed and high-speed driving scenarios, respectively. Simultaneously, a significant number of high-frequency operation points are observed in the negative torque range, indicating the presence of drag torque in the engine. Furthermore, the figure illustrates that the ICE efficiency in the conventional operation mode remains below 25 % in most operation situations. This indicates that the fuel consumption of the ICE is suboptimal during this driving conditions.

In contrast to the conventional operation mode in Figure 4.20, the ICE operation points for the hybrid mode, as shown in Figure 4.21, are shifted on the engine characteristic map into an area with high efficiency. It is observed that the low and medium torque working conditions of ICE around 1500 RPM are reduced compared to the conventional operation mode. The high-frequency points around 2000 RPM and 2500 RPM are shifted to the large torque range with high efficiency.

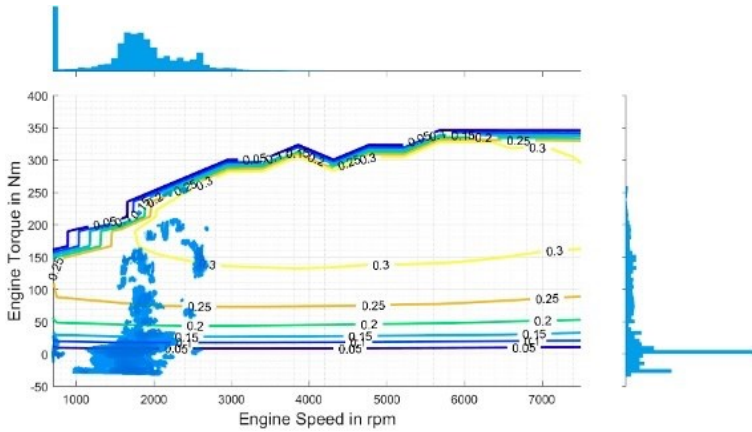


Figure 4.21: ICE operation points in the efficiency distribution diagram according to torque and speed in hybrid operation mode

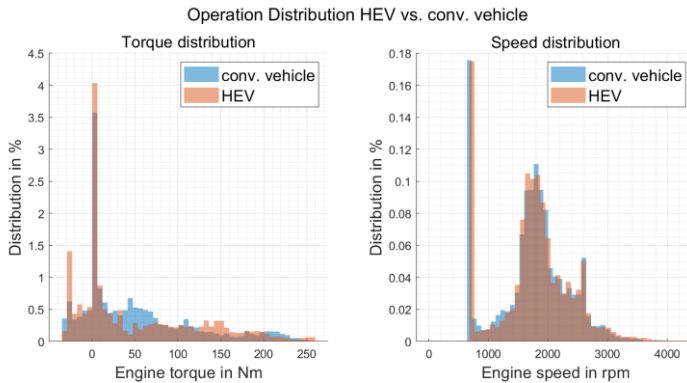


Figure 4.22: ICE operation point distribution in conventional and hybrid operation modes

In terms of frequency distribution, Figure 4.22 compares the ICE operation points in hybrid and conventional operation modes. Specifically, the distribution of torque and rotation speed is depicted, with the red bars representing the hybrid operation mode and the blue bars denoting the conventional operation mode. Since the same DCT shifting logic, which depends on the vehicle velocity, is used for hybrid and conventional operation modes, the ICE speed distributions in both modes are comparable. In comparison, the torque distribution of the hybrid mode is very different from the conventional mode, showing more operation points in high torque areas, where better fuel consumption efficiency can be detected.

Figure 4.23 details how the EM operation points are distributed in the HEV mode within the WLTC driving cycle. The EM high-frequency operation points are mainly distributed between 4000 RPM and 7000 RPM, while the motor braking maximum torque is clearly outlined. Moreover, when the HEV is at a standstill, the EM is also on standby, which corresponds to the high-frequency operation points that occur near the origin.

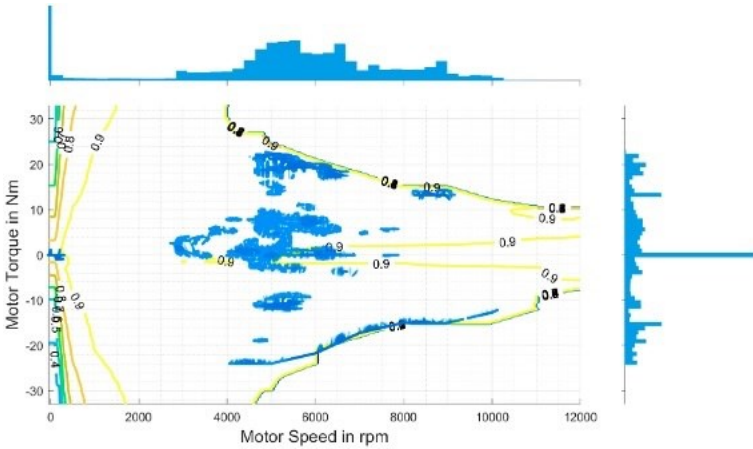


Figure 4.23: EM operation points in hybrid operation mode with the distribution diagram for torque and speed

4.5.4 Performance of the control strategy

The EMS relies on the control strategy to enable the torque distribution considering the battery recharging. This section analyzes the performance of the control strategy based on the A-ECMS by comparing it to the variant based on ECMS and summarizes its characteristics. Both of them are expended with the additional costs, as described in Section 4.4.3. In the following, both of these strategies are referred to as A-ECMS and ECMS.

As described before, A-ECMS is an adaptive approach that changes its equivalence factor along with the variation of battery SOC, therefore contributing to the EMS covering more application scenarios without fine-tuning the parameters. The ECMS does not have this advantage. In essence, it uses a constant equivalence factor determined by prior experience and practice rather than a SOC tracking approach. Figure 4.24 shows the variation of the battery SOC under the hybrid operation mode with both approaches for illustrating the recharging control performance.

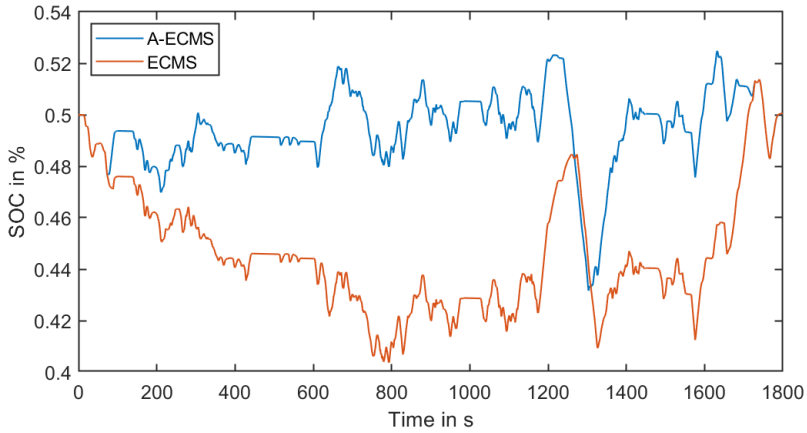


Figure 4.24: SOC comparison between ECMS and A-ECMS

The SOC for both approaches starts at the same level in the initial phase of the simulation and converges to a comparable end value. As the simulation progresses, the SOC curves gradually differ due to the dynamic adjustment of the equivalence factor in the A-ECMS method, which is based on the SOC difference between the current and target values. Although the two SOC curves no longer overlap during the simulation, their overall trends are consistent for most parts of the SOC curves. This consistency can be attributed to the unchanged parameters used in constructing the costs within the cost function, except for the parameter in the instantaneous cost $C1(t)$. Table 4.3 provides a comparison of the SOC for both approaches at the beginning and end of the simulation. The notable advantage of the A-ECMS lies in its real-time adjustment of parameters based on SOC, ensuring that the battery SOC does not persistently use a wide range of the SOC. It is enabled to prevent critically low levels during the entire driving cycle.

Table 4.3: variation of the battery SOC during WLTC driving simulation

	SOC _{Start}	SOC _{End}	Max. ΔSOC
ECMS	50 %	50.04 %	11.0 %
A-ECMS	50 %	50.02 %	9.3 %

However, better SOC maintainability does not mean better torque distribution to all speed scenarios. Figure 4.25 shows the probability distribution of the torque and speed distribution for HEV propulsion units under the control of the ECMS and A-ECMS.

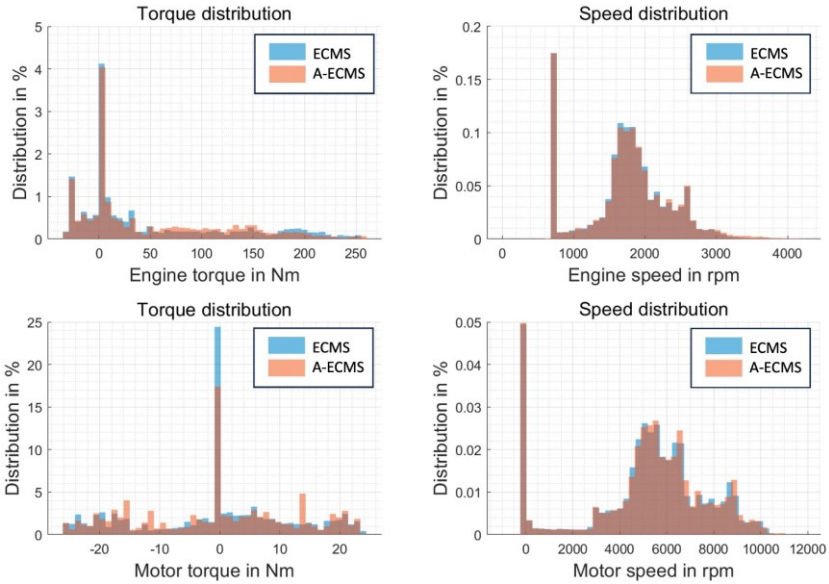


Figure 4.25: ICE and EM torque distribution under hybrid operation mode with ECMS and A-ECMS as control strategy for the EMS

The speed distribution of both the ICE and EM are highly similar. Under the control of A-ECMS, the EM operates more frequently with negative torque, while the EM is more frequently in standstill under the ECMS control. This indicates that the EM frequently works as a generator for recharging the battery, particularly with a medium torque ranging from -15 Nm to -10 Nm. This behavior is associated with the stable SOC variation shown in Figure 4.24. For maintaining a stable SOC, the battery must be frequently recharged. Comparing the overall efficiency of the ICE and EM for both control approaches reveals comparable efficiencies of the propulsion units in both operation modes: approximately 31.6 % for the ICE and 86.5 % for the EM. However, the A-ECMS-based approach stands out for its ability to maintain a stable battery SOC.

5 Results of the drive-off procedure evaluation

In this section, drive-off procedures simulated using the vehicle simulation model are objectively characterized. Initially, drive-off dynamics are evaluated through descriptive statistical methods. Subsequently, subjective criteria used in the test subject study 1 are performed by employing objectivation models for the drive-offs. Then, the ecological evaluations concerning thermal clutch load and fuel consumption are considered ecological evaluation criteria, taking into account the presence or absence of EM support. This comparison allows for the exploration of EM's potential in the evaluated aspects. Lastly, the improvement of the thermal clutch load caused by the EM support is analyzed regarding the entire driving cycle within the total lifetime to clarify the enhancements derived from these drive-off scenarios. Following this, an outlook of the thermal clutch load potential during upshifting is given.

5.1 Subjective and ecological evaluation of the drive-off procedure

5.1.1 Analysis of the drive-off procedures

As outlined in Section 4.4.1, this work implemented a drive-off controller based on LUTs to determine the desired outputs of the engine torque and speed. These LUTs are used in practical applications and provided by the industrial research partner. Due to confidential agreements, they may only be published anonymously without showing details on axillary scale, as shown in Figure 5.1. A notable point is that the drive torque requested for the ICE does not linearly increase with the APP beyond 50 %. The increase is linear up to 50 % of the APP, but after this threshold, the drive torque remains nearly constant as long as the engine speed is below 1500 RPM. Subsequently, the engine torque shows a further increase beyond this angular speed. It is important to note that the drive-off process is already completed as the clutch is engaged at this time point when the end of the drive-off is defined. The area used for determining the engine desire torque during drive-offs is marked with a red frame in Figure 5.1. Consequently, drive-off procedures for APPs greater than 50 % have identical dynamics before the clutch engagement. For this reason, the investigation primarily focuses on the drive-offs with APPs from 10 % to 50 %, in 10 % increments. Each drive-off is conducted both with and without the support of the EM and reaches a similar speed at the end of the drive-off. This comparison illuminates the EM's contribution to the hybrid powertrain.

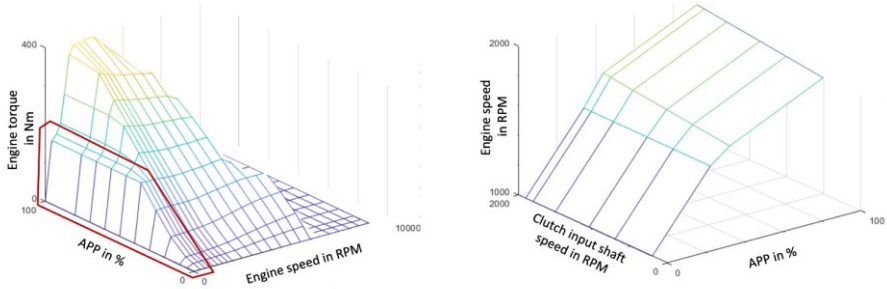


Figure 5.1: LUTs for determining the desired engine torque and speed of the drive-off controller

Figure 5.2 and Figure 5.3 provide a comparison of drive-offs with and without the support of the EM based on APPs. Each drive-off is demonstrated with the help of speed and torque diagrams to illustrate the changes during the synchronization process. On the left side of the figures, drive-offs without EM assistance are illustrated, while on the right side, drive-offs with the support of the EM are shown. Diagrams (b) and (d) of Figure 5.2 illustrate drive-offs at APPs of 10 % and 20 %, representing purely electric drive-offs. Drive-offs with APPs above 20 % are performed in hybrid mode, as displayed in diagrams (b), (d), and (f) in Figure 5.3. It indicates that the EMS prefers the EM for driving the vehicle off when the EM can provide sufficient power. Otherwise, the ICE is utilized to assist the EM in realizing the desired power output. This preference for the EM is influenced by the high instantaneous fuel consumption cost of the ICE during drive-offs, which is calculated with the first product term in Equation (4.42) when the current SOC approaches the target SOC. In these situations, the penalty function does not significantly increase the weight of electrical energy. Consequently, the EM is more likely to operate as the primary drive.

As mentioned, the drive-offs supported by the EM are performed purely electrically at 10 % and 20 % APPs, which are shown in the diagrams (b) and (d) of Figure 5.2. The clutch remains disengaged and does not transfer torque. The increasing engine torque serves to accelerate the crankshaft against friction and inertia resistance so that both drive-offs with and without EM support have comparable engine speed curves, ensuring similar acoustic comfort and synchronization duration of the clutch. This provides equivalence in end vehicle kinematics at the end of the drive-offs, allowing for a meaningful comparison of fuel consumption and thermal load.

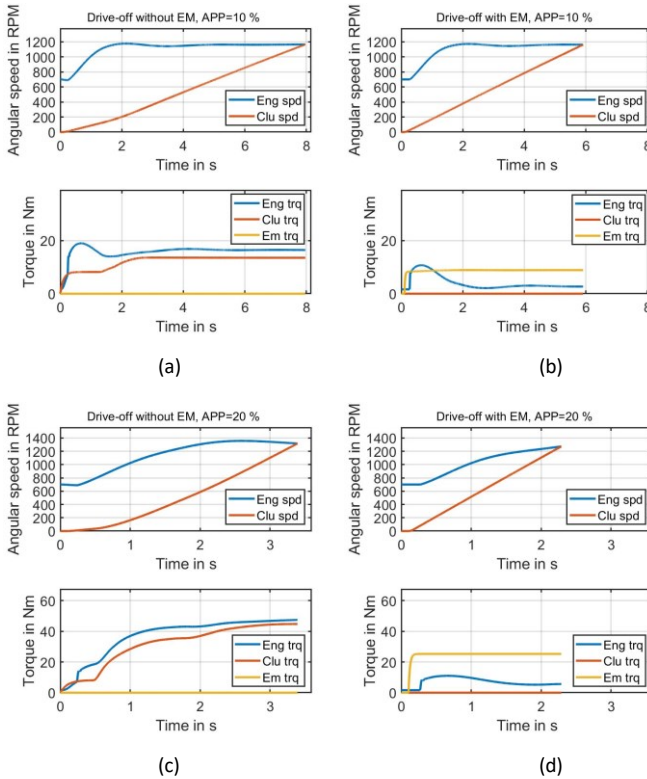


Figure 5.2: Electric drive-off procedures for the APPs of 10 % and 20 %, supported without (left) and with (right) EM

In diagram (b) of Figure 5.3, the drive-off with an APP of 30 % operates firstly with the maximum EM torque, resulting in an acceleration of 1.26 m/s^2 . Subsequently, the ICE engages with the increasing acceleration caused by the increase in drive torque. For other drive-offs with APPs of 40 % and 50 %, as shown in diagrams (d) and (f) in Figure 5.3, the vehicle is driven off by the EM and the ICE simultaneously. Additionally, the EM shows a faster torque response than the ICE and operates at maximum torque most of the time. Shortly before engagement, the EM torque gradually decreases, and the ICE takes over as the primary drive source. This shift is due to the reduction in instantaneous fuel consumption cost for the ICE, resulting from improved operating points, and the increasing cost of electrical energy caused by the reduction in SOC. In these scenarios, the EM consistently operates at maximum torque most of the time, with the ICE compensating for additional drive torque required.

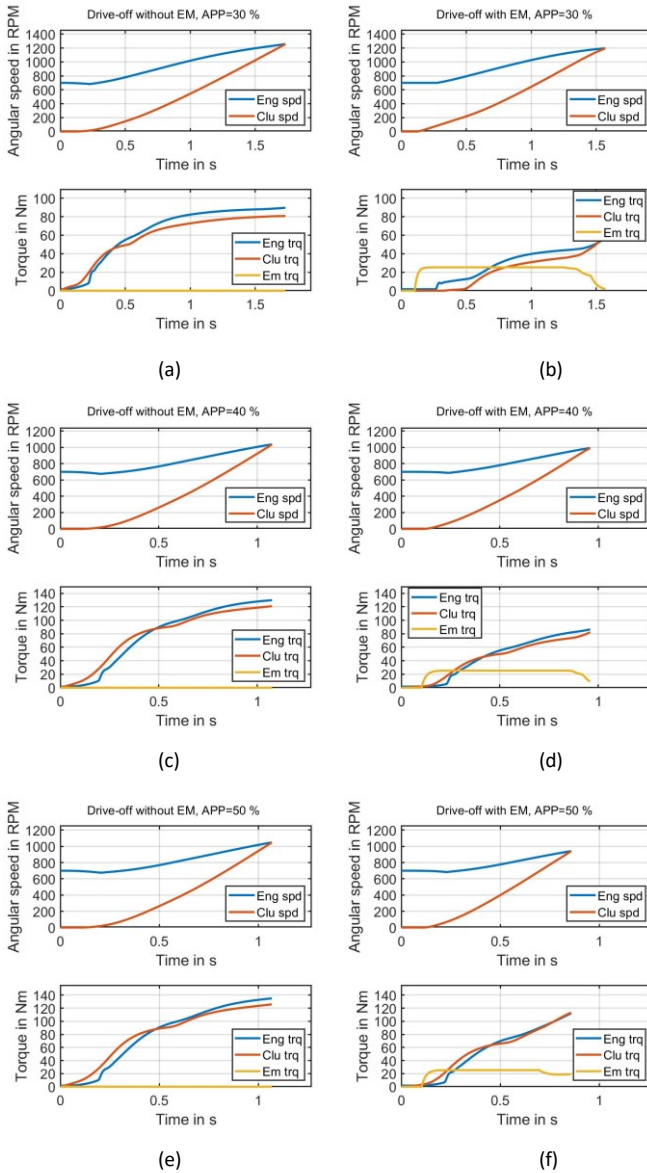



Figure 5.3: Hybrid drive-off procedures for the APPs from 30 % to 50 %, supported without (left) and with (right) EM



In the diagrams, another noticeable phenomenon is the initial increase in clutch torque above the ICE torque, which subsequently falls below it. This behavior is attributed to the drive-off controller. At the start of the drive-offs, the engine speed needs to be reduced, representing a negative engine speed error. To achieve this, the controller increases the last torque supplied by the clutch.

Table 5.1 presents an overview of the drive-off characteristics corresponding to the diagrams in Figure 5.2 and Figure 5.3. These characteristics are compared for different APPs, both with and without EM support. A clear trend emerges: as the APP increases, so does the drive torque and the acceleration of the vehicle. The minimum acceleration, observed at 10 % APP, is 0.33 m/s^2 , while the maximum reaches 3.24 m/s^2 at 50 % APP. Notably, the drive-off with the support of EM at 20 % APP is performed continuously with a maximum EM torque of 25.3 Nm without the support of ICE, as the clutch transfers zero torque. This 20 % value is a threshold value for the APP between purely electrical and hybrid drive-offs in the observed powertrain.

A small difference in drive-off duration can be observed between the drive-offs with and without EM support. Drive-offs assisted by the EM are performed faster than the drive-offs without. The load is shifted to the EM, allowing the clutch to transfer zero or only a part of the load. When comparing the slopes of the clutch output plate speeds, it becomes clear that the clutch accelerates faster, reaches the predefined engine speed earlier, and shows different dynamics. Consequently, it leads to a small deviation between the velocities after drive-off with and without EM support.

Moreover, the mean jerks between these drive-offs exhibit notable differences. This is due to the rapid response of the EM, leading to a fast torque output and a quick acceleration buildup. Consequently, the driver perceives a higher jerk during these electric or hybrid drive-offs. A particular case is the electric drive-off at 20 % APP, showing a mean jerk of approximately 20 m/s^3 , whereas the drive-off without EM support at the same APP has a mean jerk of only 0.42 m/s^3 . By comparing the torque curves in diagrams (c) and (d) of Figure 5.2, it becomes evident that the ICE torque increases significantly more slowly than the EM torque. These torque variations mirror the differences in the acceleration curves. These distinctions will be quantified in the next section through subjective evaluation aspects.

Table 5.1: Characteristic values of drive-offs with and without EM support according to APPs

Drive-offs		Max. Engine torque (Nm)	Max. EM torque (Nm)	Mean. Clutch torque (Nm)	Duration (s)	Velocity after drive-off (m/s)	Max. acceleration (m/s ²)	Mean jerk (m/s ³)
APP: 10 %	Without EM	19.0	0	12.2	7.1	2.47	0.41	0.15
	With EM	10.7	8.9	0.00	6.0	2.46	0.48	4.13
APP: 20 %	Without EM	47.5	0	31.5	3.4	2.80	1.23	0.42
	With EM	11.0	25.3	0.0	2.3	2.71	1.36	20.27
APP: 30 %	Without EM	89.7	0	58.6	1.7	2.69	2.33	1.80
	With EM	57.7	25.3	21.9	1.6	2.55	2.19	2.41
APP: 40 %	Without EM	129.9	0	78.5	1.1	2.24	3.24	4.26
	With EM	86.7	25.3	43.6	1.0	2.14	3.20	4.87
APP: 50 %	Without EM	135.0	0	80.1	1.1	2.26	3.24	4.45
	With EM	112.6	25.3	54.3	0.9	2.04	3.24	8.52

5.1.2 Subjective and ecological evaluation

Subjective evaluation

Initially, the simulated drive-offs are evaluated through objectivated subjective criteria employing the logistic regression model. Specifically, the evaluation models for sportiness, jerkiness, and comfort are utilized, as detailed in Section 2.4.3. By using the drive-off maximum acceleration and the mean jerk as inputs, the subjective evaluations of the drive-off dynamics can be estimated. Table 5.2 provides the evaluation results of drive-off dynamics at different APPs, comparing scenarios with and without EM support. The values represent the likelihood of a subjective evaluation for each criterion.

Table 5.2: Subjective evaluation of the drive-off dynamics using the evaluation models

Drive-offs		Max. acceleration (m/s ²)	Mean jerk (m/s ³)	Sportiness evaluation	Jerkiness evaluation	Comfort evaluation
APP: 10 %	Without EM	0.41	0.15	0.01 %	0.13 %	99.95 %
	With EM	0.48	4.13	0.05 %	0.72 %	99.42 %
APP: 20 %	Without EM	1.23	0.42	0.11 %	0.40 %	99.80 %
	With EM	1.36	20.27	38.40 %	93.47 %	0.34 %
APP: 30 %	Without EM	2.33	1.80	2.65 %	2.60 %	97.81 %
	With EM	2.19	2.41	2.25 %	2.80 %	97.45 %
APP: 40 %	Without EM	3.24	4.26	35.75 %	17.90 %	73.22 %
	With EM	3.20	4.87	37.69 %	20.99 %	66.92 %
APP: 50 %	Without EM	3.24	4.45	37.08 %	19.05 %	70.97 %
	With EM	3.24	8.52	66.74 %	54.93 %	18.07 %

The APP increase indicates a higher demand for acceleration, leading to changes in the perception of the drive-off dynamics. The results clearly demonstrate the trend: as the APP increases, both maximum acceleration and mean jerk rise. Consequently, drive-offs become sportier and jerkier, resulting in reduced overall comfort. The presence of the EM amplifies sportiness and jerkiness, impacting comfort, especially at higher pedal positions. This suggests that while EM enhances the dynamic aspects of drive-offs, it does this at the cost of smooth and comfortable driving. This analysis offers insights into the driving experience across different driving styles. In the following

section, a detailed explanation of the perceived changes corresponding to the alterations in APP is provided.

At lower APPs (10 % and 20 %), the drive-offs without EM support exhibit gradual acceleration, leading to a comfortable and smooth experience. The increase in maximum acceleration at these levels influences the sportiness slightly but maintains overall comfort. Jerkiness remains minimal at lower APPs, indicating a smooth and comfortable drive. Even with slight increases, the drive-offs maintain a pleasant experience. However, with EM support at 20 % APP, a high mean jerk leads to a significant jerky perception and significantly impact on the comfort evaluation.

At medium APPs (30 % and 40 %), the maximum acceleration and mean jerk increase as the APP becomes higher. This enhances sportiness, but there is still a balance between dynamics and comfort, keeping comfort at moderate levels. The drive-offs become jerkier. By comparing the drive-offs with and without EM support at the same APPs, maximum acceleration is slightly reduced, but the sportiness evaluation becomes higher due to the increase in the mean jerk. Contrarily, this leads to a decrease in comfort.

At high APP (50 %), the drive-offs show significant mean jerk, resulting in a sporty driving experience. However, this increase in jerk value comes at the cost of other evaluation criteria. The drive-off becomes considerably less smooth and comfortable. In drive-off with the support of EM, comfort dramatically decreases, and the sportiness and jerkiness significantly rise in comparison to the drive-off without EM support.

Ecological evaluation according to thermal load in the clutch

After the subjective evaluation, the ecological evaluation follows, including the aspects of thermal load and fuel consumption evaluation. Table 5.3 presents detailed information regarding various characteristic values related to thermal loads at different APPs, with and without the support of the EM. It offers insights into how different APPs and the support of the EM affect drive-offs. The data presented includes mean clutch torque, drive-off duration, heat generation, and maximum clutch temperature during each drive-off. By comparing the values between drive-offs with and without EM support at different APPs, the table illustrates the impact of EM support on heat generation and temperature levels in the clutch during the drive-offs.

Table 5.3: Thermal load and temperature in the clutch during drive-offs with different APPs

Drive-offs		Mean Clutch torque (Nm)	Duration (s)	Heat generation (J)	Max. clutch temperature (°C)
APP: 10 %	Without EM	12.2	7.05	5496.80	99.56
	With EM	0.00	5.97	0.00	85.00
APP: 20 %	Without EM	31.5	3.39	6435.28	106.57
	With EM	0.0	2.29	0.00	85.00
APP: 30 %	Without EM	58.6	1.74	4253.34	100.34
	With EM	21.9	1.57	938.94	88.59
APP: 40 %	Without EM	78.5	1.08	3102.87	96.57
	With EM	43.6	0.96	1300.61	89.97
APP: 50 %	Without EM	80.1	1.07	3134.45	96.69
	With EM	54.3	0.86	1387.74	90.30

By examining the heat generated during drive-offs without the support of the EM, as listed in Table 5.3, the drive-offs with APPs below 30 % produce significant heat due to a long slipping time. For APPs above 30 %, the heat generation increases slightly with increasing APPs due to the small increment of the clutch torque and the slipping time. Notably, the EM proves highly effective in significantly reducing clutch heat across all APPs. In special cases of pure electric drive-offs, where the clutch disengages, no heat is generated in the clutch. In hybrid drive-offs, the heat generation increases with increasing APPs. Assuming that the vehicle operates within the 10 % to 50 % APP range with equal proportions, the heat generation can be reduced by 83.82 % due to the support of the EM.

According to the comparison between the drive-offs with and without the EM support, the most significant heat reduction occurs during electric drive-offs at 10 % or 20 % APP, reaching a reduction of 100 %. Even during hybrid drive-off, a heat reduction can be achieved by up to 78 %. The lowest reduction is about 55.6 % at 50 % APP. Accordingly, the maximum friction surface temperatures follow similar trends, showing a maximum reduction of 21.57 °C and a minimum reduction of about 6.40 °C. This is illustrated in Figure 5.4. It highlights the EM's effectiveness in reducing heat generation, contributing to enhanced clutch performance and lifetime.

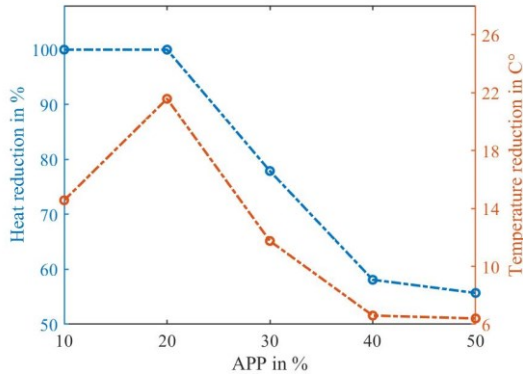


Figure 5.4: Reduction of heat and surface temperature during drive-offs according to the APPs by using the EM

The potential of EM in reducing friction surface temperatures during drive-offs suggests the possibility of reducing energy consumption in the hydraulic system. This leads to the investigation of the idea of reducing the flow rate of the friction oil during hybrid drive-off. Previous research [127] analyzed the energy consumption of the hydraulic system during a test cycle of 120 seconds, which is a part of the experimental measurements used for this work. During this test cycle, the transmission is shifted up to the highest gear and then down to the lowest. The study found that cooling accounted for about 42.8 % of the total energy consumption in the hydraulic system, which corresponds to 3400 J out of 7940 J.

For conducting this investigation, the APP of 50 %, which exhibits the lowest temperature reduction, is evaluated according to the efficiency of the cooling system at reduced flow rates of 0.5 l/min, 1 l/min, and 3 l/min compared to the standard 5 l/min used in the experiment. Figure 5.5 shows the simulation results. Each simulation is performed for the operation that starts with drive-off and follows a short period of normal driving in first gear. The maximum temperature represents the time of the drive-off end when the clutch is engaged. This investigation aims to explain the potential for energy savings in the hydraulic system associated with hybrid drive-offs.

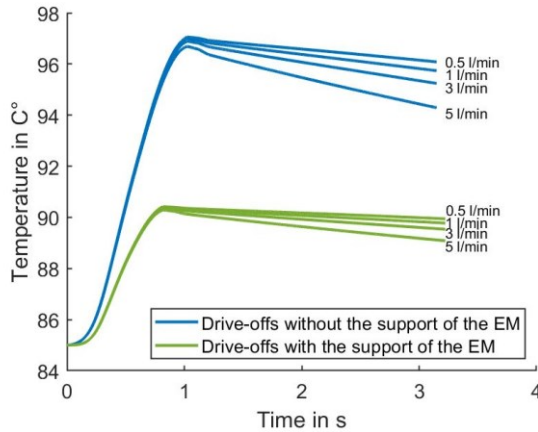


Figure 5.5: Cooling performance at different flow rates for drive-offs with and without the EM support at an APP of 50 %

The temperature variations during drive-offs, followed by normal driving, are illustrated by the blue and green curves, representing drive-offs without the EM support and those with EM support, respectively. Each curve peak signifies the termination of frictional heat generation due to the engaged clutch. Notably, different flow rates marginally influence temperature changes and maximum temperatures during drive-offs. This is due to the limited heat absorption capacity of the friction oil from the relatively small convection surface, consisting of the grooves and outer surface of the friction plate pack.

For the drive-offs without EM support, which have a high-temperature difference between friction oil and friction plate, the higher flow rate proves a better cooling performance for the engaged clutch. At the flow rate of 5 l/min, the clutch temperature declines rapidly compared to other flow rates. In contrast, drive-offs supported by the EM have slight differences in temperature drop less than 2 °C between low and high flow rates. This observation indicates the potential to reduce the friction oil flow rate during hybrid drive-offs for archiving energy conservation within the hydraulic system.

Ecological evaluation according to fuel consumption

Evaluating the fuel consumption improvement during drive-offs with EM support requires a systematic approach. Since the MHVs can recharge the battery during subsequent driving. It allows an analysis of the influence of the EM support on drive-off fuel consumption with a neutral SOC. Achieving SOC neutrality, battery recharging through recuperation and ICE charging must be considered in this process, taking into account the load point upshifting for the ICE and the energy

recuperation during deceleration based on the driving cycle. Based on this, the following approach is proposed:

1. **Drive-Off procedures:** For each APP, the drive-off procedure is initially conducted both with and without EM support.
2. **Subsequent driving:** Following the drive-off, the vehicle operates in hybrid mode, recharging the battery to its initial SOC through recuperation.
3. **Equivalence factors determination:** The Equivalence Factors of the EMS are determined individually for each simulation scenario using the shooting method.

The shooting method iteratively adjusts related parameters for the equivalence factors. It starts with initial values for parameters, refining these parameters iteratively until the final SOC matches the desired value, set at 50 % in this work.

With the help of this approach, only the difference exists between the drive-offs with and without EM support for each APP, ensuring identical vehicle states at the start and end of the driving cycle. The fuel consumption difference of both simulations indicates the consumed fuel for recovering the electric energy consumed during hybrid drive-off. Battery recharge can be considered through a representative driving scenario including frequent deceleration phases. A portion of the WLTC, representing urban traffic, is selected and shown in Figure 5.6. It covers a travel distance of about 1.5 km. The red and blue segments in the curve denote the drive-off procedure and subsequent driving, respectively, revealing dynamic vehicle behavior with multiple deceleration phases.

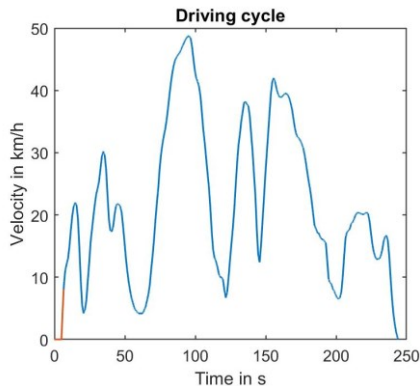


Figure 5.6: Driving cycle for testing the fuel consumption improvement during drive-offs with EM support and recharging the battery with consideration of the energy recuperation

Relying solely on recuperation during deceleration to recharge the battery is insufficient within the chosen driving cycle. To ensure SOC neutrality, the ICE must be engaged with a load point upshifting to charge the battery through the EM during subsequent driving. Figure 5.7 illustrates the distribution of both charging methods during the drive-off with 10 % APP as an example. During the deceleration phases in the driving cycle, the EM operates with an average braking torque of about 8.4 Nm, often below its maximum torque. Since the recuperation performance depends on the driving cycle, it results in identical recuperation performance across all simulations. However, the frequency of ICE load point upshifting varies for different APP levels. The more electrical energy is consumed, the more frequently the ICE engages in load point upshifting, consequently increasing the fuel consumption needed to recharge the battery. It can be seen that the fuel consumption for battery charging differs in Table 5.4.

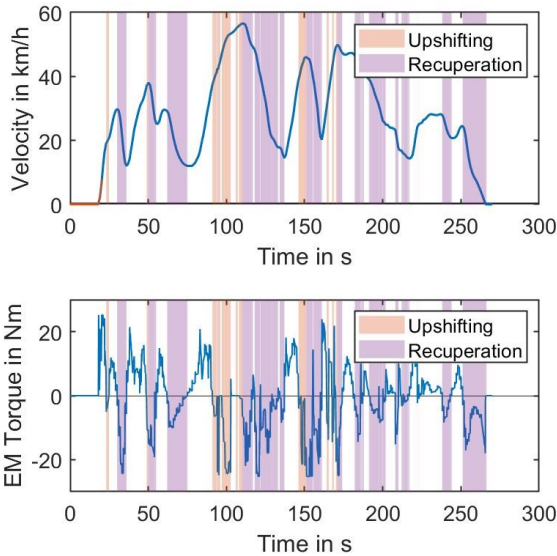


Figure 5.7: Distribution of the battery recharge by recuperation and ICE load point upshifting for drive-off with an APP of 10 %

The fuel consumption improvements (FCIs) for the drive-offs with the EM support are investigated in the following according to APPs from 10 % to 50 %. Driving simulations are conducted to calculate electrical energy and fuel consumption after-drive-off. The scenarios with and without the EM support are compared. The difference between the fuel consumption after drive-offs represents the fuel consumption improvement achieved through EM support during the drive-off phase.

However, this improvement also includes a part of the electric energy consumed by the EM. In order to compensate this, the fuel consumption must be used for battery recharging. It can be calculated by subtracting the total fuel consumptions of both driving cycles with and without the support of the EM. Finally, the effective FCIs, considering the fuel consumption for battery recharging, are determined under the condition of SOC neutrality. The simulation and calculation results are presented in Table 5.4.

Table 5.4: Fuel consumption improvement during drive-offs considering energy recuperation

Drive-offs		Electrical energy consumption (Wh)	Fuel cons. after drive-off (g)	FCI after drive-off (g)	Fuel cons. for battery charging (g)	Effective FCI (g)
APP: 10 %	Without EM	0	6.03	1.58	0.80	0.78
	With EM	2.2	4.45			
APP: 20 %	Without EM	0	4.75	1.38	0.98	0.40
	With EM	2.5	3.38			
APP: 30 %	Without EM	0	4.01	0.60	0.48	0.12
	With EM	1.3	3.41			
APP: 40 %	Without EM	0	3.56	0.35	0.44	-0.09
	With EM	0.7	3.21			
APP: 50 %	Without EM	0	3.57	0.38	0.45	-0.07
	With EM	0.6	3.19			

As the APP increases, there is a trend of decreasing electrical energy and fuel consumption. However, this does not imply a statement that higher APP always results in less energy consumption. This variation is due to the shortened drive-off durations across different APPs. The ratio between fuel consumption for battery charging and electrical energy consumption during drive-off represents a conversion factor for the hybrid powertrain controlled by a control strategy based on A-ECMS. This factor depends on the energy recuperation performance in the driving cycle. Regarding the simulated condition in this work, the conversion factor ranges from 0.1 g/kJ to 0.2 g/kJ, which indicates the fuel consumption quantity for producing 1 kJ of electrical energy.

The effective FCI shows that enhancing fuel efficiency is most noticeable at lower APPs and gradually decreases as APP increases. The most significant improvements are observed at APPs of 10 %

and 20 %, primarily due to pure electrical drive-offs and their extended durations. Longer electrical drive-off durations result in greater fuel consumption improvements when taking into account energy recovery during subsequent driving. Although these longer drive-offs consume more electrical energy (approximately 0.46 % and 0.53 % of the battery capacity) and use more fuel to recharge the battery (0.80 g and 0.98 g), the net fuel consumption improvements remain considerable, amounting to 0.78 g and 0.4 g, compared to 0.12 g at the 30 % APP. Additionally, a modern vehicle uses additional ecological functions like the start-stop function to improve fuel consumption. Assuming the ICE is deactivated and reactivated with a start-stop function, facilitating a transition to engine propulsion from the end of the drive-off. The fuel consumption during electrical drive-offs (4.45 g and 3.38 g) can be reduced by 0.18 g and 0.21 g, accounting for the energy required to accelerate the engine crankshaft to match the actual vehicle speed before engaging the engine with the drivetrain. These deductions are based on the assumption that the engine crankshaft accelerates with an angular acceleration of 300 rad/s².

In the drive-off at 30 % APP, the ICE operates with lower torque but for a more extended duration compared to the drive-off at 40 % and 50 % APPs, as illustrated in Figure 5.3. It demonstrates a fuel consumption improvement of 0.12g.

The drive-offs with APP of 40 % and 50 % exhibit similar characteristics and are conducted within a very brief timeframe, as can be seen in Table 5.1. Furthermore, the drive torques in these cases are also greater than those in other drive-offs. The simulation results show that the fuel consumption for recovering the electrical energy consumed during drive-offs is more than the saved fuel in these drive-offs. Thus, the potential for fuel consumption improvement through EM support is limited in these scenarios.

In the subsequent analysis, the drive-offs are analyzed concerning the overall energy efficiency during drive-offs. The overall energy efficiency of a powertrain refers to the effectiveness with which the powertrain converts the energy input into useful work. It is a measure of how much of the energy from the fuel or electrical source is effectively utilized to propel the vehicle while accounting for inefficiencies in all components of the powertrain, such as the engine, electric motor, and transmission system. Additionally, losses due to factors like friction, heat dissipation, and other mechanical inefficiencies must be accounted for. The efficiency is often expressed as a percentage, indicating what portion of the input energy is converted into useful work, which corresponds to the kinetic energy of the movement in the context of a vehicle.

In the scope of this work, the energy input W_{input} consists of the chemical W_{chem} and electrical energy W_{elec} consumed by ICE and EM during the drive-offs. It is shown in diagram (a) of Figure 5.8. Diagram (b) in Figure 5.8 illustrates the energy output W_{output} and the losses. The energy output is the vehicle's kinetic energy $W_{kinetic}$. The blue bars represent the kinetic energy and the light blue bars indicate the mechanical energy losses, for example due to friction in the transmission and

differential. The ratio between energy output and energy input indicates the overall energy efficiency η_{overall} for the drive-off, as shown in Equation (5.1).

$$\eta_{\text{overall}} = \frac{W_{\text{output}}}{W_{\text{input}}} = \frac{W_{\text{kinetic}}}{W_{\text{chem}} + W_{\text{elec}}} \quad (5.1)$$

Figure 5.8 comparably illustrates the energy inputs in diagram (a) and energy outputs and losses in diagram (b) during drive-offs with and without the support of the EM. The ICE is activated during drive-offs. The sum of the energy output and losses, the cumulative value of the colored bars, is identical to the energy input, recognizable by comparing the bar length for each drive-off between the diagrams.

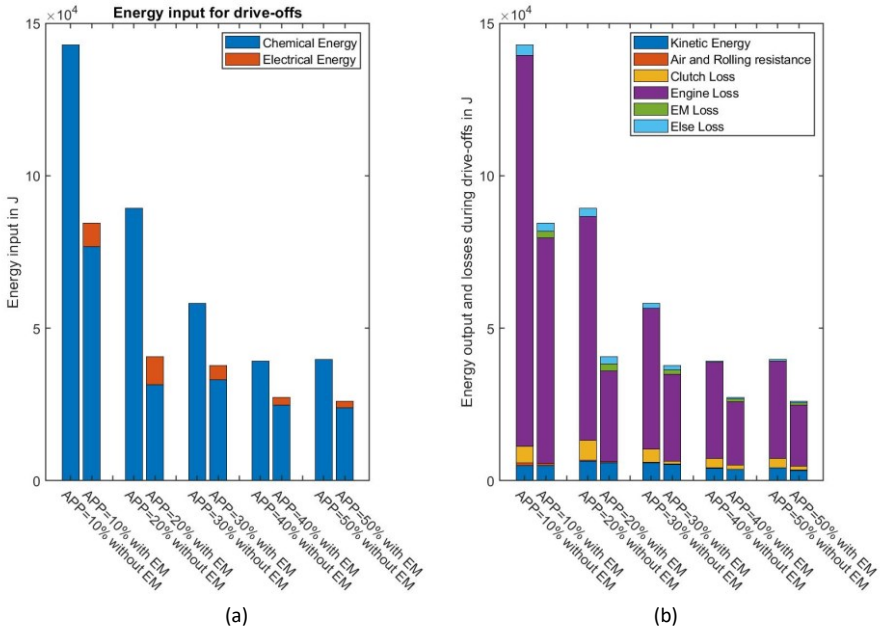


Figure 5.8: Energy inputs (a) and Energy outputs and losses (b) during drive-offs with and without the support of the EM

During drive-offs with APPs of 10 % and 20 %, the vehicle requires substantial energy inputs when operating without EM support. This heightened demand is primarily due to the long drive-off duration, leading to increased energy losses in various components of the powertrain. Consequently, the overall energy efficiencies in these scenarios are notably low, calculating at 4.1 % and 7.5 %. These inefficiencies are also reflected in the ICE, operating at efficiencies of 10.37 % and 14.81 %,

respectively.

However, when EM support is introduced, a remarkable transformation occurs. The total energy inputs and associated losses decrease significantly, almost halving in comparison to drive-offs without the EM support. As a result, the overall energy efficiencies increase to 6.65 % and 15.36 % for the same APPs.

Furthermore, the drive-offs with EM support at 10 % and 20 % APPs necessitate considerable chemical energy inputs to maintain the operation of the ICE. When the ICE is deactivated in these scenarios, the overall energy efficiency can be improved to 49.2 % and 42.64 % at these APPs, respectively. In these electric drive-offs, the EM operates with efficiencies of 74.36 % and 74.99 %, underlining the efficiency gains achieved by employing pure electric drive in the powertrain.

The drive-offs at 30 %, 40 %, and 50 % APPs remarkably require decreased energy inputs despite demanding higher drive torques compared to lower APP drive-offs. The total energy inputs for drive-offs supported by the EM are slightly lower than those without the EM support. Consequently, their overall energy efficiencies are enhanced, reaching 14.4 %, 13.9 %, and 13.1 %, compared to 10.4 %, 10.6 %, and 10.7 % for drive-offs without EM support. This improvement is due to the high efficiency of the EM.

The drive-offs without EM support demonstrate a progressive increase in overall efficiency, ranging from 4.1 % to 10.7 %, corresponding to the APPs from 10 % to 50 %. In comparison, the most efficient drive-off occurs with EM support at 20 % APP, showing an efficiency of 15.36 %. This is closely followed by the drive-off at 30 % APP, indicating improvements in overall efficiency due to EM support.

Diagram (b) in Figure 5.8 show that the ICE and clutch are the primary contributors to energy losses when comparing drive-offs with and without the EM support at different APPs. The increase in overall efficiency can be mainly attributed to the reduction in losses within these components.

In summary, the EM demonstrates significant contributions at lower pedal positions, particularly in pure electric drive-offs. It efficiently drives the vehicle, leading to substantial reductions in energy consumption and fuel usage. As the pedal position increases, the EM still plays a vital role, albeit in combination with the ICE. Even though higher drive torques are required, the overall energy inputs decrease due to the EM's effective support. Across all scenarios, the integration of the EM consistently enhances overall efficiency. Comparing drive-offs with and without EM support, it becomes evident that energy losses, particularly in the ICE and clutch components, are significantly reduced. This loss reduction directly contributes to the overall efficiency increase.

Connection between subjective and ecological evaluation aspects in the mild hybrid powertrain

Examining the simulation results focusing on drive-offs within the investigated mild hybrid powertrain allows for identifying the relationship between subjective evaluations and objective metrics in this specific powertrain concept, encompassing driving dynamics and ecological aspects. This analysis is conducted across different APPs, revealing distinct drive-off dynamics. The relationship between subjective impressions and ecological impact helps calibration engineers strike a balance between vehicle performance and efficiency. Optimizing vehicle dynamics to enhance sportiness while minimizing negative ecological effects ensures that the vehicle remains competitive in terms of both driving pleasure and environmental responsibility. Many regions have stringent regulations regarding emissions and fuel efficiency. Calibration engineers must calibrate vehicle dynamics to comply with these regulations. Understanding how subjective impressions align with ecological impact allows engineers to make informed decisions that meet regulatory requirements while maintaining a positive driving experience. The summarized results are presented in Table 5.5.

The maximum acceleration increases with higher APPs, indicating a more dynamic driving experience. This is in line with the general expectation that higher APP leads to a sportier feel during drive-offs. Sportiness evaluation correlates positively with maximum acceleration, supporting the statement that a more dynamic acceleration is perceived as sportier. However, the impact of mean jerk, for example, at 20 % APP, may introduce some trade-offs in the perceived sportiness. The mean jerk measures the smoothness of acceleration changes. Higher values of mean jerk suggest a less smooth acceleration, significantly impacting subjective evaluations of jerkiness and comfort. Higher mean jerk values are generally associated with higher jerkiness and lower comfort evaluation. The increasing APP indicates higher heat generation and ICE efficiency but decreasing EM efficiency. The highest overall efficiency of the powertrain is identified at APP of 20 % with 15.36 % compared to 6.65 % at 10 % APP, which is the lowest overall efficiency.

The connection between subjective and ecological aspects is intricate. Higher sportiness, as perceived by users, is generally associated with more dynamic driving, but this might compromise the thermal load in the clutch and the overall efficiency of the powertrain.

The challenge lies in optimizing the drive-off process to balance these subjective and ecological considerations. As explained before, the high jerkiness at 20 % APP is caused by the highly dynamic character of the EM, which can also lead to an increase in the sportiness evaluation. Adjustments in the application of EM at different APPs can be further investigated to find an optimal compromise between sportiness, comfort, and ecological aspects.

Table 5.5: Subjective and ecological evaluations of the drive-offs in the mild hybrid powertrain

Drive-offs	Max. acceleration (m/s ²)	Mean jerk (m/s ³)	Sportiness evaluation	Jerkiness evaluation	Comfort evaluation	Heat generation (J)	ICE efficiency	EM efficiency	Overall efficiency
APP: 10 %	0.48	4.13	0.05 %	0.72 %	99.42 %	0.00	3.39 %	74.36 %	6.65 %
APP: 20 %	1.36	20.27	38.40 %	93.47 %	0.34 %	0.00	5.41 %	74.99 %	15.36 %
APP: 30 %	2.19	2.41	2.25 %	2.80 %	97.45 %	938.94	13.96 %	69.75 %	14.43 %
APP: 40 %	3.20	4.87	37.69 %	20.99 %	66.92 %	1300.61	15.96 %	63.82 %	13.86 %
APP: 50 %	3.24	8.52	66.74 %	54.93 %	18.07 %	1387.74	16.43 %	61.49 %	13.17 %

5.2 Ecological evaluation of the thermal clutch load regarding the driving cycle

A driving cycle represents the typical sequence of driving conditions a vehicle experiences during its operation. It consists of various phases, including acceleration, cruising, and deceleration, and often involves upshifting and downshifting, during which the thermal load is also generated in the clutch. While the integration of an EM into the powertrain is found to significantly improve the thermal load during the drive-off phase, the question arises as to how much of the total thermal load in the entire lifetime of the clutch is accounted for by the thermal load during the drive-off phase. By understanding this aspect, the necessity of using EM during drive-off can be analyzed.

For a holistic ecological evaluation of the thermal load reduction in the clutch, the EM contribution during the shifting is also questioned. It can illustrate the distribution of the EM contribution to the thermal load reduction. Therefore, it is important to investigate the specific improvements made by the EM system during subsequent driving. Together with the analysis results in the previous section, it provides a holistic understanding of how EM contributes to eco-friendly driving, not only during the drive-off phase but also across the subsequent gear-shifting phase.

5.2.1 Proportion of the drive-off thermal load in the lifetime of the clutch

For determining the proportion of drive-off thermal load in the entire lifetime of the clutch, the endurance experiment measurements are utilized. The experiment's nature is detailed in Section 4.3.2. In this experiment, the drive load generated in the test powertrain is doubled to ensure an equivalent thermal load in the clutch over a shorter experimental duration, which is also known as an accelerated experiment. The experimental data show a heat-mileage ratio of 15.35 kJ/km, representing the average heat generated per kilometer. By calculating the heat generated during drive-off phases and comparing it to the total heat produced over the entire lifetime, it is determined that each individual drive-off contributes an average heat of about 10 kJ, and the drive-offs account for 9.62 % of the total heat generated throughout the clutch's lifetime. It indicates a potential maximum lifetime enhancement of 9.62 % if drive-offs were consistently conducted solely with the EM. This percentage decreases when hybrid drive-offs are performed.

5.2.2 Outlook for the potential during shifting

Although the EM shows benefits in minimizing heat during drive-offs, it's important to note that this phase accounts for just about 10 % of the total heat generated throughout the clutch's lifetime. Further research can delve into using the EM to reduce thermal load during sequential shifts after drive-off. This raises a research question: How much can the EM contribute to reduce heat generation during subsequent gear shifts? Investigating this aspect can provide advancements in heat reduction research in clutches.

To address this question, a gear-upshifting process is executed with the vehicle model. The vehicle accelerates up to 30 m/s with a constant acceleration of 0.4 m/s², corresponding to an APP of 10 %. During this process, sequential gear shifting from 1st to 7th is conducted in two driving modes, without and with the EM support separately. The study focuses on heat generation in both clutches, specifically comparing the clutch that takes over the drive load during shifts in each scenario. clutch C1 is observed during shifts to odd-numbered gears, while clutch C2 is observed during shifts to even-numbered gears. The aim is to compare heat generation between the two driving modes to determine the EM's effectiveness in reducing clutch heat during gear shifts.

The shifting process at 1st gear corresponds to the drive-off procedure with 10 % APP, which was previously analyzed. The focus of the analysis shifts to the gear shifting from 2nd to 7th gears. The simulation results are shown in Table 5.6: Heat generation in the clutch C1 and clutch C2 for gear shifting from 2nd to 7th, providing insights into the impact of EM support on heat generation during sequential gear shifts.

Table 5.6: Heat generation in the clutch C1 and clutch C2 for gear shifting from 2nd to 7th

Gear shifting to	Heat generation without the EM support (J)	Heat generation with the EM support (J)	Heat comparison (J)	Heat comparison in percentage
2 nd	144.12	139.11	5.01	3.48 %
3 rd	295.45	156.43	139.02	47.05 %
4 th	142.57	138.22	4.35	3.05 %
5 th	228.54	68.62	159.92	69.97 %
6 th	164.82	136.38	28.44	17.26 %
7 th	194.67	161.20	33.47	17.19 %

The heat comparison indicates the difference in heat generation between driving modes without and with EM support. Notably, at the gear shifting of the 2nd and 4th gears, there is a marginal difference in heat generation between both modes. Similarly, the heat generation during 6th and 7th gear shifting is slightly improved. In these shifting processes, the clutch load and shifting durations are comparable. Since the EMS tends to avoid excessive use of electric energy during hybrid driving, the drive load does not significantly shift to the EM side.

In comparison, the 3rd and 5th gear shifting show significant reductions in heat generation, amounting to 47.05 % and 69.97 %, respectively. To explain these reductions, the shifting processes at 3rd gear for both driving modes, without and with the EM support, are illustrated in Figure 5.9. It shows a drive upshift process from 2nd gear to 3rd gear.

The drive upshift sequence can be divided into three main phases: preparation, torque transfer, and speed adjustment. Initially, before the shift command is given, the engine drives the vehicle

through clutch C2, which remains engaged to transmit driving torque. When a shift command is given, the preparation phase begins. In this phase, the target gear (3rd gear in this case) is engaged by a form-lock mechanism using the synchronizer. This engagement causes the speed of clutch C1 to decrease in accordance with the gear ratio of the target gear. Next, in the torque transfer phase, friction torque is generated by controlling the hydraulic pressure applied to clutch C1, allowing it to enter a slipping state. As clutch C1 takes over the drive load, clutch C2 gradually becomes load-free by the end of this phase. Finally, the speed adjustment phase takes place. The engine speed is reduced to match the rotational speed required by the new gear. During this phase, the engine speed is adapted to the new speed of the target gear by reducing the engine torque.

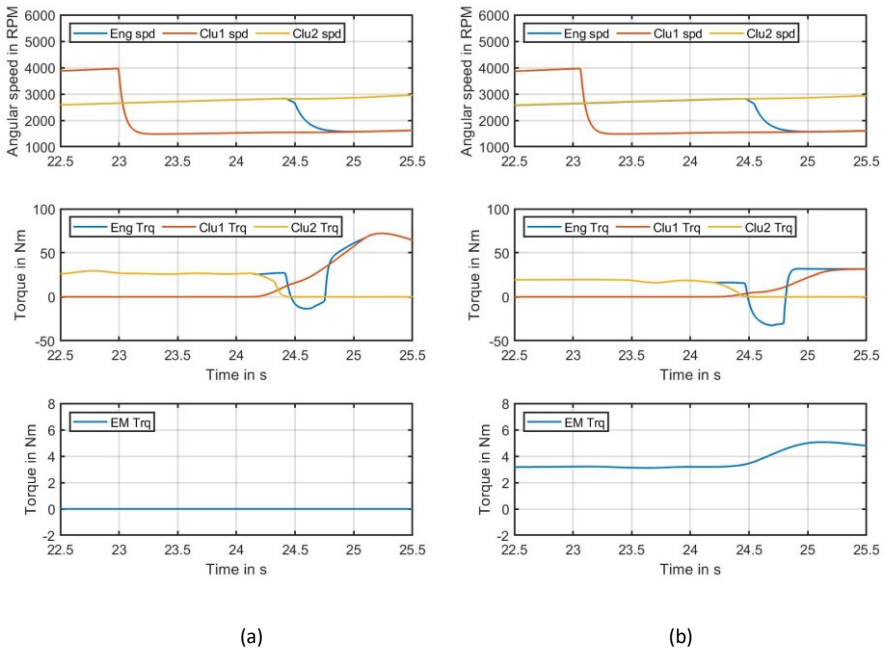


Figure 5.9: Gear shifting at 3rd gear without (a) and with (b) the EM support

As shown in the illustration, the shifting durations for both driving modes are nearly identical, approximately 1 second. The torque transfer occurs first and consumes about 0.5 seconds, followed by a speed adjustment, which also takes around 0.5 seconds. During the speed adjustment phase, the engine speed is reduced by decreasing the engine torque, which corresponds to the torque drop in the diagram. In this way, the engine crankshaft is decelerated by the torque load from the clutch. The negative torque reflects the drag torque in the engine. This character can be

derived from Figure 4.2. By comparing the torques in clutch 1, the clutch torque in hybrid operation reaches a value that is almost half as high as in operation without EM support. This leads to a halving of the heat generation in the clutch.

This analysis reveals that the EM support can effectively reduce the heat generation in the clutch during sequential gear shifting when the EM operates as a drive, corresponding to the load points downshifting in the ICE. However, during load point upshifting, where the EM functions as a generator, the situation changes. The ICE must supply recharging torque in addition to providing drive torque. This results in higher torque levels. Consequently, the clutch experiences increased thermal load due to the elevated drive torque.

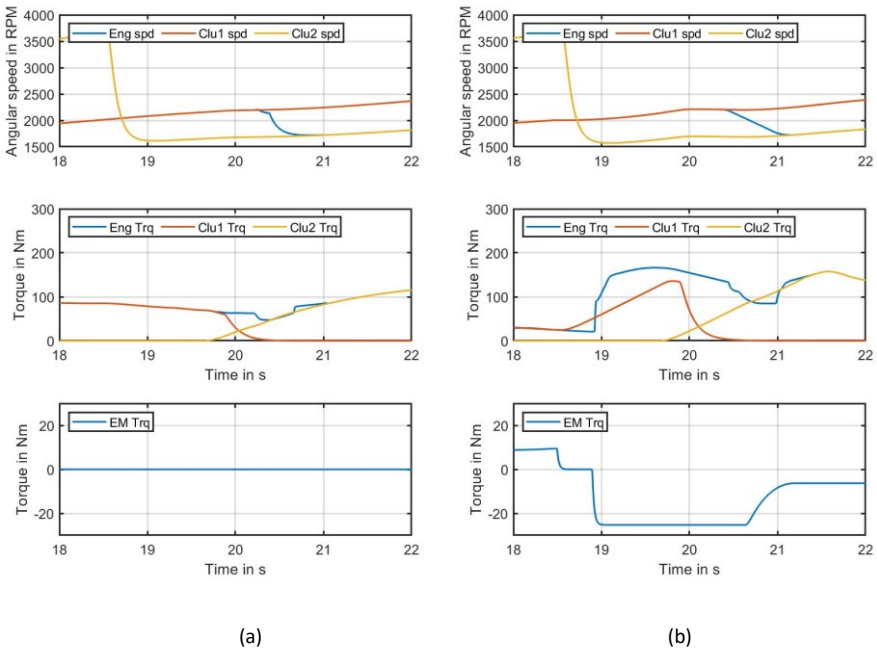



Figure 5.10: Gear shifting at 4th gear without (a) and with (b) the EM support during load point upshifting of the ICE

To illustrate this, further simulation is conducted with the same settings as before but with an acceleration of 0.7 m/s^2 . In this simulation, a load point upshifting is performed at 4th gear, as shown in Figure 5.10. It can be seen that the ICE torque increases just before 19 seconds. This torque is initially transmitted via the first clutch and then shifted to the second clutch by shifting gears. During this time, the EM operates as a generator with a charging torque at the maximum



torque first and then with a decreased charging torque. The friction torque in the second clutch increases to about 150 Nm, compared to about 100 Nm in the gear shifting without the EM support. The heat generation accounts for 1143 J compared to 247 J. It shows a fourfold increase in heat generation in a load point upshifting scenario.

The results indicate that the heat reduction occurs specifically during load point downshifting in the ICE, with no observed reduction during upshifting. This finding underscores the correlation between heat reduction through the use of the EM and the control strategy employed by the EMS during shifting. The results highlight the strategic consideration of the interplay between the gear shifting and the EM operation while recharging. However, the results clearly demonstrate the valuable role of employing the EM during gear shifting to effectively reduce heat generation.

6 Conclusion and perspectives

This work has presented an evaluation process for the drive-off procedure in a mild hybrid powertrain regarding subjective and ecological evaluation criteria. With the help of these criteria, the relation between the subjective driving impression and the ecological evaluation aspects of fuel consumption and thermal load in the clutch can be established according to varying drive-off dynamics. The outcome can help calibration engineering by facilitating the calibration process by considering the impact of alterations in drive-off dynamics on the aforementioned ecological facets and the user experience. The outcome also provides the fundamental knowledge for the design of the EMS and the clutch system in the mild hybrid powertrain. According to the research results, it is not always favorable to use the EM during the drive-off procedure to improve fuel economy. Additionally, the EM support can effectively reduce the thermal load in the clutch during drive-off and gear shifting when the EM functions as a drive. In the following, a conclusion of the conducted work and the perspectives are given in detail.

6.1 Conclusion


According to the literature research addressing the basics of subjective evaluation and the ecological evaluation regarding vehicle dynamics, which is introduced in Chapter 2, a disconnection between subjective evaluations of drive-off behavior and the calibration process with regard to the ecological evaluation is detected.

In the research field of human perception regarding driving dynamics, the focus lies mainly on the determination of the JNT (Just Noticeable Threshold) and the correlation of the subjective rating and the objective measurements in the context of ride comfort or vehicle handling. This work proposes a definition named EDT (Evaluation Difference Threshold), describing the stimulus intensity changes for generating a variation of an evaluation of the drive-off dynamics. In total, three test subject studies are carried out with the help of a driving simulator for determining the EDTs of the maximum acceleration, mean jerk, response time, and engine speed changes according to dynamics and acoustic evaluations. In these studies, as introduced in Chapter 3, descriptive statistical methods are used to illustrate the evaluation results and statistical tests are performed to investigate the influence of the considered factors. For determining the factor influence and interaction effect between the factors, MANOVA is used, which provides an advantage of examining multiple factors simultaneously. After this, the factors are examined by using ANOVA to determine whether the influence is significant on each evaluation criterion. In the last step, the EDTs of the influence factors are determined according to the evaluation criteria by using pairwise comparisons. The nonlinearity of the stimulus intensity is determined, matching the psychophysical theory introduced in [87] and [109].

Furthermore, the evaluation criteria, sportiness, jerkiness, and comfort, are objectivated according to the factors, maximum acceleration and mean jerk, in the test subject study 1. The objectivation models are built for each criterion by using logistic regression models. The simulated drive-offs are evaluated afterward with the help of objectivation models. The EDTs of the response time and the engine speed changes, determined in test subject studies 2 and 3, are considered in the vehicle simulation model in order to ensure the investigation aspect of focusing on a comfort-oriented powertrain. Additional constraints for this purpose are set according to the recorded vehicle measurements for comfort driving. The engine torque output and the clutch torque increase rates are fine-tuned and limited.

For the ecological evaluation, a hybrid modeling approach is introduced in Chapter 4, including the powertrain component modeling and the control module. It combines a forward modeling approach for the drive-off procedure and a backward modeling approach instead of a driver model for controlling the post-drive-off phase in order to precisely follow the reference driving cycle. This hybrid approach offers a robust method for simulating the drive-off behavior with the consideration of both powertrain limitations and cycle accuracy. It fulfills the requirement of maintaining SOC neutrality because the mild hybrid powertrain does not have an external power supply. With this requirement, the fuel consumption in the drive-off with and without the EM support can be directly analyzed without the necessity of converting the consumed electric energy into chemical energy. Although there is available conversion factor in the literature, it is highly dependent on the powertrain performance and driving cycle. Thus, the recharging of the battery by the ICE or during deceleration through energy recuperation must be considered. For this purpose, a control strategy named extended A-ECMS is deployed by extending the A-ECMS with additional costs of traction power error, high engine torque jerk, and hard constraints of the drives. These costs take the drivability, driving comfort, and powertrain limits into account. In addition to maintaining the SOC of the battery, this strategy also controls the interplay between the ICE and the EM, deciding the coordination of both drives to maintain the minimum fuel consumption according to the current driving conditions. Furthermore, a realistic drive-off control strategy is implemented to control the drive-off procedure. Both of these strategies are essential parts of the control module in the vehicle simulation model and ensure a reality-close simulation of the studied powertrain.

Based on this vehicle model, the ecological evaluation regarding fuel consumption and the thermal load generation in the clutch are performed. The findings in Chapter 5 show that fuel consumption improvement can be obtained by using EM during drive-offs with low APPs. In this study case, it refers to APPs below 40 %. The reason for this finding is the long synchronization duration of the clutch, during which the frictional heat is continuously generated, and the unfavorable efficiency of the ICE and the clutch. In comparison, the EM shows a high efficiency of more than 70 %, while the ICE operates only at about 10 % during drive-off. The low efficiency of the ICE and the energy losses in the clutch become dominant for the energy consumption in the drive-offs without the EM



support at low APPs. Consequently, the benefit of EM efficiency is becoming dominant in the drive-offs with the EM support. With the increasing APP, the drive-off duration can be significantly reduced. This disadvantage of the ICE and the clutch becomes unpronounced. Although the fuel consumption can be improved during the drive-off phase, this benefit will be compensated by the consumed fuel for recharging the battery. When observing the entire drive cycle, the fuel consumption for the battery recharging is comparable or even more than the saved fuel consumption during drive-offs.

By analyzing the thermal load during drive-off and sequential upshifting, the EM can effectively reduce the thermal load generation in the clutch by shifting the drive load to the EM side. It indicates that this advantage can be obtained in pure electric driving or hybrid driving with load point downshifting. In the case of load point upshifting, the thermal load generation increases significantly. This point should be noticed, particularly for the control strategy design of the mild hybrid powertrain. The findings underscore the multifaceted ecological advantages associated with the EM support during drive-off and gear shifting. These advantages encompass not only immediate thermal load reduction but also extend to improvements in clutch durability and the overall optimization of powertrain components, aligning with the goals of sustainable and efficient vehicle design. The thermal load is strongly correlated to the lifetime of the friction material and the friction oil in the clutch system, as introduced in Section 2.3.2. Less thermal load generation can optimize the clutch working condition and decelerate the degradation speed. Furthermore, this advantage also provides the potential to reduce friction oil flow rate for saving the energy consumption in the hydraulic system and the potential of downsizing the friction components.

By aligning the subjective and ecological evaluation regarding the variation of drive-off dynamics, a connection between the user experience and calibration engineering can be established. It guides the calibration engineers in aiming to fine-tune drive-off characteristics according to user preferences and the ecological aspects. It can facilitate the calibration process to improve the calibration effectiveness.

In the realm of mild hybrid powertrains, the control strategy needs to optimize efficiency, reduce ecological impact, and consider critical factors such as fuel consumption and thermal load in the clutch. The results of the ecological evaluation can be guidelines for designing control strategies aiming to achieve optimal fuel consumption improvement and thermal load generation in the drive-off elements.

6.2 Perspectives

The fuel consumption improvement of the 48 V mild hybrid powertrain depends on control strategy in the EMS, recuperation performance and driving cycle. In this work, a part of the WLTC, which represents urban driving, is used to analyze fuel consumption improvement by shifting

torque to the EM during drive-off procedures with consideration of energy recuperation during deceleration. However, the recuperation performance depends on this driving cycle. Other driving cycles offering different energy recuperation performances can be taken into account in further investigation.

It is interesting to investigate the influence of the driving cycle on the improvement of fuel consumption by using EM and to clarify the dependence between the EM performance in fuel consumption improvement and the driving cycles. As shown in the results of this work, the highly dynamic character of the EM extends the potential of sporty powertrain tuning. This point can be taken into account in the development of the EM controller with the aim of improving the sporty or comfortable evaluation of the drive-off with optimal fuel consumption. In addition, the control strategy of the EMS also plays an important role in the mild hybrid powertrain.

This work also shows that the EM can help to reduce the frictional thermal load in the clutch, which is a key factor for the clutch component aging. This topic can be involved in further research with the help of the developed clutch degradation model, aiming to investigate the thermal load development at different health states of the clutch or to design the clutch control system with a compensation controller for adapting the changing of the CoF. Furthermore, a subsequent topic is the lifetime of the battery, which varies depending on the operation of the EM. If the EM is frequently shifted between drive and generator operation, it accelerates cyclic degradation of the battery [128]. With the help of a battery aging model, the change in the battery lifetime can be considered when developing a control strategy for an EMS. In future research of this kind, it would be valuable to explore the battery aging rate with respect to the operation of the EM.

Appendix A Questionnaire for test subject study 1

Appendix A1 Introduction

Versuchsanweisungen

In der bevorstehenden Untersuchung sollen verschiedene Anfahrvorgänge im Fahrsimulator hinsichtlich Komforts und Sportlichkeit untersucht werden. Ihnen werden dazu verschiedene Ausprägungen von Anfahrvorgängen präsentiert, die Sie bewerten sollen.

Alle Beschleunigungs-, Anfahr- und Bremsvorgänge erfolgen automatisiert. Im Fahrszenario werden Sie ausschließlich geradeaus fahren. Sie werden also automatisiertes Fahren erleben und müssen weder Lenken, noch das Gaspedal oder Bremspedal betätigen.

Vorbereitung

Die Versuchsleitung wird Sie durch den gesamten Versuch führen. Zuerst wird im Fahrsimulator ihre Sitzposition eingestellt. Daraufhin werden Sie die Kopfhörer und die Oculus Rift aufziehen. Die Fahrgastzelle wird während des Versuchs nicht geschlossen.

Versuchsablauf

Eingewöhnungsphase: Stellen Sie sich vor, dass Sie sich auf einer Landstraße befinden und an einer Ampel stehen. Sie fahren dann an, um Ihre Endgeschwindigkeit (ca. 35km/h) zu erreichen. Bitte konzentrieren Sie sich bei der Fahrt lediglich auf den Anfahrvorgang selbst (die Beschleunigung von 0km/h auf 20km/h). Hier erleben Sie erst zwei Anfahrvorgänge als Orientierung für die spätere Bewertung und anschließend sollen Sie diese mit folgenden Kriterien bewerten.

Versuchsteil: Sie werden insgesamt 9 unterschiedlich ausgeprägte Anfahrvorgänge erleben. Jeder zu bewertende Anfahrvorgang wird einmal gefahren. Anschließend stellt Ihnen die Versuchsleitung die folgenden Fragen zur Bewertung von Komfort und Sportlichkeit des gerade erlebten Anfahrvorgangs:

Den Anfahrvorgang empfand ich als...	1	2	3	4	5	
unsportlich	<input type="radio"/>	<input type="radio"/>	<input type="radio"/>	<input type="radio"/>	<input type="radio"/>	sportlich
flüssig	<input type="radio"/>	<input type="radio"/>	<input type="radio"/>	<input type="radio"/>	<input type="radio"/>	ruckartig
unkomfortabel	<input type="radio"/>	<input type="radio"/>	<input type="radio"/>	<input type="radio"/>	<input type="radio"/>	komfortabel

Die Bewertung soll sich lediglich auf die Beschleunigung von 0km/h auf 20km/h beziehen.

Bitte lassen Sie bei der Bewertung weitere Vorgänge, wie Schaltvorgänge oder das anschließende Bremsen, außer Acht!

Abschluss: Nach Beendigung des Versuchsteils, erhalten Sie noch einen kurzen Fragebogen.

Beschreibungen verschiedener Fahrstile:

Fahrstil	Beschreibung
komfortabel	eher ausgewogene und komfortorientierte Fahrweise
sportlich	eher sportliche und dynamische Fahrweise/ in einer Weise geartet, die dem Sport als imponierender Leistung gleich, ähnelt
flüssig	Ablaufender Fahrstil, keine merkwürdigen Anregungen
ruckartig	Eine kurze und sprunghafte Bewegung
agil	Schnelle Bewegung, ohne großen Kraftaufwand
träge	Arm an Bewegung, verzögerte Fahrweise

Appendix A2 Pre-questionnaire

Welche der folgenden Autoklassen nutzen Sie regelmäßig? (Mehrfachnennung sind möglich)	
0	Kleinwagen (z.B. Audi A1, BMW Mini, VW Polo)
0	Kompaktklasse (z.B. Audi A3, BMW 1er, Mercedes A-Klasse, VW Golf)
0	Mittelklasse inkl. Kombi (z.B. Audi A4, Mercedes C-Klasse, VW Passat)
0	Obere Mittelklasse (z.B. Audi A6, BMW 5er, Mercedes E-Klasse)
0	Oberklasse (z.B. Audi A8, BMW 7er, Mercedes S-Klasse)
0	SUV (z.B. BMW X4, Mercedes GLC, Porsche Cayenne)
0	Sportwagen (z.B. BMW Z4, Mercedes SLK, Porsche 911)
0	Vans (z.B. BMW 2er Active Tourer, Opel Zafira, VW Sharan)
0	Sonstiges: _____

Wie viele Kilometer sind Sie ungefähr im letzten Jahr gefahren?	
0	Bis 2.000 km
0	2.001
0	5.001
0	10.001 – 15.000 km
0	15.001 – 20.000 km
0	Mehr als 20.000 km
0	Ich weiß nicht

Im Vergleich zu anderen Autofahrern fahre ich / bin ich im Straßenverkehr überwiegend:						
sportlich	0	0	0	0	0	gemütlich
risikobereit	0	0	0	0	0	vorsichtig
offensiv	0	0	0	0	0	defensiv
mutig	0	0	0	0	0	ängstlich
sicher	0	0	0	0	0	unsicher
schnell	0	0	0	0	0	langsam
Aufmerksam	0	0	0	0	0	ablenkbar

Appendix A3 Questionnaire for test phase (Example: drive-off 4)

Trajektorie __4__ Den Anfahrvorgang empfand ich als...						
	1	2	3	4	5	
unsportlich	0	0	0	0	0	sportlich
flüssig	0	0	0	0	0	ruckartig
unkomfortabel	0	0	0	0	0	komfortabel

Appendix A4 Post-questionnaire

Beispiel: Wie hoch waren die geistigen Anforderungen der Aufgabe? (z.B. Denken, Entscheiden, Rechnen, Erinnern, Beobachten, Suchen, usw.) Bitte markieren Sie Ihre Antwort auf den Strichen.



Wie hoch waren die geistigen Anforderungen der Aufgabe? (z.B. Denken, Entscheiden, Rechnen, Erinnern, Beobachten, Suchen, usw.)



Wie hoch waren die körperlichen Anforderungen der Aufgabe? (z.B. drücken, ziehen, drehen, kontrollieren, usw.)



Wie erfolgreich haben Sie die geforderte Aufgabe Ihrer Ansicht nach durchgeführt? (z.B. Zufriedenheit mit der Aufgabenbewältigung)



Ausgehend von Ihrem aktuellen Befinden, wie gern möchten Sie noch einmal im Simulator fahren?

Sehr ungern	1	2	3	4	5	6	7	8	9	10	Sehr gern
	<input type="radio"/>	<input type="radio"/>	<input type="radio"/>	<input type="radio"/>	<input type="radio"/>	<input type="radio"/>	<input type="radio"/>	<input type="radio"/>	<input type="radio"/>	<input type="radio"/>	

Im folgenden Fragebogen werden Ihnen Fragen zum/zur Realitätsgrad/Realitätsnähe der Simulatorfahrten gestellt. Bitte wählen Sie bei jeder Frage eine der fünf Bewertungsmöglichkeiten.

	1	2	3	4	5
Wie stufen Sie die Realitätsnähe des Beschleunigungsverhaltens des Simulators, unabhängig von dem Motorgeräusch, ein?	<input type="radio"/>	<input type="radio"/>	<input type="radio"/>	<input type="radio"/>	<input type="radio"/>
	Wenn sehr gering , weshalb?				
Ist es Ihnen aufgefallen, dass die Motorgeräusche aller Anfahrvorgänge unterschiedlich sind	Ja / Nein				
Wie stufen Sie den Einfluss des Motorgeräusches auf die Bewertung der Beschleunigung ein?	<input type="radio"/>	<input type="radio"/>	<input type="radio"/>	<input type="radio"/>	<input type="radio"/>
	Wenn sehr hoch , weshalb?				

Weitere Anmerkung:

Appendix B Questionnaire for test subject study 2

Appendix B1 Introduction

Aufklärungsbogen

Die Richtlinien der Deutschen Forschungsgemeinschaft (DFG) sehen vor, dass sich die Teilnehmer_innen an empirischen Studien mit ihrer Unterschrift explizit und nachvollziehbar einverstanden erklären, dass sie freiwillig an unserer Forschung teilnehmen.

Aus diesem Grund möchten wir Sie bitten, die nachfolgenden Erläuterungen zum Inhalt der Studie zu lesen und untenstehende Einverständniserklärung zu unterzeichnen, sofern Sie damit einverstanden sind.

Gegenstand der Studie/des Experiments

In der bevorstehenden Untersuchung sollen verschiedene Anfahrvorgänge mit Fahrsimulator hinsichtlich Agilität untersucht werden. Ihnen werden dazu verschiedene Ansprechzeiten präsentiert, die Sie bewerten sollen.

Ablauf der Studie/des Experiments

Im Fahrszenario werden Sie ausschließlich geradeaus fahren. Sie werden also aktiv anfahren und nach der Anforderung der Versuchsleitung das Gaspedal betätigen.

Vorbereitung:

Ansprechzeit der Gaspedalzustellung wird als die Zeitspanne zwischen der Betätigung des Gaspedals und die erste Wahrnehmung der Bewegung des Fahrzeugs definiert.

Die Versuchsleitung wird Sie durch den gesamten Versuch führen. Zuerst wird im Fahrsimulator ihre Sitzposition eingestellt. Daraufhin werden Sie die Kopfhörer und die Oculus Rift aufziehen.

Versuchsablauf:

Eingewöhnungsphase: Stellen Sie sich vor, dass Sie sich auf einer Landstraße befinden und an einer Ampel stehen. Sie fahren dann mit 20 %, 40 % oder 60 % der Gaspedalzustellung an. Bitte konzentrieren Sie sich bei der Fahrt lediglich auf den Anfahrvorgang selbst. Hier erleben Sie erst zwei Anfahrvorgänge als Orientierung für die spätere Bewertung und anschließend sollen Sie diese mit folgenden Kriterien bewerten.

Versuchsteil:

Sie werden insgesamt 9 unterschiedlich ausgeprägte Anfahrvorgänge erleben. Jeder zu bewertende Anfahrvorgang wird einmal gefahren. Anschließend stellt Ihnen die Versuchsleitung die folgenden Fragen zur Bewertung von Agilität, Sportlichkeit, Ruckartigkeit und Komfort des gerade erlebten Anfahrvorgangs:

Den Anfahrvorgang empfand ich als...						
	1	2	3	4	5	
träge	0	0	0	0	0	agil
unsportlich	0	0	0	0	0	sportlich
unkomfortabel	0	0	0	0	0	komfortabel

Die Bewertung soll sich lediglich auf den Anfahrvorgang beziehen. Bitte lassen Sie bei der Bewertung weitere Vorgänge, wie Schaltvorgänge oder das anschließende Bremsen, außer Acht!

Beschreibungen verschiedener Fahrstile:

Fahrstil	Beschreibung
komfortabel	eher ausgewogene und komfortorientierte Fahrweise
sportlich	eher sportliche und dynamische Fahrweise/ in einer Weise geartet, die dem Sport als imponierender Leistung gleicht, ähnelt
flüssig	Ablaufender Fahrstil, keine merkwürdigen Anregungen
ruckartig	Eine kurze und sprunghafte Bewegung
agil	Schnelle Bewegung, ohne großen Kraftaufwand
träge	Arm an Bewegung, verzögerte Fahrweise

Appendix B2 Questionnaire for test phase (Example: drive-off 4)

Trajektorie __4__ Den Anfahrvorgang empfand ich als...						
	1	2	3	4	5	
träge	0	0	0	0	0	agil
unsportlich	0	0	0	0	0	sportlich
unkomfortabel	0	0	0	0	0	komfortabel

Appendix C Calculation equations for the Magic Formula parameters

In general, the curve of the longitudinal friction coefficient needs to be fitted by a large amount of experimental data. If the fitted curve of longitudinal friction coefficient is known, the definition of the above parameters can be expressed by the following:

$$\begin{aligned}
 D &= \mu_{\text{Tire},x}(\lambda_m) \\
 &= \mu_{\text{max}} \\
 C &= 1 + \left| \left(1 - \frac{2}{\pi} \cdot \arcsin \frac{\lim_{\lambda \rightarrow \infty} \mu_{\text{Tire},x}(\lambda)}{D} \right) \right| \\
 &= 1 + \left| \left(1 - \frac{2}{\pi} \cdot \arcsin \frac{\mu_{\text{slip}}}{D} \right) \right| \\
 B &= \frac{\left. \frac{d\mu_{\text{Tire},x}(\lambda)}{d\lambda} \right|_{\lambda=0}}{C \cdot D} \\
 &= \frac{C_{\lambda, \text{origin}}}{C \cdot D} \\
 E &= \frac{B \cdot \lambda_m - \tan\left(\frac{\pi}{2 \cdot C}\right)}{B \cdot \lambda_m - \arctan(B \cdot \lambda_m)}
 \end{aligned}$$

where μ_{slip} is the longitudinal friction coefficient in the case of full slip, $C_{\lambda, \text{origin}}$ is the stiffness of friction curve at the origin and λ_m indicates the slip rate corresponding to μ_{max} .

The related parameter for calculating Magic Formula factors:

μ_{max}	μ_{slip}	$C_{\lambda, \text{origin}}$	λ_m
1.3	0.87	30	0.1

Reference

- [1] K. Tammi, T. Minav, and J. Kortelainen, “Thirty Years of Electro-Hybrid Powertrain Simulation,” *IEEE Access*, vol. 6, pp. 35250–35259, 2018, doi: 10.1109/ACCESS.2018.2850916.
- [2] G. Conway, A. Joshi, F. Leach, A. García, and P. K. Senecal, “A review of current and future powertrain technologies and trends in 2020,” *Transp. Eng.*, vol. 5, p. 100080, Sep. 2021, doi: 10.1016/j.treng.2021.100080.
- [3] S. Ou, D. Gohlke, and Z. Lin, “Quantifying the impacts of micro- and mild- hybrid vehicle technologies on fleetwide fuel economy and electrification,” *eTransportation*, vol. 4, p. 100058, May 2020, doi: 10.1016/j.etrans.2020.100058.
- [4] S. Lauer, M. Perugini, and F. Graf, “48 Volt High Power – Much More than a Mild Hybrid,” presented at the 29th Aachen Colloquium Sustainable Mobility 2020, Aachen, Jul. 2020.
- [5] S. Hayslett, K. van Maanen, W. Wenzel, and T. Husain, “The 48-V Mild Hybrid: Benefits, Motivation, and the Future Outlook,” *IEEE Electrification Mag.*, vol. 8, no. 2, pp. 11–17, 2020, doi: 10.1109/MELE.2020.2985481.
- [6] N. Lingesten, “Wear behavior of wet clutches,” Licentiate thesis, Luleå tekniska universitet, Luleå, 2016. [Online]. Available: <https://www.diva-portal.org/smash/record.jsf?pid=diva2%3A991361&dsid=3536>
- [7] M. Li, M. M. Khonsari, D. M. C. McCarthy, and J. Lundin, “On the wear prediction of the paper-based friction material in a wet clutch,” *Wear*, vol. 334–335, pp. 56–66, 2015, doi: 10.1016/j.wear.2015.04.005.
- [8] A. Ompusunggu, T. Janssens, F. Al-Bender, P. Sas, H. Brussel, and S. Vandenplas, “Contact Stiffness Characteristics of a Paper-Based Wet Clutch at Different Degradation Levels,” *17th Int. Colloq. Tribol. 2010 - Solving Frict. Wear Probl.*, vol. 1, 2010.
- [9] W. Ost, P. Baets, and J. Degrieck, “The tribological behaviour of paper friction plates for wet clutch application investigated on SAE#II and pin-on-disk test rigs,” *Wear*, vol. 249, no. 5, pp. 361–371, 2001, doi: 10.1016/S0043-1648(01)00540-3.
- [10] N. Fatima, “Degradation Mechanism of Automatic Transmission Fluid by Water as a Contaminant,” *Proc. Inst. Mech. Eng. Part J J. Eng. Tribol.*, vol. 229, no. 1, pp. 74–85, 2015, doi: 10.1177/1350650114542477.
- [11] T. Newcomb, M. Sparrow, B. Ciupak, Y. Hadad, and J. Hassert, “The Effect of Lower Viscosity Automatic Transmission Fluid on Glaze Chemistry,” *SAE Int. J. Fuels Lubr.*, vol. 1, no. 1, pp. 1469–1479, 2009, doi: 10.4271/2008-01-2395.

- [12] K. Berglund, P. Marklund, and R. Larsson, "Lubricant ageing effects on the friction characteristics of wet clutches," *Proc. Inst. Mech. Eng. Part J J. Eng. Tribol.*, vol. 224, no. 7, pp. 639–647, 2010, doi: 10.1243/13506501JET734.
- [13] K. Berglund, P. Marklund, H. Lundh, and R. Larsson, "Prediction of driveline vibrations caused by ageing the limited slip coupling," *Proc. Inst. Mech. Eng. Part J. Automob. Eng.*, vol. 230, no. 12, pp. 1687–1698, 2016, doi: 10.1177/0954407015619505.
- [14] R. "Barney" Carlson, H. Lohse-Busch, M. Duoba, and N. Shidore, "Drive Cycle Fuel Consumption Variability of Plug-In Hybrid Electric Vehicles Due to Aggressive Driving," presented at the SAE World Congress & Exhibition, Warrendale, PA, United States, 2009. doi: 10.4271/2009-01-1335.
- [15] Z. Liu, A. Ivanco, and Z. S. Filipi, "Impacts of Real-World Driving and Driver Aggressiveness on Fuel Consumption of 48V Mild Hybrid Vehicle," *SAE Int. J. Altern. Powertrains*, vol. 5, no. 2, pp. 249–258, 2016, doi: 10.4271/2016-01-1166.
- [16] G. Lenaers, "Real Life CO₂ Emission and Consumption of Four Car Powertrain Technologies Related to Driving Behaviour and Road Type," presented at the 9th International Conference on Engines and Vehicles, Warrendale, PA, United States, 2009. doi: 10.4271/2009-24-0127.
- [17] J. Thomas, S. Huff, B. West, and P. Chambon, "Fuel Consumption Sensitivity of Conventional and Hybrid Electric Light-Duty Gasoline Vehicles to Driving Style," *SAE Int. J. Fuels Lubr.*, vol. 10, no. 3, 2017, doi: 10.4271/2017-01-9379.
- [18] P. Jardin, "Philippe Jardin - Personalisierte Klassifizierung des Fahrstils durch maschinelles Lernen," Dissertation, Technische Universität Darmstadt, Darmstadt, 2023. Accessed: Aug. 23, 2023. [Online]. Available: <http://www.shaker.de/de/content/catalogue/index.asp?lang=de&ID=8&ISBN=978-3-8440-9016-1>
- [19] M. Schmiedt, P. He, and S. Rinderknecht, "Target State Optimization: Drivability Improvement for Vehicles with Dual Clutch Transmissions," *Appl. Sci.*, vol. 12, no. 20, Art. no. 20, Jan. 2022, doi: 10.3390/app122010283.
- [20] D. Simon, "Entwicklung eines effizienten Verfahrens zur Bewertung des Anfahrverhaltens von Fahrzeugen," Dissertation, Universität Rostock, 2010. doi: 10.18453/rosdok_id00000901.
- [21] P. He, E. Kraft, and S. Rinderknecht, "Objektivierung subjektiver Kriterien für die Bewertung von Anfahrvorgängen," in *Fachtagung VDI MECHATRONIK 2022*, 2022, pp. 139–144.
- [22] E. Kraft, "Test und Applikation von Anfahrvorgängen in virtueller Realität," Dissertation, Technische Universität Darmstadt, Darmstadt, 2023. Accessed: Aug. 23, 2023. [Online]. Available: <https://www.shaker.eu/en/content/catalogue/index.asp?lang=en&ID=8&ISBN=978-3-8440-9159-5&search=yes>

- [23] J. M. Slicker and R. N. K. Loh, "Design of robust vehicle launch control system," *IEEE Trans. Control Syst. Technol.*, vol. 4, no. 4, pp. 326–335, Jul. 1996, doi: 10.1109/87.508881.
- [24] K. van Berkel, T. Hofman, A. Serrarens, and M. Steinbuch, "Fast and smooth clutch engagement control for dual-clutch transmissions," *Control Eng. Pract.*, vol. 22, pp. 57–68, Jan. 2014, doi: 10.1016/j.conengprac.2013.09.010.
- [25] H. Naunheimer, B. Bertsche, G. Lechner, J. Ryborz, and W. Novak, *Fahrzeuggetriebe: Grundlagen, Auswahl, Auslegung und Konstruktion*, 2nd ed. in VDI-Buch. Heidelberg: Springer-Verlag, 2007. [Online]. Available: <http://nbn-resolving.org/urn:nbn:de:bsz:31-epflicht-1609127>
- [26] A. Dutta *et al.*, "Model-based and model-free learning strategies for wet clutch control," *Mechatronics*, vol. 24, no. 8, pp. 1008–1020, Dec. 2014, doi: 10.1016/j.mechatronics.2014.03.006.
- [27] R. Fischer, F. Kückükay, G. Jürgens, and B. Pollak, *Das Getriebebuch*, 2nd ed. in Der Fahrzeugantrieb. Wiesbaden: Springer Vieweg, 2016. [Online]. Available: <https://doi.org/10.1007/978-3-658-13104-3>
- [28] K. Nowatschin *et al.*, "Multitronic - hirzelDas neue Automatikgetriebe von Audi," *ATZ - Automob. Z.*, vol. 102, no. 9, pp. 746–753, Sep. 2000, doi: 10.1007/BF03224308.
- [29] K. Wehbi, D. Bestle, and J. Beilharz, "Automatic calibration process for optimal control of clutch engagement during launch," *Mech. Based Des. Struct. Mach.*, vol. 45, no. 4, pp. 507–522, Oct. 2017, doi: 10.1080/15397734.2016.1250221.
- [30] L. Battiato, H. Wolff, and W. Nover, "Schaltvorgaenge und Anfahrbeschleunigung des Normalfahrers im Innerortsverkehr," *Verkehrsunfall Fahrzeugtechnik*, vol. 36, pp. 201–212, 1998.
- [31] R. Krause, "Anfahrbeschleunigungen im alltäglichen Straßenverkehr," *Verkehrsunfall Fahrzeugtechnik*, vol. 40, pp. 105–108, 2002.
- [32] Gosberger wissenschaftlicher Arbeitskreis, "Anfahrbeschleunigungen für die Praxis," *Verkehrsunfall Fahrzeugtechnik*, vol. 30, pp. 252–254, 1992.
- [33] M. G. Jasinski and F. Baldo, "A method to identify aggressive driver behaviour based on enriched gps data analysis," in *Proceedings of the GEOProcessing*, Nice, France, 2017.
- [34] Andreas Balazs, "Optimierte Auslegung von ottomotorischen Hybridantriebssträngen unter realen Fahrbedingungen," Doctoral Thesis, RWTH Aachen University, Aachen, 2015. doi: 10.13140/RG.2.2.10274.84163.
- [35] K. T. Chau and Y. S. Wong, "Overview of power management in hybrid electric vehicles," *Energy Convers. Manag.*, vol. 43, no. 15, pp. 1953–1968, 2002, doi: 10.1016/S0196-8904(01)00148-0.
- [36] K. Reif, K.-E. Noreikat, and K. Borgeest, *Kraftfahrzeug-Hybridantriebe*. Wiesbaden: Vieweg+Teubner Verlag, 2012. doi: 10.1007/978-3-8348-2050-1.

- [37] O. M. Govardhan, "Fundamentals and classification of hybrid electric vehicles," *Int. J. Eng. Tech.*, vol. 3, 2017.
- [38] A. Babu and S. Ashok, "Improved parallel mild hybrids for urban roads," *Appl. Energy*, vol. 144, pp. 276–283, Apr. 2015, doi: 10.1016/j.apenergy.2014.12.007.
- [39] H. S. Das, C. W. Tan, and A. H. M. Yatim, "Fuel cell hybrid electric vehicles: A review on power conditioning units and topologies," *Renew. Sustain. Energy Rev.*, vol. 76, pp. 268–291, Sep. 2017, doi: 10.1016/j.rser.2017.03.056.
- [40] A. Babu and S. Ashok, "Energy and fuel efficient parallel mild hybrids for urban roads," *Energy Convers. Manag.*, vol. 121, pp. 305–320, Aug. 2016, doi: 10.1016/j.enconman.2016.05.047.
- [41] Y. Luo *et al.*, "Control Strategy for Electric Startup of P2.5-PHEV Based on Slope Memory and Driver's Startup Intention," *IEEE Access*, vol. 9, pp. 77044–77057, 2021, doi: 10.1109/ACCESS.2021.3081924.
- [42] V. Ngo, T. Hofman, M. Steinbuch, and A. Serrarens, "Optimal Control of the Gearshift Command for Hybrid Electric Vehicles," *IEEE Trans. Veh. Technol.*, vol. 61, no. 8, pp. 3531–3543, 2012, doi: 10.1109/TVT.2012.2207922.
- [43] D. Förster, M. Timmann, R. Inderka, J. Strenkert, and F. Gauterin, "Impact of future 48 V-systems on powertrain operation under real-driving conditions." in Proceedings. Springer Fachmedien Wiesbaden, pp. 345–360, 2020. doi: 10.1007/978-3-658-30995-4_33.
- [44] H. Yu, F. Zhang, J. Xi, and D. Cao, "Mixed-Integer Optimal Design and Energy Management of Hybrid Electric Vehicles With Automated Manual Transmissions," *IEEE Trans. Veh. Technol.*, vol. 69, no. 11, pp. 12705–12715, 2020, doi: 10.1109/TVT.2020.3018445.
- [45] F. Winke, *Transient Effects in Simulations of Hybrid Electric Drivetrains*. in Springer eBook Collection Engineering. Wiesbaden: Springer Fachmedien Wiesbaden, 2019. doi: 10.1007/978-3-658-22554-4.
- [46] J. T. B. A. Kessels, M. W. T. Koot, P. P. J. van den Bosch, and D. B. Kok, "Online Energy Management for Hybrid Electric Vehicles," *IEEE Trans. Veh. Technol.*, vol. 57, no. 6, pp. 3428–3440, 2008, doi: 10.1109/TVT.2008.919988.
- [47] S. Onori, L. Serrao, and G. Rizzoni, *Hybrid Electric Vehicles: Energy Management Strategies*, 1st ed. 2016. in SpringerLink Bücher. London: Springer London, 2016. doi: 10.1007/978-1-4471-6781-5.
- [48] A. Rezaei, J. B. Burl, and B. Zhou, "Estimation of the ECMS Equivalent Factor Bounds for Hybrid Electric Vehicles," *IEEE Trans. Control Syst. Technol.*, vol. 26, no. 6, pp. 2198–2205, 2018, doi: 10.1109/TCST.2017.2740836.
- [49] J. Han, Y. Park, and Y. Park, "A novel updating method of equivalent factor in ECMS for prolonging the lifetime of battery in fuel cell hybrid electric vehicle," *IFAC Proc. Vol.*, vol. 45, no. 30, pp. 227–232, 2012, doi: 10.3182/20121023-3-FR-4025.00059.

- [50] F. Zhang, L. Wang, S. Coskun, H. Pang, Y. Cui, and J. Xi, "Energy Management Strategies for Hybrid Electric Vehicles: Review, Classification, Comparison, and Outlook," *Energies*, vol. 13, no. 13, p. 3352, 2020, doi: 10.3390/en13133352.
- [51] K. Berglund, "Predicting wet clutch service life performance," Doctoral thesis, comprehensive summary, Luleå tekniska universitet, Luleå, 2013. [Online]. Available: <http://ltu.diva-portal.org/smash/get/diva2:999654/FULLTEXT01.pdf>
- [52] A. P. Ompusunggu, P. Sas, and H. van Brussel, "Modeling and simulation of the engagement dynamics of a wet friction clutch system subjected to degradation: An application to condition monitoring and prognostics," *Mechatronics*, vol. 23, no. 6, pp. 700–712, 2013, doi: 10.1016/j.mechatronics.2013.07.007.
- [53] M. Hologerson and J. Lundberg, "Engagement behaviour of a paper-based wet clutch Part 2: Influence of temperature," *Proc. Inst. Mech. Eng. Part J. Automob. Eng.*, vol. 213, no. 5, pp. 449–455, 1999, doi: 10.1243/0954407991527017.
- [54] P. Marklund, R. Mäki, R. Larsson, E. Höglund, M. M. Khonsari, and J. Jang, "Thermal influence on torque transfer of wet clutches in limited slip differential applications," *Tribol. Int.*, vol. 40, no. 5, pp. 876–884, 2007, doi: 10.1016/j.triboint.2006.09.004.
- [55] M. Hologerson, "Influence of operating conditions on friction and temperature characteristics of a wet clutch engagement," *Lubr. Sci.*, vol. 7, no. 2, pp. 99–114, 2006, doi: 10.1002/tt.3020070202.
- [56] S. Li, M. T. Devlin, S. H. Tersigni, T.-C. Jao, K. Yatsunami, and T. M. Cameron, "Fundamentals of Anti-shudder Durability: Part I - Clutch Plate Study," in *SAE Technical Paper Series*, Warrendale, PA, United States, 2003. doi: 10.4271/2003-01-1983.
- [57] C. G. Slough, M. P. Everson, R. C. Jaklevic, D. J. Melotik, and W. Shen, "Clutch Shudder Correlated to ATF Degradation through Local Friction vs. Velocity Measurements by a Scanning Force Microscope," *Tribol. Trans.*, vol. 39, no. 3, pp. 609–614, 1996, doi: 10.1080/10402009608983573.
- [58] Y. Yang and R. C. Lam, "Theoretical and experimental studies on the interface phenomena during the engagement of automatic transmission clutch," *Tribol. Lett.*, vol. 5, no. 1, pp. 57–67, 1998, doi: 10.1023/A:1019196331003.
- [59] A. Ompusunggu, J.-M. Papy, S. Vandenplas, P. Sas, and H. Brussel, "Condition Monitoring Method for Automatic Transmission Clutches," *Int. J. Progn. Health Manag. ISSN 2153-2648*, vol. 3, p. 14, 2012.
- [60] P. He, A. Eßer, S. Rinderknecht, and M. Schmiedt, "A Degradation Model of a Wet Friction Clutch based on Theoretical and Experimental Analysis and the Application for a Condition Monitoring Method," in *22nd International VDI Congress Drive*, in VDI-Berichte. , Düsseldorf: VDI Verlag, 2022, pp. 303–320. doi: 10.51202/9783181024010-303.
- [61] E. B. Goldstein, *Wahrnehmungspsychologie: der Grundkurs*, 9. Auflage. Heidelberg: Springer, 2015. doi: 10.1007/978-3-642-55074-4.

- [62] R. F. Schmidt, F. Lang, and M. Heckmann, *Physiologie des Menschen: Mit Pathophysiologie*, 31. überarbeitete und aktualisierte Auflage. in Springer-Lehrbuch. Berlin, Heidelberg: Springer, 2011.
- [63] S. M. Highstein, R. R. Fay, and A. N. Popper, Eds., *The Vestibular System*, vol. 19. in Springer Handbook of Auditory Research, vol. 19. New York, NY: Springer, 2004. doi: 10.1007/b97280.
- [64] M.-T. Nguyen, J. Pitz, W. Krantz, J. Neubeck, and J. Wiedemann, “Subjective Perception and Evaluation of Driving Dynamics in the Virtual Test Drive,” *SAE Int. J. Veh. Dyn. Stab. NVH*, vol. 1, no. 2, Art. no. 2017-01-1564, Mar. 2017, doi: 10.4271/2017-01-1564.
- [65] A. Kumar, E. Sällström, S. Sebben, B. Jacobson, and K. Amiri, “Prediction of Drivers’ Subjective Evaluation of Vehicle Reaction Under Aerodynamic Excitations,” *Hum. Factors*, p. 00187208231157935, Feb. 2023, doi: 10.1177/00187208231157935.
- [66] H. Guan, C. G. Duan, and P. P. Lu, “Subjective Evaluation of Braking System and Dynamics Analysis,” *Appl. Mech. Mater.*, vol. 644–650, pp. 76–80, 2014, doi: 10.4028/www.scientific.net/AMM.644-650.76.
- [67] T. Schubert, F. Friedmann, and H. Regenbrecht, “The Experience of Presence: Factor Analytic Insights,” *Presence*, vol. 10, pp. 266–281, Jun. 2001, doi: 10.1162/105474601300343603.
- [68] H. Kingma, “Thresholds for perception of direction of linear acceleration as a possible evaluation of the otolith function,” *BMC Ear Nose Throat Disord.*, vol. 5, no. 1, p. 5, 2005, doi: 10.1186/1472-6815-5-5.
- [69] P. R. Grant and B. Haycock, “The Influence of Jerk on Perceived Simulator Motion Strength,” *J. Aircr.*, vol. 45, no. 4, pp. 1190–1197, 2008, doi: 10.2514/1.33757.
- [70] F. Soyka *et al.*, “Does Jerk Have to be Considered in Linear Motion Simulation?,” in *AIAA Modeling and Simulation Technologies Conference*, Chicago, Illinois, 2009. doi: 10.2514/6.2009-6245.
- [71] T. Müller, H. Hajek, L. Radić-Weißenfeld, and K. Bengler, “Can You Feel the Difference? The Just Noticeable Difference of Longitudinal Acceleration,” *Proc. Hum. Factors Ergon. Soc. Annu. Meet.*, vol. 57, no. 1, pp. 1219–1223, 2013, doi: 10.1177/1541931213571271.
- [72] T. A. Müller, “Ermittlung vestibulärer Wahrnehmungsschwellen zur zielgerichteten Gestaltung der Fahrzeug-Längsdynamik,” Dissertation, Technische Universität München, München, 2015.
- [73] Müller, T. and Hajek, H. and Frank, T. and Bengler, Klaus, “Das menschliche Auflösungsvermögen von Dynamikveränderungen im Fahrzeug,” presented at the Conference on Future Automotive Technology, 2014. [Online]. Available: <https://mediatum.ub.tum.de/1320005>
- [74] T. H. Rockwell, J. N. Snider, Ohio State University. Department of Industrial Engineering. Systems Research Group, and United States. Public Health Service, *An Investigation of Variability in Driving Performance on the Highway*. Systems Research Group, Department of Industrial Engineering, Ohio State University, 1965. [Online]. Available: <https://books.google.de/books?id=6h4JQAAMAAJ>

- [75] Howard I. P., “The perception of posture, self motion, and the visual vertical,” *Handb. Percept. Hum. Perform.*, p. 18.1-18.61, 1986.
- [76] E. Baumgartner, A. Ronellenfitsch, H.-C. Reuss, and D. Schramm, “Using a dynamic driving simulator for perception-based powertrain development,” in *Transportation Research Part F: Traffic Psychology and Behaviour*, vol. 61, pp. 281–290. doi: 10.1016/j.trf.2017.08.012.
- [77] R. L. Henderson and M. L. Edwards, *Driver Performance Data Book*. U.S. Department of Transportation, National Highway Traffic Safety Administration, 1987. [Online]. Available: <https://books.google.de/books?id=Sc0mcAAACAAJ>
- [78] P. Erler, “Untersuchung von vorausschauenden Motion-Cueing-Algorithmen in einem neuartigen längsdynamischen Fahrsimulator,” Dissertation, Technische Universität Darmstadt, Darmstadt, 2019. doi: 10.25534/TUPRINTS-00011838.
- [79] C. Deubel, S. Ernst, and G. Prokop, “Objective evaluation methods of vehicle ride comfort—A literature review,” *J. Sound Vib.*, vol. 548, p. 117515, Mar. 2023, doi: 10.1016/j.jsv.2022.117515.
- [80] M. Kim, K.-W. Kim, and W. Yoo, “Method to objectively evaluate subjective ratings of ride comfort,” *Int. J. Automot. Technol.*, vol. 12, Dec. 2011, doi: 10.1007/s12239-011-0095-8.
- [81] H. Ghanwat, S. Gosavi, M. Chasker Sr, V. Bagal, and R. Hagawane, “Ride and Comfort Measurements - A Challenge of Subjective and Objective Correlation,” *SAE Int. J. Adv. Curr. Pract. Mobil.*, vol. 4, no. 3, Art. no. 2021-26-0445, Sep. 2021, doi: 10.4271/2021-26-0445.
- [82] T. Ali Böke *et al.*, “Correlation between objective and subjective tests for vehicle ride comfort evaluations,” *Proc. Inst. Mech. Eng. Part J. Automob. Eng.*, vol. 237, no. 4, pp. 706–721, Mar. 2023, doi: 10.1177/09544070221080362.
- [83] P. Maier, “Entwicklung einer Methode zur Objektivierung der subjektiven Wahrnehmung von antriebsstrangerregten Fahrzeugschwingungen,” Dissertation, Karlsruher Institut für Technologie, Karlsruhe, 2011. [Online]. Available: <https://books.google.de/books?id=ojeQMwEACAAJ>
- [84] K. Wolff, R. Kraaijeveld, and J. Hoppermans, “Objective evaluation of subjective driving impressions,” *2008 JSAE Annu. Cong Yokohama SAE Pap.*, vol. 8, p. 0222, 2008.
- [85] J. Chen, S. Wang, D. Liu, F. Cai, and Z. Yang, “Correlation between Subjective and Objective Evaluations of Steering Performance of Passenger Vehicles”, Accessed: Sep. 07, 2023. [Online]. Available: <https://oa.mg/work/10.1061/jhtrcq.0000659>
- [86] H. A. S. Ash, “Correlation of subjective and objective handling of vehicle behaviour,” Doctoral Thesis, University of Leeds, Leeds, West Yorkshire, England, 2002. Accessed: Sep. 06, 2023. [Online]. Available: <https://etheses.whiterose.ac.uk/609/>

- [87] M. Spering and T. Schmidt, *Allgemeine Psychologie kompakt 1: Wahrnehmung, Aufmerksamkeit, Denken, Sprache*, 3. überarbeitete und erweiterte Auflage., vol. 1. in *Allgemeine Psychologie kompakt*, vol. 1. Weinheim: Beltz, 2017.
- [88] K. Backhaus, B. Erichson, W. Plinke, and R. Weiber, *Multivariate Analysemethoden: Eine anwendungsorientierte Einführung*. Berlin, Heidelberg: Springer Berlin Heidelberg, 2018. doi: 10.1007/978-3-662-56655-8.
- [89] P. Erler and S. Rinderknecht, *A newly developed 3 DOF driving simulator for longitudinal dynamics perception investigation*. in *Proceeding of the DSC 2017 Europe Driving Simulation & Virtual Reality Conference and Exhibition*. 2017. [Online]. Available: <https://tubiblio.ulb.tu-darmstadt.de/90251/>
- [90] G. Reymond and A. Kemeny, “Motion Cueing in the Renault Driving Simulator,” *Veh. Syst. Dyn.*, vol. 34, no. 4, pp. 249–259, 2000, doi: 10.1076/vesd.34.4.249.2059.
- [91] M. Fischer, “Motion-Cueing-Algorithmen für eine realitätsnahe Bewegungssimulation,” Dissertation, Technische Universität Braunschweig, Braunschweig, 2009. doi: 10.24355/DBBS.084-200910051056-0.
- [92] E. L. Groen and W. Bles, “How to use body tilt for the simulation of linear self motion,” *J. Vestib. Res. Equilib. Orientat.*, vol. 14, no. 5, pp. 375–385, 2004.
- [93] F. Colombet, Z. Fang, and A. Kemeny, “Tilt thresholds for acceleration rendering in driving simulation,” *SIMULATION*, vol. 93, no. 7, pp. 595–603, Jul. 2017, doi: 10.1177/0037549716675955.
- [94] E. Kraft, A. Viehmann, P. Erler, and S. Rinderknecht, “Virtuelle Fahrerprobungen von Antriebssystemen im Fahr Simulator,” *ATZ - Automob. Z.*, vol. 123, no. 3, pp. 42–47, 2021, doi: 10.1007/s35148-020-0652-4.
- [95] A. Al-Samari, “Study of emissions and fuel economy for parallel hybrid versus conventional vehicles on real world and standard driving cycles,” *Alex. Eng. J.*, vol. 56, no. 4, pp. 721–726, 2017, doi: 10.1016/j.aej.2017.04.010.
- [96] F. Orecchini *et al.*, “Energy consumption of a last generation full hybrid vehicle compared with a conventional vehicle in real drive conditions,” *Energy Procedia*, vol. 148, pp. 289–296, 2018, doi: 10.1016/j.egypro.2018.08.080.
- [97] R. Bao, V. Avila, and J. Baxter, “Effect of 48 V Mild Hybrid System Layout on Powertrain System Efficiency and Its Potential of Fuel Economy Improvement,” presented at the WCX™ 17: SAE World Congress Experience, in *SAE Technical Paper Series*. Warrendale, PA, USA: SAE International, 2009. doi: 10.4271/2017-01-1175.
- [98] M. Melaika, S. Mamikoglu, and P. Dahlander, “48V Mild-Hybrid Architecture Types, Fuels and Power Levels Needed to Achieve 75g CO₂/km,” presented at the WCX SAE World Congress Experience, in *SAE Technical Paper Series*. Warrendale, PA, USA: SAE International, 2009. doi: 10.4271/2019-01-0366.

- [99] D. Förster, L. Decker, M. Doppelbauer, and F. Gauterin, “Analysis of CO2 reduction potentials and component load collectives of 48 V-hybrids under real-driving conditions,” *Automot. Engine Technol.*, vol. 6, no. 1–2, pp. 45–62, 2021, doi: 10.1007/s41104-021-00076-3.
- [100] Y. Jiang, Y. Zheng, Y. Guo, and M. Cong, “Regenerative Braking Control Strategy to Improve Braking Energy Recovery of Pure Electric Bus,” *SAE Int. J. Veh. Dyn. Stab. NVH*, vol. 4, no. 3, 2020, doi: 10.4271/10-04-03-0015.
- [101] I. Pielecha, W. Cieřlik, and A. Szałlek, “Energy recovery potential through regenerative braking for a hybrid electric vehicle in an urban conditions,” *IOP Conf. Ser. Earth Environ. Sci.*, vol. 214, no. 1, p. 012013, 2019, doi: 10.1088/1755-1315/214/1/012013.
- [102] J. M. Luján, A. Garcia, J. Monsalve-Serrano, and S. Martínez-Boggio, “Effectiveness of hybrid powertrains to reduce the fuel consumption and NOx emissions of a Euro 6d-temp diesel engine under real-life driving conditions,” *Energy Convers. Manag.*, vol. 199, p. 111987, 2019, doi: 10.1016/j.enconman.2019.111987.
- [103] P. He, A. Kappes, Y. Cui, and S. Rinderknecht, “The Potential of a Hybrid Powertrain in Fuel Consumption and Thermal Drive-Off Element Load for Drive-Off Procedures regarding Driving Styles,” *SAE World Congr. 2023*, 2023.
- [104] S. R. Serge and J. D. Moss, “Simulator Sickness and the Oculus Rift: A First Look,” *Proc. Hum. Factors Ergon. Soc. Annu. Meet.*, vol. 59, no. 1, pp. 761–765, Sep. 2015, doi: 10.1177/1541931215591236.
- [105] J. T. Reason, “Motion Sickness Adaptation: A Neural Mismatch Model,” *J. R. Soc. Med.*, vol. 71, no. 11, pp. 819–829, Nov. 1978, doi: 10.1177/014107687807101109.
- [106] J. D. Moss, J. Austin, J. Salley, J. Coats, K. Williams, and E. R. Muth, “The effects of display delay on simulator sickness,” *Displays*, vol. 32, no. 4, pp. 159–168, Oct. 2011, doi: 10.1016/j.displa.2011.05.010.
- [107] N. Salkind, *Encyclopedia of research design Band I*. SAGE Publications, 2010. doi: 10.4135/9781412961288.
- [108] E. Schmider, M. Ziegler, E. Danay, L. Beyer, and M. Bühner, “Is It Really Robust?,” *Methodology*, vol. 6, no. 4, pp. 147–151, 2010, doi: 10.1027/1614-2241/a000016.
- [109] C. Becker-Carus and M. Wendt, *Allgemeine Psychologie: Eine Einführung*, 2. Auflage. Berlin, Heidelberg: Springer Berlin Heidelberg, 2017. [Online]. Available: <http://nbn-resolving.org/urn:nbn:de:bsz:31-epflicht-1531815>
- [110] N. Dillen, M. Ilievski, E. Law, L. E. Nacke, K. Czarniecki, and O. Schneider, “Keep Calm and Ride Along: Passenger Comfort and Anxiety as Physiological Responses to Autonomous Driving Styles,” in *Proceedings of the 2020 CHI Conference on Human Factors in Computing Systems*, Honolulu, HI, USA, Apr. 2020, pp. 1–13. doi: 10.1145/3313831.3376247.

- [111] S. Skoda, J. Steffens, and J. Becker-Schweitzer, “Einfluss von Fahrzeuggeräuschen auf die subjektive Bewertung von Beschleunigung,” presented at the DAGA, Darmstadt, 2012.
- [112] Y. Cui, “Development of an energy management strategy for a 48V hybrid drive system of a vehicle,” Student work, Technische Universität Darmstadt, Darmstadt, 2022.
- [113] P. Sendur, J. L. Stein, H. Peng, and L. S. Louca, “An Algorithm for the Selection of Physical System Model Order Based on Desired State Accuracy and Computational Efficiency,” in *Dynamics Systems and CControl*, Washington, DC, USA, May 2008, pp. 891–902. doi: 10.1115/IMECE2003-41529.
- [114] F. Zheng, Y. Xing, J. Jiang, B. Sun, J. Kim, and M. Pecht, “Influence of different open circuit voltage tests on state of charge online estimation for lithium-ion batteries,” *Appl. Energy*, vol. 183, pp. 513–525, 2016, doi: 10.1016/j.apenergy.2016.09.010.
- [115] D. Karnopp, “Computer Simulation of Stick-Slip Friction in Mechanical Dynamic Systems,” *J. Dyn. Syst. Meas. Control*, vol. 107, no. 1, pp. 100–103, Mar. 1985, doi: 10.1115/1.3140698.
- [116] Guang Rao, “Modellierung und Simulation des Systemverhaltens nasslaufender Lamellenkupplungen,” Dissertation, Technische Universität Dresden, Dresden, 2011. [Online]. Available: <https://tud.qucosa.de/api/qucosa%3A25774/attachment/ATT-0/>
- [117] S. Jung, T.-Y. Kim, and W.-S. Yoo, “Advanced slip ratio for ensuring numerical stability of low-speed driving simulation. Part I: Longitudinal slip ratio,” *Proc. Inst. Mech. Eng. Part J. Automob. Eng.*, vol. 233, no. 8, pp. 2000–2006, 2019, doi: 10.1177/0954407018759738.
- [118] N. Sina, V. Esfahanian, M. R. H. Yazdi, and S. Azadi, “Introducing the Modified Tire Power Loss and Resistant Force Regarding Longitudinal Slip,” *SAE Int. J. Passeng. Cars - Mech. Syst.*, vol. 11, no. 2, Art. no. 06-11-02-0014, Apr. 2018, doi: 10.4271/06-11-02-0014.
- [119] H. B. PACEJKA and I. J. M. BESSELINK, “Magic Formula Tyre Model with Transient Properties,” *Veh. Syst. Dyn.*, vol. 27, no. sup001, pp. 234–249, 1997, doi: 10.1080/00423119708969658.
- [120] P. W. A. Zegelaar, “The dynamic response of tyres to brake torque variations and road unevennesses,” Doctoral Thesis, Technical University Delft, Delft, Niederlande, 1998. Accessed: Oct. 12, 2023. [Online]. Available: <https://repository.tudelft.nl/islandora/object/uuid%3Ac623e3fc-b88a-4bec-804a-10bc7e94124>
- [121] M. Blundell and D. Harty, “Tyre Characteristics and Modelling,” in *The Multibody Systems Approach to Vehicle Dynamics*, 2nd ed., Butterworth-Heinemann, 2014, pp. 335–450. doi: 10.1016/B978-0-08-099425-3.00005-4.
- [122] G. Rill, “First Order Tire Dynamics,” in *III European Conference on Computational Mechanics*, Dordrecht: Springer Netherlands, 2006, pp. 776–776. doi: 10.1007/1-4020-5370-3_776.
- [123] P. Stephan, “Berechnungsmethoden für Wärmeleitung, konvektiven Wärmeübergang und Wärmestrahlung,” in *VDI-Wärmeatlas*, Berlin, Heidelberg: Springer, 2013, pp. 23–36. doi: 10.1007/978-3-642-19981-3_4.

-
- [124] C. Hirzel, “Ein Beitrag zur Synthese und Analyse elektrifizierter Fahrzeuggetriebestrukturen aus einer Kombination von Stirnrad- und Planetengetrieben mit Fokus auf die systematische Realisierung einer hinreichenden Gangverteilung,” Doctoral Thesis, Martin-Luther-Universität Halle-Wittenberg, Halle (Saale) und Wittenberg, Germany, 2018. doi: 10.25673/13435.
- [125] M. Tutuianu *et al.*, “Development of the World-wide harmonized Light duty Test Cycle (WLTC) and a possible pathway for its introduction in the European legislation,” *Transp. Res. Part Transp. Environ.*, vol. 40, pp. 61–75, Oct. 2015, doi: 10.1016/j.trd.2015.07.011.
- [126] M. Gis and M. Bednarski, “Comparative studies of harmful exhaust emission from a hybrid vehicle and a vehicle powered by spark ignition engine,” *IOP Conf. Ser. Mater. Sci. Eng.*, vol. 421, p. 042022, Oct. 2018, doi: 10.1088/1757-899X/421/4/042022.
- [127] Z. Liu, P. He, and S. Rinderknecht, “A Combined Theoretical and Experimental Investigation of the Overall Energy Consumption in a Wet Dual Clutch System During a Driving Profile,” in *ASME 2021 International Mechanical Engineering Congress and Exposition*, 2021. doi: 10.1115/IMECE2021-71198.
- [128] J. Schmalstieg, S. Käbitz, M. Ecker, and D. U. Sauer, “A holistic aging model for Li(NiMnCo)O₂ based 18650 lithium-ion batteries,” *J. Power Sources*, vol. 257, pp. 325–334, Jul. 2014, doi: 10.1016/j.jpowsour.2014.02.012.